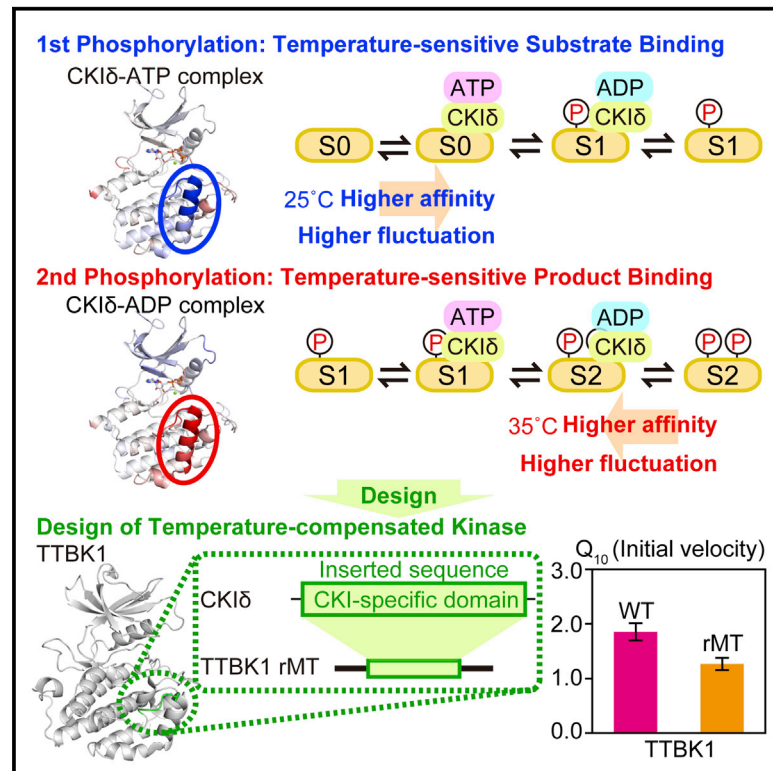


Molecular Cell

Temperature-Sensitive Substrate and Product Binding Underlie Temperature-Compensated Phosphorylation in the Clock

Graphical Abstract



Authors

Yuta Shinohara, Yohei M. Koyama, Maki Ukai-Tadenuma, ..., Takashi Umehara, Kazuki Tainaka, Hiroki R. Ueda

Correspondence

uedah-tyk@umin.ac.jp

In Brief

The circadian clock is able to compensate for fluctuations in temperature, and Shinohara et al. reveal two underlying mechanisms: “lower substrate affinity to CKI δ -ATP complex” and “higher product affinity to CKI δ -ADP complex.” They also identify a key CKI-specific domain that is necessary for temperature compensation.

Highlights

- Temperature-sensitive affinity can counteract the speedup of phosphorylation
- CKI δ agonist ATA is identified by inhibitor screening of dephosphorylation activity
- K224D mutation significantly changed the temperature dependency of circadian rhythm
- Temperature compensation is conferred by inserting CKI-specific domain around K224



Temperature-Sensitive Substrate and Product Binding Underlie Temperature-Compensated Phosphorylation in the Clock

Yuta Shinohara,¹ Yohei M. Koyama,^{1,2,3} Maki Ukai-Tadenuma,¹ Takatsugu Hirokawa,^{4,5} Masaki Kikuchi,⁶ Rikuhiko G. Yamada,¹ Hideki Ukai,¹ Hiroshi Fujishima,¹ Takashi Umehara,^{6,7} Kazuki Tainaka,^{8,9} and Hiroki R. Ueda^{1,8,10,*}

¹Laboratory for Synthetic Biology, RIKEN Quantitative Biology Center, 1-3 Yamadaoka, Suita, Osaka 565-0871, Japan

²Laboratory for Computational Molecular Design, RIKEN Quantitative Biology Center, 6-2-4 Furuedai, Suita, Osaka 565-0874, Japan

³Research and Development Project of Special Purpose Supercomputers for Drug Design, RIKEN Quantitative Biology Center, 6-2-4 Furuedai, Suita, Osaka 565-0874, Japan

⁴Molecular Profiling Research Center for Drug Discovery (molprof), National Institute of Advanced Industrial Science and Technology (AIST), 2-4-7 Aomi, Koto-ku, Tokyo 135-0064, Japan

⁵Division of Biomedical Science, Faculty of Medicine, University of Tsukuba, 1-1-1 Tennodai, Tsukuba-shi, Ibaraki 305-8575, Japan

⁶Epigenetics Drug Discovery Unit, RIKEN Center for Life Science Technologies, 1-7-22 Suehiro-cho, Tsurumi-ku, Yokohama 230-0045, Japan

⁷PRESTO, Japan Science and Technology Agency (JST), 4-1-8 Honcho, Kawaguchi, Saitama 332-0012, Japan

⁸Department of Systems Pharmacology, Graduate School of Medicine, The University of Tokyo, 7-3-1 Hongo, Bunkyo-ku, Tokyo 113-0033, Japan

⁹System Pathology for Neurological Disorders, Brain Research Institute, Niigata University, 1 Asahimachi, Chuo-ku, Niigata 951-8585, Japan

¹⁰Lead Contact

*Correspondence: uedah-tky@umin.ac.jp

<http://dx.doi.org/10.1016/j.molcel.2017.08.009>

SUMMARY

Temperature compensation is a striking feature of the circadian clock. Here we investigate biochemical mechanisms underlying temperature-compensated, CKI δ -dependent multi-site phosphorylation in mammals. We identify two mechanisms for temperature-insensitive phosphorylation at higher temperature: lower substrate affinity to CKI δ -ATP complex and higher product affinity to CKI δ -ADP complex. Inhibitor screening of ADP-dependent phosphatase activity of CKI δ identified aurintricarboxylic acid (ATA) as a temperature-sensitive kinase activator. Docking simulation of ATA and mutagenesis experiment revealed K224D/K224E mutations in CKI δ that impaired product binding and temperature-compensated primed phosphorylation. Importantly, K224D mutation shortens behavioral circadian rhythms and changes the temperature dependency of SCN's circadian period. Interestingly, temperature-compensated phosphorylation was evolutionary conserved in yeast. Molecular dynamics simulation and X-ray crystallography demonstrate that an evolutionally conserved CKI-specific domain around K224 can provide a structural basis for temperature-sensitive substrate and product binding. Surprisingly, this domain can confer temperature compensation on a temperature-sensitive TTBK1. These findings suggest the temperature-sensitive substrate- and

product-binding mechanisms underlie temperature compensation.

INTRODUCTION

The circadian clock is a molecular mechanism underlying endogenous, self-sustained oscillations with a period of ~ 24 hr manifest in diverse physiological and metabolic processes. Its striking and defining feature is its ability to maintain constant period length over a wide range of temperatures (known as “temperature compensation”) (Hastings and Sweeney, 1957; Hogenesch and Ueda, 2011; Millius and Ueda, 2017; Pittendrigh, 1954). This characteristic is evolutionarily conserved in a wide range of organisms from photosynthetic bacteria (Kondo et al., 1993) to warm-blooded mammals (Izumo et al., 2003; Tsuchiya et al., 2003). Although mammals are warm blooded, it is known that temperature gradients exist between the body's skin and core (Lenhardt and Sessler, 2006), which indicates that the temperature compensation is also important for mammals to keep the circadian rhythm among tissues. Since the rate of most enzymatic reactions doubles or triples with every 10°C increase in temperature (i.e., $Q_{10} = 2-3$) (Segel, 1975), the temperature compensation of the circadian period ($Q_{10} = 0.8-1.4$) (Dunlap et al., 2004) has attracted the attention of a broad spectrum of researchers from different disciplines (Hogenesch and Ueda, 2011; Millius and Ueda, 2017). However, despite many genetic and molecular studies, the detailed biochemical mechanisms underlying temperature compensation remain poorly understood (Hogenesch and Ueda, 2011; Millius and Ueda, 2017).

The simplest explanation for temperature compensation of the circadian clock is that the key period-determining reactions

are insensitive to temperature. Indeed, Pittendrigh proposed the existence of a temperature-insensitive component in the clock system in 1954 (Pittendrigh, 1954), and in 1968, he and his colleagues demonstrated that both the wave form and the period of a circadian oscillation are invariant with temperature (Zimmerman et al., 1968). However, the idea of temperature-insensitive biochemical reaction is counterintuitive, as elementary chemical processes are highly temperature sensitive (Segel, 1975). Exceptions first came from the observations of the cyanobacterial clock, where temperature-insensitive biochemical reactions have been observed in vitro (Nakajima et al., 2005; Tomita et al., 2005). Although the clock proteins in cyanobacterial clock seem distinct from other clock systems, the temperature-insensitive biochemical reactions were also discovered in mammals, where we observed that CKI δ / ϵ -dependent phosphorylation, a period-determining process in the mammalian circadian clock, had temperature compensation in vitro and in cellulo (Isojima et al., 2009). Here, we show two mechanisms underlie temperature compensation: “lower substrate affinity to CKI δ -ATP complex at higher temperature” and “higher product affinity to CKI δ -ADP complex at higher temperature.”

RESULTS

Temperature-Sensitive Binding of a Substrate to an Enzyme Underlies the Temperature Compensation of CKI δ -Dependent Single-Serine Phosphorylation

In a previous study, we demonstrated that CKI δ -dependent phosphorylation was temperature compensated in vitro (Isojima et al., 2009). Interestingly, temperature dependency of the phosphorylation by the catalytic domain of wild-type CKI δ (Δ CKI δ ; 2–317 residues of CKI δ to delete C-terminal regulatory domain) is highly affected by the peptide sequence of their substrate. For example, although the phosphorylation of casein by Δ CKI δ is highly temperature sensitive, it is temperature compensated for β TrCP- (RKKKPHSGSSGYGSLGNSGHEH LMSQTSSSDSN) and FASPS- (RKKKTEVSAHLSSLTLPKAE SVSLTSQ) peptides that include typical CKI-substrate motif S-X-X-S (Gallego and Virshup, 2007). However, these peptides contain more than twelve and nine possible phosphorylation sites, respectively, whose complexity confounds a detailed biochemical understanding of temperature-compensated phosphorylation. Therefore, in this study, we introduced derivatives of a simple synthetic peptide (CKItide; KRRRALpSVASLPGL), which is used as a substrate for CKI. In the following analysis, we introduced a CKItide derivative (*CKItide; KRRRALSVASLPGL), which includes only a single S-X-X-S motif. In order to precisely quantify the amount of substrate and phosphorylated peptides, we used a capillary electrophoresis-based mobility shift assay system (Figure S1A). The initial velocity of Δ CKI δ -dependent phosphorylation from a two-serine substrate *CKItide to double-phosphorylated product CKItide (2pS) (KRRRALpSVApSLPGL) at low-concentration substrate (20 μ M) seemed highly temperature compensated over a wide range of temperatures from 20°C to 45°C (Figure S1B). Initial velocities were also temperature compensated for a wide range of substrate concentrations (Figures 1A and S1C), although the

substrate inhibition observed for 640 μ M at 25°C indicated the deviation from the Michaelis-Menten model.

We further simplified the two-serine substrate because it seemed still too complex to determine the detailed kinetic parameters for each process. We thus prepared a series of single-serine substrates, *CKItide(S10X) (KRRRALSVAXLPGL), by mutating the second serine (at position 10) of *CKItide to an amino acid X. As a negative control, we utilized Δ TTBK1 (a catalytic domain of wild-type Tau-tubulin kinase 1, TTBK1) because TTBK family is one of the closest neighbors to CKI family in mammalian kinases (Manning et al., 2002). Interestingly, the phosphorylation reactions of all single-serine substrates by Δ CKI δ were also temperature compensated, whereas those by Δ TTBK1 were temperature sensitive (Figure 1B). These results suggest that a single-serine substrate is sufficient for temperature-compensated, Δ CKI δ -dependent phosphorylation.

To determine each kinetic parameter (Figure 1C) of phosphorylation activity of Δ CKI δ , which showed ATPase activity (Figure S1D), we used a single-serine substrate *CKItide(S10A) (KRRRALSVAAALPGL) and evaluated how its phosphorylation is dependent on the concentration of ATP (Figures 1D and S1E). Interestingly, the catalytic efficiency ($k_{\text{catTS}}/K_{\text{mTS}}$) was temperature compensated whereas the catalytic constant (k_{catTS}) and the Michaelis constant (K_{mTS}) were highly sensitive to temperature (Figure 1D). Hence, the apparent temperature compensation of $k_{\text{catTS}}/K_{\text{mTS}}$ would be attributed to the counterbalance between the temperature-dependent increase in k_{catTS} and temperature-dependent decrease in the affinity between Δ CKI δ and a single-serine substrate ($1/K_{\text{mTS}}$).

To validate the role of enzyme-substrate binding in the temperature compensation of Δ CKI δ -dependent phosphorylation, we measured the phosphorylation activity of a series of alanine mutants of *CKItide by Δ CKI δ (Figure S1F). Since the phosphorylation of R4A, S7A, and V8A mutant peptides was remarkably suppressed, we considered that these residues would participate in the enzyme-substrate binding. The previous study demonstrated that the phosphorylation activity of CKI was increased by introducing a negatively charged residue such as aspartate and glutamate to the –3 position from the residue to phosphorylate in the substrate (Flotow and Roach, 1991). We focused on the arginine at the position 4 (R4) because it was located at the –3 position from the serine at position 7 of the single-serine substrate *CKItide(S10A). We synthesized a new substrate, *CKItide(R4D,S10A), by replacing the arginine at the position 4 (R4) with the aspartate (D). Although $k_{\text{cat}}/K_{\text{m}}$ in the phosphorylation of the single-serine substrate *CKItide(S10A) was temperature compensated (Figure 1E), that of *CKItide (R4D,S10A) was sensitive to temperature with temperature-independent K_{m} (Figure 1F). We next focused on the serine at the position 7 (S7) because it was located at the –3 position from the second serine (S10). We synthesized a new substrate, *CKItide(S7D), by replacing S7 with the aspartate (D). We found that $k_{\text{cat}}/K_{\text{m}}$ in the phosphorylation of *CKItide(S7D) was sensitive to temperature with temperature-independent K_{m} (Figure S1G). Taken together, temperature-compensated phosphorylation of the single-serine substrates could be achieved by the temperature-sensitive interaction between enzyme and substrate.

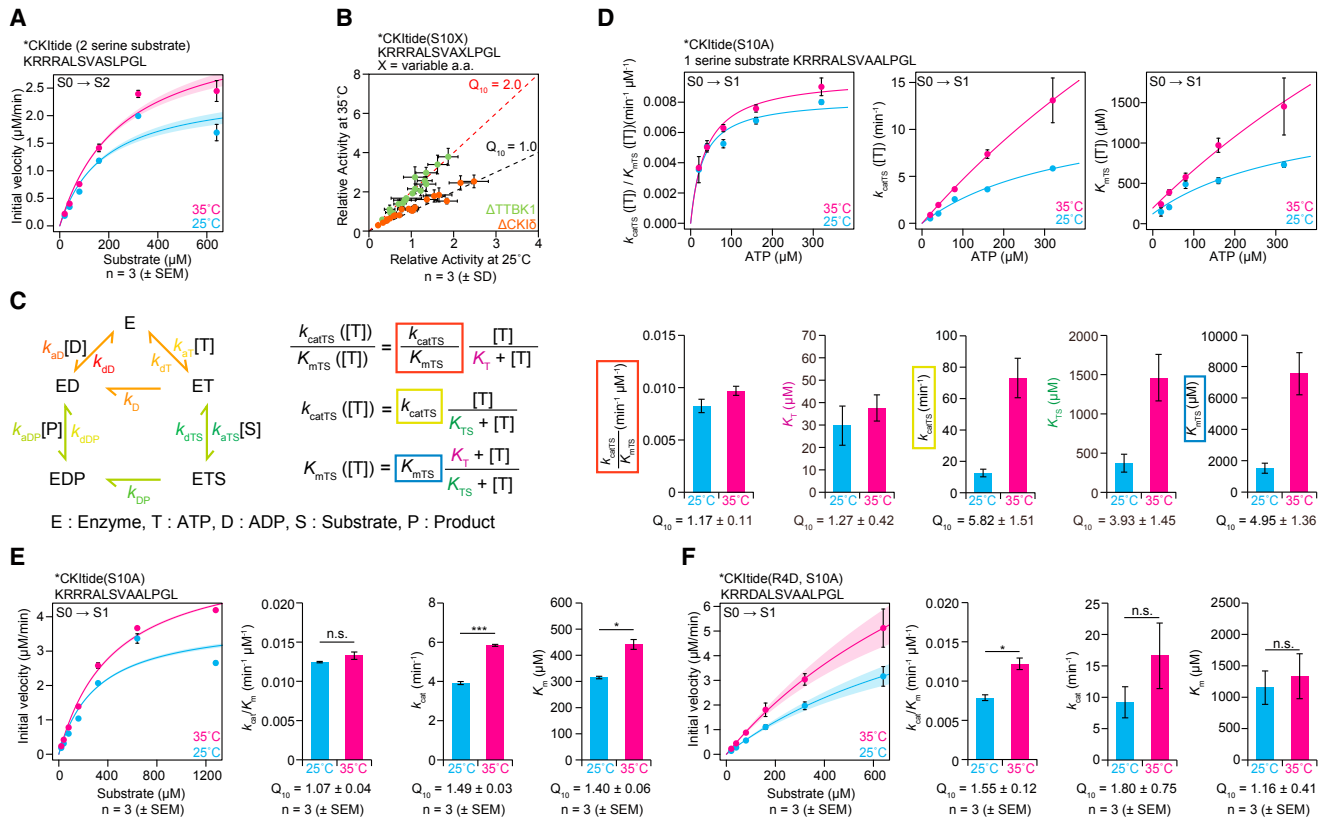


Figure 1. Temperature-Sensitive Binding of a Substrate to an Enzyme Underlies the Temperature Compensation of CKI δ -Dependent Single-Serine Phosphorylation

(A) Substrate saturation curves of Δ CKI δ -dependent phosphorylation on a two-serine substrate *CKIide at 25°C and 35°C. (B) Temperature dependency of Δ CKI δ - or Δ TTBK1-dependent phosphorylation for a series of single-serine substrates, *CKIide(S10X). Activities at 25°C for *CKIide were set as 1.0 in the relative activity. Data are mean \pm SD (n = 3). (C) A computational model of single-serine phosphorylation (left) and its kinetic parameters (right). (D) Temperature and ATP dependency of kinetic parameters (upper), and ATP-saturation kinetic parameters in (C) (lower) for Δ CKI δ -dependent phosphorylation on single-serine substrate *CKIide(S10A). Data are parameter \pm SE estimated from the nonlinear least-square fitting (n = 1). (E and F) Substrate saturation curves (left) and kinetic parameters (right) of Δ CKI δ -dependent phosphorylation on single-serine substrate *CKIide(S10A) (E) and *CKIide(R4D, S10A) (F) with 640 μ M ATP at 25°C and 35°C. For (A), (E), and (F), data are mean \pm SEM (n = 3); *p < 0.05, ***p < 0.001, and n.s. (not significant); two-tailed Welch's t test. Solid line and shade represent mean \pm SEM of curves of Michaelis-Menten model with estimated parameters. See also Figure S1.

Temperature-Sensitive and ADP-Dependent Binding of a Product to an Enzyme Underlies the Temperature Compensation of CKI δ -Dependent Multi-site Phosphorylation

Multi-site phosphorylation after priming phosphorylation seems critical in mammalian circadian clock because we recently found that the multi-site phosphorylation in a clock protein, CRY1, worked as a molecular timer by additively contributing to the period determination of mammalian circadian clocks (Ode et al., 2017). Therefore, we investigated CKIide, which contains a phosphorylated serine. We found that the production rate of CKIide(2pS) decelerated only after 10 min (Figure S2A), which was in contrast to the almost constant production rate of CKIide(2pS) from *CKIide (Figure S1C). Although the observed non-linear behavior made it difficult to determine the accurate kinetic parameters, the phosphorylation of CKIide was also

temperature compensated, especially for higher substrate concentrations described by k_{cat} (Figure 2A).

Initial velocities of CKIide phosphorylation both at 35°C and 25°C were significantly decelerated by the addition of ADP or a mixture of ADP and CKIide(2pS) (Figures 2B, S2B, and S2C), suggesting the phosphorylation of CKIide could be inhibited by ADP and CKIide(2pS). Isothermal titration calorimetry (ITC) revealed that Δ CKI δ and ADP form a stable binary complex with temperature-insensitive affinity (Figure S2D). Interestingly, the ADP-dependent binding of CKIide(2pS) to Δ CKI δ was strengthened for higher temperature (Figure 2C). In addition, the binding was exothermic, and enthalpically and entropically favored (Figure 2C).

Since the binding of a product to an enzyme is the first step toward a reverse reaction, we hypothesized that the high affinity of CKIide(2pS) to Δ CKI δ may result in the reverse reaction (dephosphorylation) of CKIide(2pS) by Δ CKI δ . To verify this

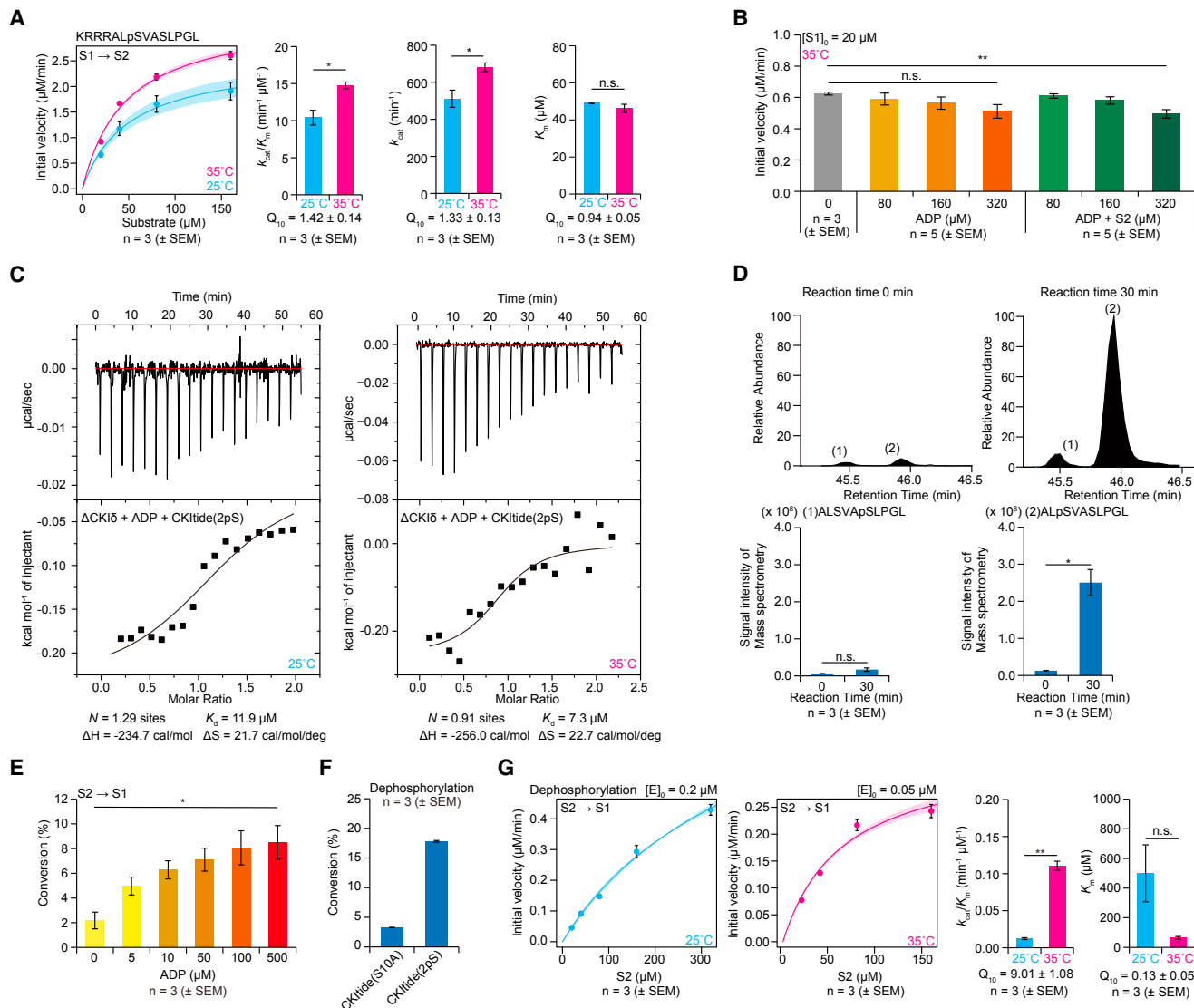


Figure 2. Temperature-Sensitive and ADP-Dependent Binding of a Product to an Enzyme Underlies the Temperature Compensation of CKIδ-Dependent Multi-site Phosphorylation

(A) Substrate saturation curves (left) and kinetic parameters (right) of phosphorylation on a single-phosphoserine substrate CKItide at 25°C and 35°C.

(B) Initial velocities of CKItide phosphorylation at 35°C with initial ADP or mixture of ADP and CKItide(2pS).

(C) ITC assay for the binding of CKItide(2pS) to ΔCKIδ in the presence of ADP at 25°C (left) and 35°C (right).

(D) Mass spectrometry for dephosphorylated peptides produced by ΔCKIδ from CKItide(2pS) in the presence of ADP.

(E) ADP concentration dependency of dephosphorylation activity by ΔCKIδ on CKItide(2pS).

(F) Substrate specificity of ADP-dependent dephosphorylation activity by ΔCKIδ.

(G) Substrate saturation curves (left) and kinetic parameters (right) of ΔCKIδ-dependent dephosphorylation on a CKItide(2pS) at 25°C and 35°C.

For (A), (B), and (D)–(G), data are mean ± SEM ($n = 5$ for B with ADP or ADP + S2 and $n = 3$ otherwise); * $p < 0.05$, ** $p < 0.01$, and n.s. (not significant); two-tailed Welch's t test. For (A) and (G), solid line and shade represent mean ± SEM of curves of Michaelis-Menten model with estimated parameters. See also Figure S2.

hypothesis, we incubated double-phosphorylated CKItide(2pS) in the presence of 1 mM ADP and then measured the state of the peptide by mass spectrometry. We noted that a single-phosphorylated pS-X-X-S product was specifically yielded (Figure 2D). In addition, the dephosphorylation was significantly facilitated by an ADP concentration (Figure 2E), much more favorable in CKItide(2pS) compared to CKItide(S10A) (KRRRALpSVAALPGL) (Figure 2F), and markedly enhanced by

the increase of temperature (Figure S2E). According to k_{cat}/K_m , the observed dephosphorylation was highly temperature sensitive (Figure 2G). In particular, K_m values indicate that an affinity of CKItide(2pS) to ΔCKIδ-ADP at 35°C is higher than that at 25°C, which is consistent with the ITC assay (Figure 2C). Therefore, temperature-compensated phosphorylation of CKItide might be explained by the balance between thermal acceleration of phosphorylation and thermal retardation of ΔCKIδ turnover

multi-site phosphorylation from S0 to S2 at 35°C. The perturbation of k_{aTS0} , k_{dTTS0} , k_{DS1} , and k_{dDS1} , all of which related to S0 to S1 reaction, affected the concentration of S2 (Figure 3B), suggesting the rate-limiting step in this multi-site phosphorylation would be priming phosphorylation from S0 to S1. Consistent with the initial crude analysis of experimental data (Figure 1E), k_{cat}/K_m for the priming phosphorylation (Figure 3C) was temperature compensated, whereas k_{cat}/K_m for other reactions such as ATPase activity (Figure S4A) or dephosphorylation from S2 to S1 (Figure S4B) was temperature sensitive. The perturbation of association (k_{aTS0}) and dissociation (k_{dTTS0}) rate between substrate S0 and ATP-bound enzyme (ET) strongly affected Q_{10} of k_{cat}/K_m (Figure 3C). These results imply that temperature-sensitive substrate-binding mechanism (weaker at higher temperature) could effectively counteract temperature-sensitive enzyme activity (faster at higher temperature).

In order to understand the molecular mechanism underlying the observed temperature compensation in Δ CKI δ -dependent phosphorylation of CKI tide (Figure 2A), we next focused on the phosphorylation from S1 to S2 at 35°C. Compared with S0 to S2 (Figure 3B), the perturbation of various rate parameters affected the concentration of S2 for S1 to S2 (Figure S4C). We noted that k_{cat} for S1 to S2 (Figure 3D) was temperature compensated, which is consistent with the initial crude analysis of experimental data (Figure 2A). Interestingly, the perturbation of dissociation rate (k_{dDS2}) between product S2 and ADP-bound enzyme (ED) strongly affected Q_{10} of k_{cat} (Figure 3D). Furthermore, by slowing down k_{dDS2} (i.e., strengthen the affinity between S2 and ED), k_{cat} at 35°C decreased and lowered Q_{10} . In addition to the kinetic parameter, Q_{10} of mean time course of S2 concentration also decreased for higher substrate concentrations by slowing down k_{dDS2} (dashed lines in panel k_{dDS2} in Figure S4C). These results imply that the temperature-sensitive product-binding mechanism (stronger at higher temperature) could effectively counteract with the temperature-sensitive enzyme activity (faster at higher temperature). The detailed analysis revealed that the temperature-sensitive substrate-binding mechanism would be important for a priming phosphorylation, whereas the temperature-sensitive product-binding mechanism would be critical for the following phosphorylation.

Identification of a Chemical, ATA, that Inhibits ADP-Dependent Product Binding of CKI δ by Comprehensive Chemical Screening

If we could find specific chemicals competing with putative substrate- and product-binding processes, we could use such chemical inhibitors to identify putative substrate- and product-binding sites and further investigate the underlying molecular mechanisms. Previously, we have discovered several CKI δ inhibitors from LOPAC¹²⁸⁰ library, which would potentially antagonize the substrate-binding step (Isojima et al., 2009). However, temperature compensation of the mammalian circadian clock was still preserved even under high concentrations of such potent inhibitors. Therefore, we focused on chemicals competing with a stable complex formation between Δ CKI δ -ADP and product. Such chemicals were hypothesized to inhibit the dephosphorylation, and therefore

would work as a CKI δ agonist by acceleration of Δ CKI δ turnover in phosphorylation. Based on this hypothesis, we first screened 1,259 chemical compounds in LOPAC¹²⁸⁰ library for chemical inhibitors of dephosphorylation activity (Figure 4A). The chemical screening reliably identified 13 candidates, including known CKI δ kinase inhibitors such as SB 202190 and SP600125 (Bain et al., 2007) (Figures S5A and 4B). We evaluated the inhibitory specificity of dephosphorylation against phosphorylation among these chemicals and characterized aurintricarboxylic acid (ATA) as a dephosphorylation-specific inhibitor (Figures 4C and 4D). As we expected, ATA strongly inhibited dephosphorylation activity and inversely enhanced phosphorylation activity of Δ CKI δ in a dose-dependent manner (Figures 4E and 4F). Importantly, we found that ATA significantly changed Q_{10} of Δ CKI δ -dependent phosphorylation (Figure 4F), supporting the significant contribution of a stable product-binding process to temperature-compensated phosphorylation predicted by the computational model.

Identification of Putative ATA-Binding Site of CKI δ by In Silico Docking Simulation

According to ITC assay, ATA could bind to Δ CKI δ with a stoichiometry of approximately 2:1 (Figure 4G). High concentration of ATA could inhibit ATPase activity of Δ CKI δ in addition to an inhibition of dephosphorylation activity, implying an ATA molecule could bind to an ATP-binding site of Δ CKI δ (Figure S5B). To predict another ATA-binding site of Δ CKI δ , we searched putative druggable sites on Δ CKI δ -ATP complex, which were roughly divided into five binding regions (A to E) (Figure 4H). Among these putative ATA-binding sites, C5 site displayed the smallest binding-free energy (Figure 4I). The same binding site was also predicted by an ATA analog (NS-05199909), which also enhanced phosphorylation activity (Figures S5C–S5E). In these docking simulations, the carboxyl group of ATA and NS-05199909 was estimated to make hydrogen bonds to the guanidinium group of Arg178, the amino group of Lys130 and Lys224, and the amide backbone of Gly215 (Figures 4I and S5E).

Comprehensive Genetic Screening Identified K224D and K224E Mutants of CKI δ that Impaired ADP-Dependent Product Binding and Temperature Compensation of Multi-site Phosphorylation

Previously reported crystal structures of mammalian CKI δ have identified four binding sites of phosphate analogs (Long et al., 2012; Longenecker et al., 1996) (Figure 5A). Combined with the prediction of ATA-binding site, R178 and K224 residues were found to be the most prominent candidates for mediating enzyme-phosphopeptide binding (Figure 5B).

R178C mutant of CKI δ , which is well known as *tau* mutant (Lowrey et al., 2000), shortens the circadian period of mammalian circadian clocks by destabilizing PER protein (Meng et al., 2008). Although *tau* mutant in a Syrian hamster affected temperature compensation in the circadian period of peripheral clocks (Tosini and Menaker, 1998), the mouse *tau* mutant (Meng et al., 2008) had an intact temperature-compensated circadian period in vivo and temperature-compensated phosphorylation of β TrCP-peptide in vitro (Isojima et al., 2009)

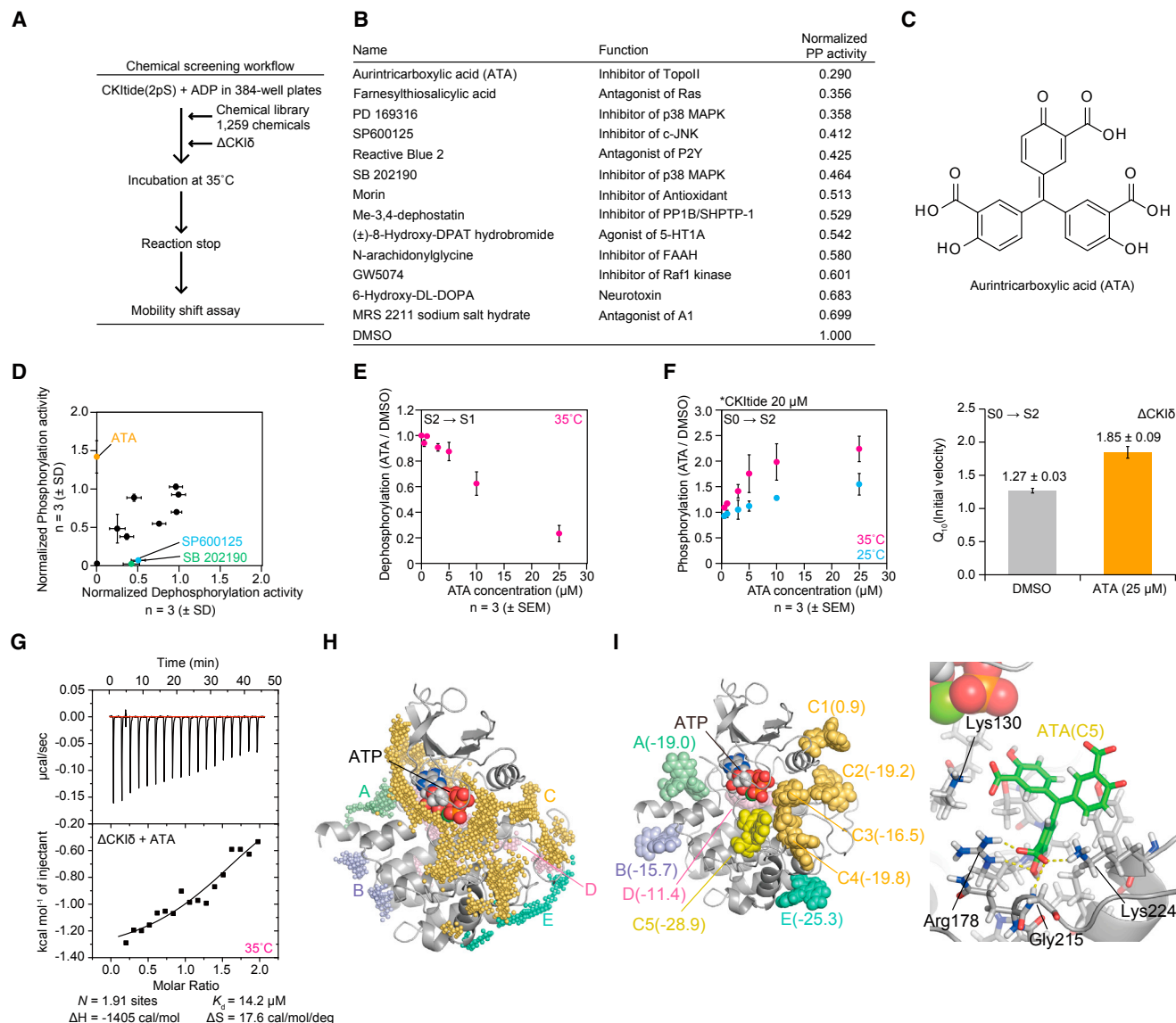


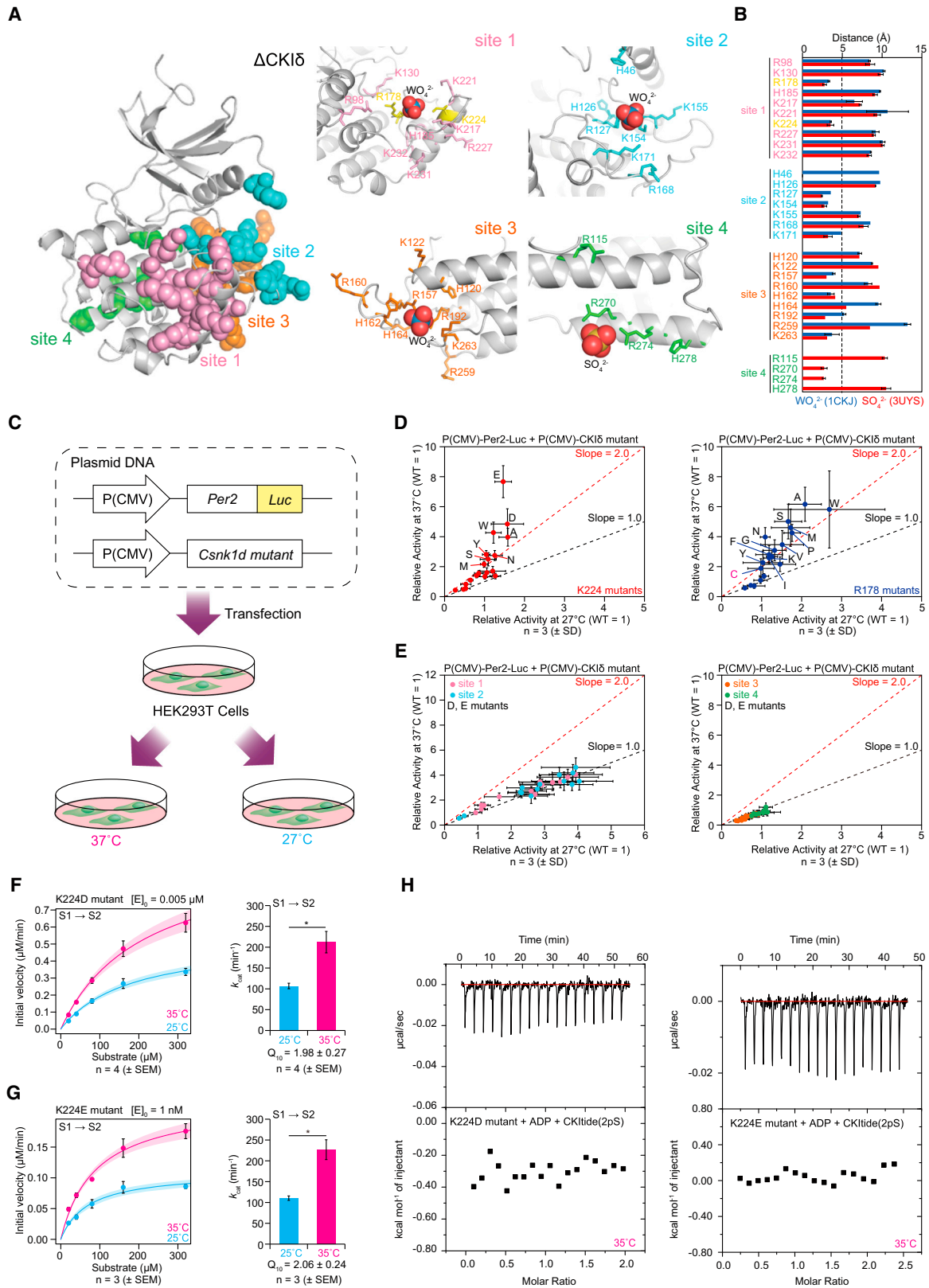
Figure 4. Identification of ATA that Inhibits ADP-Dependent Product Binding of CKI δ by Comprehensive Chemical Screening and Putative ATA-Binding Site of CKI δ by In Silico Docking Simulation

- (A) The workflow of the chemical inhibitor screening against Δ CKI δ -dependent dephosphorylation activity.
- (B) The first chemical screening identified 13 candidates (over 3 SD).
- (C) Chemical structure of ATA.
- (D) The second chemical screening to evaluate the specificity of chemical inhibitors to dephosphorylation activity against phosphorylation activity, which characterized ATA as a dephosphorylation-specific inhibitor. Data are mean \pm SD (n = 3).
- (E) Δ CKI δ -dependent dephosphorylation on a double-phosphorylated CKItide(2pS) was inhibited by ATA in a dose-dependent manner. Data are mean \pm SEM (n = 3).
- (F) Temperature and ATA concentration dependency of Δ CKI δ -dependent phosphorylation on *CKItide. Data are mean \pm SEM (n = 3).
- (G) ITC assay for the binding of ATA to Δ CKI δ at 35°C.
- (H) Putative druggable sites on Δ CKI δ -ATP complex identified by SiteMap program, which were roughly divided into five binding regions (A to E).
- (I) Putative ATA binding sites identified by in silico docking simulation. The binding-free energy (kcal/mol) was indicated in parentheses (left). The detailed structure of putative ATA-binding site C5 with the lowest binding-free energy was indicated in the right panel. See also Figure S5.

despite a significant acceleration of circadian period (Meng et al., 2008) and phosphorylation reaction (Isojima et al., 2009). Thus, there remains a discrepancy between the relationship of phosphorylation-dependent period acceleration by the

tau mutation to temperature compensation in the mammalian circadian clock.

We examined a series of CKI δ mutants of K224 as well as R178 for their effect on temperature dependency of



(legend on next page)

CKI δ -dependent phosphorylation measured by the stability of the PER2::LUC protein in HEK293T cells, which do not harbor functional circadian oscillators (Isojima et al., 2009) (Figure 5C). A number of K224 and R178 mutants significantly promoted the degradation of PER2::LUC protein in a temperature-dependent manner (Figure 5D); however, these mutations did not alter temperature dependency of the stability of the LUC protein alone (Figures S6A and S6B). Interestingly, the charge-deleted R178 mutants significantly altered temperature dependency of CKI δ -dependent phosphorylation measured by the stability of the PER2::LUC protein (Figure 5D). The charge-inversed K224 mutants (K224D/E) also remarkably changed temperature dependency (Figure 5D). On the other hand, temperature dependency was not altered by D/E mutations of all the other candidate residues in four sites (Figures 5B, 5E, S6A, and S6C), highlighting K224 as a unique residue. As a negative control, we selected H185, which was also a basic residue located in site 1, but did not directly interact with phosphate analogs (Figure 5B) or ATA (Figure 4I). Then, we confirmed that all H185 mutants did not significantly promote the degradation of PER2::LUC or LUC proteins in a temperature-dependent manner (Figures S6D and S6E).

Since the charge inversion of K224 markedly facilitated CKI δ -dependent phosphorylation at higher temperature when measured by the stability of the PER2::LUC protein (Figure 5D), we hypothesized that K224D/E mutants might fail to counteract the activated phosphorylation activity at higher temperature due to the unstable enzyme-phosphopeptide complex formation. To verify this hypothesis, we investigated the phosphorylation activity of K224D/E mutants against CKI δ tide. As expected, both mutants exhibited remarkably accelerated initial velocities at higher temperature, and also demonstrated temperature dependency for k_{cat} (Figures 5F and 5G) and k_{cat}/K_m (Figures S6F and S6G) in spite of temperature-insensitive K_m (Figures S6F and S6G). In the ITC assay, we could not detect any signals for the binding of CKI δ tide(2pS) to both mutants with ADP (Figure 5H). These results suggested that K224D/E mutants of CKI δ impair ADP-dependent product binding, probably by inducing phosphopeptide release via electrostatic repulsion. These results also confirmed that ADP-dependent product binding was critical in the temperature compensation of CKI δ -dependent multi-site phosphorylation.

K224D Mutation Remarkably Shortens Behavioral Circadian Rhythm in Mammalian Circadian Clocks

Since K224D/E mutants of CKI δ exhibited more than four times greater degradation activity of PER2 protein at higher temperature compared to wild-type CKI δ (Figure 5D), circadian periods of these mutant mice would be expected to be shortened as was observed in that of CKI ϵ (*tau*) mutant mice (Meng et al., 2008). To investigate in vivo significance of K224 mutants, we generated embryonic stem cell-derived mice (ESC mice) of these mutants (Figure S7A; STAR Methods) (Ode et al., 2017). Although K224E knockin mice failed to be created, wild-type CKI δ and K224D knockin mice (named WT-KI and K224D-KI mice, respectively) were successfully generated. We then analyzed the behavioral circadian rhythms of WT-KI and K224D-KI mice by monitoring their locomotor activity in the light-dark (LD) cycle, constant light (LL), or constant darkness (DD) conditions (Figures 6A, S7B, and S7C). Interestingly, K224D-KI mice showed markedly shorter circadian period (19.6 ± 1.2 hr) than WT-KI mice (23.7 ± 0.1 hr) in DD condition while no significant circadian period difference was observed in LD condition (Figures 6A and S7D). The strikingly shortened circadian period was comparable to that of CKI ϵ (*tau*) mutant mice (20.0 ± 0.1 hr) (Meng et al., 2008). In addition, altered behavioral circadian rhythms of K224D-KI mice in DD condition were adjusted by second LD cycles, and circadian period length of K224D-KI mice in LL condition was again shorter than that of WT-KI mice (Figure S7E).

K224D Mutation Significantly Changed the Temperature Dependency of Circadian Rhythm of SCN in Mammalian Circadian Clocks

It is difficult to evaluate how K224D mutation of CKI δ contributes to temperature dependency of circadian rhythms in organisms because of the homeostasis of body temperature in warm-blooded mammals. Thus, we instead investigated temperature dependency of circadian rhythms in suprachiasmatic nucleus (SCN). To record endogenous circadian rhythms of SCN slices, WT-KI or K224D-KI mice were mated with PER2::Luciferase (PER2::LUC) protein-fused reporter mice by in vitro fertilization (Yoo et al., 2004). Time course of luciferase activity in each long-term cultured organotypic SCN slice was monitored by photomultiplier tubes (PMTs) under different temperature

Figure 5. Comprehensive Genetic Screening Identified K224D and K224E Mutants of CKI δ that Impaired ADP-Dependent Product Binding and Temperature Compensation of Multi-site Phosphorylation

- (A) Overview (left) and close-up views (right) of four binding sites of phosphate analogs such as tungstate and sulfate ions.
 (B) Minimum distance between phosphate analogs and basic amino acids (H, R, and K). Data are mean \pm SD, whose sample n is the number of chains for specified site and PDB ID.
 (C) Workflow of the dual-luciferase assay to examine a series of CKI δ mutants for their effect on temperature dependency of phosphorylation measured by the stability of the PER2::LUC protein in HEK293T cells.
 (D) K224 and R178 mutations significantly promoted the degradation of PER2::LUC protein in a temperature-dependent manner.
 (E) The aspartate or glutamate mutation of all other candidate residues in four sites did not promote the degradation of PER2::LUC protein in a temperature-dependent manner.
 For (D) and (E), data are mean \pm SD ($n = 3$).
 (F and G) Temperature and substrate concentration dependency of the phosphorylation activity on a single-phosphorylated CKI δ tide by (F) K224D and (G) K224E mutants. Data are mean \pm SEM (F, $n = 4$; G, $n = 3$); * $p < 0.05$; two-tailed Welch's t test. Solid line and shade represent mean \pm SEM of curves of Michaelis-Menten model with estimated parameters.
 (H) ITC assay for the binding of CKI δ tide(2pS) to K224D (left) and K224E (right) mutants in the presence of ADP.
 See also Figure S6.

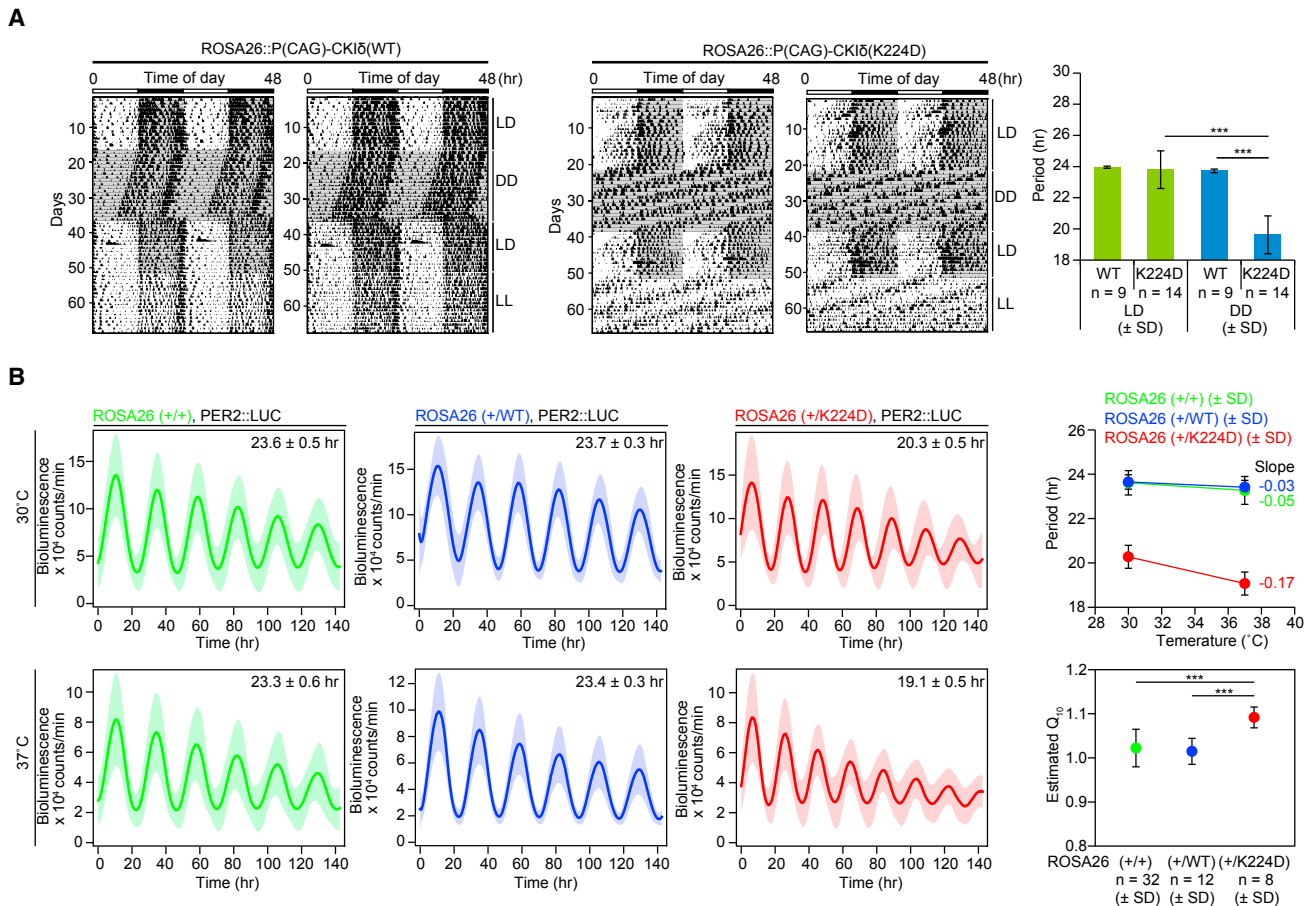


Figure 6. K224D Mutation of CKI δ Remarkably Shortened Behavioral Circadian Rhythm and Significantly Changed the Temperature Dependency of Circadian Rhythm of SCN in Mammalian Circadian Clocks

(A) Locomotor activity of wild-type CKI δ knockin mice (WT-KI mice; left) and K224D mutant knockin mice (K224D-KI mice; middle) in the light-dark (LD) cycle, constant light (LL), or constant darkness (DD) conditions. Behavioral period in LD and DD conditions (right). Data are mean \pm SD ($n = 9$ for WT and $n = 14$ for K224D); *** $p < 0.001$; two-tailed Welch's t test.

(B) Temperature dependency of circadian rhythms of *Per2^{Luc}* SCN of the control mice without knockin (first column), WT-KI mice (second column), and K224D-KI mice (third column); the circadian period (top right); and the estimated Q_{10} (bottom right). The shaded band represents 1 SD from the mean. Data are mean \pm SD ($n = 32$ for control mice without knockin, $n = 12$ for WT-KI mice, and $n = 8$ for K224D-KI mice); *** $p < 0.001$; two-tailed Welch's t test.

See also [Figure S7](#) and [Movie S1](#).

conditions over 6 days ([Figure 6B](#); [Movie S1](#)). The circadian period and the robustness to temperature perturbation of WT-KI slices were quite similar to those of slices without the knockin ([Figures 6B](#) and [S7F](#)). On the other hand, K224D-KI slices displayed remarkably shorter circadian periods compared with WT-KI slices, closely matching with behavioral circadian rhythms in organisms. Furthermore, circadian period of K224D-KI slices was significantly shortened by temperature elevation; therefore, the estimated Q_{10} value was also significantly increased ([Figure 6B](#)). These results highlighted the importance of K224 residue in circadian period and its temperature dependency of mammalian circadian clock in the SCN.

Temperature Compensation of Multi-site Phosphorylation Is Evolutionary Conserved in CKI family

A budding yeast demonstrated temperature-compensated ultradian metabolic cycles ([Mellor, 2016](#)). Importantly,

CKI has also been reported in the period determination of ultradian metabolic cycles ([Causton et al., 2015](#)). We note that amino acid residues including K224 were highly conserved in the CKI family of budding and fission yeasts ([Figures 7A](#) and [S8A](#)). Interestingly, CKI homolog 1 ([Figure S8B](#))-dependent phosphorylation of γ CKItide is temperature compensated ([Figures 7B](#) and [S8C](#)). In addition, ATA also increased the initial velocity of this multi-site phosphorylation in a dose-dependent manner ([Figure S8D](#)). Moreover, ITC assay revealed CKI homolog 1 exhibited a remarkable affinity to CKItide(2pS) with ADP ([Figure 7C](#)). Structural alignment of newly solved budding yeast CKI homolog 1 ([Table 1](#)) with mammalian CKI δ displayed strong structural conservation ([Figures S8E](#) and [S8F](#)). Based on these results, we concluded that temperature-compensated phosphorylation was evolutionarily conserved in budding yeast CKI homolog 1.

A CKI-Specific Domain around K224 Can Provide an Evolutionally Conserved Structural Basis of Temperature Sensitivity of Substrate and Product Binding

Multiple sequence alignment revealed that TTBK1 and TTBK2 lacked the CKI-specific domain around the residue K224 (Figure 7A). The multiple structural alignment further confirmed that TTBK1 was also deficient in K217 to Q223 regions of CKI δ (Figure 7D, green shaded region), although it is difficult to judge the exact conservation for K224 of CKI δ because of the existence of K243 or K245 in TTBK1. Since TTBK1 doesn't preserve the temperature compensation, we speculated that the CKI-specific domain around K224 and K224 itself, which is critical for second-serine phosphorylation (Figure 5), might provide a structural basis of the temperature sensitivity in the substrate and product binding, and hence temperature-compensated phosphorylation.

To gain structural insights into the temperature sensitivity inherent in CKI δ , we performed molecular dynamics (MD) simulations, which predicted that K217-Q223 around α F helix was highly fluctuated (Figures 7E, S9A, and S9B; Movies S2 and S3). In addition, B factors (Figure 7F) of the newly solved Δ CKI δ -ADP complex (Table 1; Figure S9C) and previously determined apo- Δ CKI δ structure (Longenecker et al., 1996) (Figure S8F) showed higher fluctuations in K217-Q223. Furthermore, B factors of apo-CKI homolog 1 structure indicate higher fluctuations in the CKI-specific domain (K279-Q285) (Figure S8F), indicating that higher fluctuations in the CKI-specific domain were evolutionarily conserved from yeast to mammals. These results suggested that a CKI-specific domain (K217-Q223) around K224 displayed large fluctuations, which could provide an evolutionally conserved structural basis of temperature sensitivity in substrate and product binding, and hence temperature-compensated multi-site phosphorylation.

A CKI-Specific Domain around K224 Can Be a Structural Basis of Temperature Compensation of CKI δ -Dependent Multi-site Phosphorylation

To identify critical interactions for the large fluctuations, we performed potential energy principal component analysis (PEPCA) (Koyama et al., 2008, 2011) (Figures S9D-S9I). For Δ CKI δ -ADP complex at 35°C and Δ CKI δ -ATP complex at 25°C, the first prin-

cipal components identified the large conformational change of α F helix including K224 away from the loop including R178 (Figure S9B), and the first eigenvector components highlighted critical interactions, which significantly changed their minimum distance (Figures S9D-S9G). As predicted, the alanine mutations on α F helix (i.e., I228 and K232) or on its spatially adjacent regions (i.e., E197 and Q214) significantly altered temperature dependency of CKI δ -dependent phosphorylation measured by the stability of the PER2::LUC protein (Figures 7G and S10A). Taken together, these results were consistent with the hypothesis that a CKI-specific domain around K224 can be a structural basis of temperature compensation of CKI δ -dependent multi-site phosphorylation.

A CKI-Specific Domain around K224 Can Confer Temperature Compensation on TTBK1, Which Shows Temperature Sensitivity in the First- and Second-Serine Phosphorylation

In order to verify whether the CKI-specific domain around K224 residue was sufficient for temperature compensation, we next attempted to reconstitute temperature compensation in vitro by introducing the CKI-specific domain into TTBK1, which shows temperature-sensitive phosphorylation for a two-serine and for a variety of single-serine substrates (Figure 1B). To our surprise, with rationally designed TTBK1 mutant (rMT, reconstituted mutant type; Figures 7H and S10B; STAR Methods), the phosphorylation of a two-serine substrate *CKItide (Figure 7I) and a single-serine substrate *CKItide(S10A) (Figure S10D) for a lower substrate concentration (20 μ M) was temperature compensated, whereas the phosphorylation by wild-type TTBK1 was temperature sensitive. Furthermore, for a higher substrate concentration (320 μ M), when we utilized two-serine substrate *CKItide (Figure S10C), single-serine substrate *CKItide(S10A) (Figure S10D), and single-phosphorylated CKItide (Figure 7J), TTBK1 rMT significantly reduced the temperature sensitivity of the phosphorylation compared to that of wild-type TTBK1. These results, together with the results shown in Figure 5, thus demonstrated that the Q214-K224 domain could work as a regulatory module of temperature compensation in the CKI family, probably mediated through temperature-sensitive substrate- and/or product-binding mechanisms.

Figure 7. A Conserved CKI-Specific Domain around K224 Can Provide a Structural Basis for Temperature-Sensitive Substrate and Product Binding, and Confer Temperature Compensation to a Temperature-Sensitive Kinase

- (A) Multiple sequence alignment among CKI and TTBK family.
 (B) Temperature dependency of CKI homolog 1-dependent phosphorylation on a two-serine substrate.
 (C) ITC assay for the binding of CKItide(2pS) to CKI homolog 1 in the presence of ADP.
 (D) Multiple structural alignments among CKI, TTBK1, VRK2, AurA, and CDK2.
 (E) RMSF for each C $_{\alpha}$ atom of MD simulation of Δ CKI δ -ATP and Δ CKI δ -ADP complexes.
 (F) B factor for each C $_{\alpha}$ atom of X-ray crystal structure analysis of Δ CKI δ -ADP complex.
 (G) Dual-luciferase assay to examine a series of CKI δ mutants for their effect on temperature dependency phosphorylation measured by the stability of the PER2::LUC protein in HEK293T cells. Data are mean \pm SD (n = 3).
 (H) TTBK1 mutant (rMT) was rationally designed by replacing five amino acid residues (R240-D244) of TTBK1 with eleven amino acid residues (Q214-K224) of CKI δ (pink), which contained the CKI-specific domain (green) (upper). The structural alignment of TTBK1 (blue) and CKI δ (green) (lower).
 (I) Temperature dependency of phosphorylation on a two-serine substrate by TTBK1 (WT) and TTBK1 mutant (rMT).
 (J) Temperature dependency of phosphorylation on a single-phosphorylated CKItide by TTBK1 (WT) and TTBK1 mutant (rMT).
 For (B), (I), and (J), data are mean \pm SEM (B, n = 3; I, n = 5; J, n = 3); *p < 0.05, ***p < 0.001, and n.s. (not significant); two-tailed Welch's t test. See also Figures S8-S10, Table 1, and Movies S2 and S3.

Table 1. Data Collection and Refinement Statistics

Dataset	CKI δ	CKI Homolog 1
Data Collection and Processing		
X-ray source	BL26B2, SPring-8	BL26B2, SPring-8
Temperature (K)	100	100
Space group	$P2_1$	$P2_1$
Cell dimensions: a (Å)	50.14	45.50
Cell dimensions: b (Å)	130.35	97.92
Cell dimensions: c (Å)	53.18	84.74
Cell dimensions: β (°)	115.45	93.89
Wavelength (Å)	1.000	1.000
Resolution range (Å)	50.0–2.00 (2.03–2.00) ^a	50.0–1.80 (1.83–1.80)
No. of unique reflections	41687	67599
Multiplicity	3.8 (3.7)	3.7 (3.2)
Completeness (%)	100.0 (99.9)	98.4 (86.6)
R_{sym} (%) ^b	8.2 (59.6)	4.8 (57.5)
$I/\sigma(I)$	15.3 (2.2)	27.0 (2.0)
Model Refinement		
Resolution range (Å)	50–2.00 (2.04–2.00)	50–1.80 (1.85–1.80)
No. of reflections, working set	41,629	65,536
No. of reflections, test set	2,047	1,951
$R_{\text{work}}/R_{\text{free}}$ (%) ^c	18.72/24.16	15.97/20.85
RMSD for bond length (Å)	0.014	0.008
RMSD for bond angles (°)	1.667	1.226
No. of non-H atoms: protein	4671	4759
No. of non-H atoms: water molecules	311	315
No. of non-H atoms: ligand	54	–
Mean B factors (Å ²): protein	36.55	43.14
Mean B factors (Å ²): water molecule	39.76	46.62
Mean B factors (Å ²): ligand	25.64	–
Residues in the Ramachandran plot: most favored (%)	97.4	97.1
Residues in the Ramachandran plot: allowed (%)	2.6	2.9
Residues in the Ramachandran plot: outliers (%)	0	0
PDB entry	PDB: 5X17	PDB: 5X18

RMSD, root-mean-square deviation.

^aValues in parentheses are for the outermost resolution shell.

^b $R_{\text{sym}} = (\sum_h \sum_i |I_{hi} - \langle I_h \rangle|) / (\sum_h \sum_i I_{hi})$, where h indicates unique reflection indices, and i indicates symmetry equivalent indices.

^c $R_{\text{work}} = \sum |F_{\text{obs}} - F_{\text{calc}}| / \sum F_{\text{obs}}$ for all reflections; R_{free} was calculated by using randomly selected reflections.

DISCUSSION

In the current study, we showed two mechanisms, (1) “lower substrate affinity to CKI δ -ATP complex at higher temperature” and

(2) “higher product affinity to CKI δ -ADP complex at higher temperature,” underlie the temperature compensation. PER proteins function in a large complex (PER complex) over 1 MDa, including CRY and other proteins (Kim et al., 2015). Furthermore, PER2 was shown to be phosphorylated on many sites by CKI δ (Schlosser et al., 2005). Here, we briefly discuss how two mechanisms can contribute to the temperature compensation of the multi-site phosphorylation of PER proteins in PER complex. If the priming phosphorylation of PER is the rate-limiting step in PER complex, we expect that mechanism (1) will be important to keep the temperature compensation (Figures 3B and 3C). On the other hand, if the multi-site phosphorylation of PER induces the tight binding between CKI and PER complex, then the rate-limiting step becomes the dissociation of CKI from PER complex. In this case, we expect that mechanism (2) can contribute to the temperature compensation. In reality, we showed that K224D mutation increased the temperature dependency of k_{cat} (Figure 5F) and the period in the SCN slice experiment (Figure 6B). Since K224 is an important residue to recognize a phosphate (analog) in site 1 (Figures 5A, 5B, and 5H), this implies mechanism (2) is more important for the temperature compensation in PER complex. In another respect, it was proposed that the phosphorylation of two sites in PER could contribute differently to the temperature compensation (Zhou et al., 2015). One CKI target unprimed site is β TrCP binding site and the other primed site by unknown kinase is FASPS mutant site (Isojima et al., 2009). Since two regions are different in the priming conditions, mechanisms (1) and (2) may be able to contribute to the two sites in a different way to realize the temperature compensation in PER complex.

The observed temperature dependency in substrate binding and product release is intrinsically encoded in CKI δ structure, which is supported by temperature-sensitive fluctuations of a CKI-specific domain around K224 revealed by MD simulations (Figures 7E and S9A), and the large fluctuations observed by X-ray crystallography (Figures 7F and S8F). Furthermore, it is supported by the impaired temperature dependency of CKI δ -dependent phosphorylation measured by PER2::LUC degradation in a series of mutations on a CKI-specific domain or on its spatially adjacent regions (Figures 5 and 7). Finally, we successfully conferred temperature-compensated phosphorylation on temperature-sensitive TTBK1 by replacing the original R240-D244 residues of TTBK1 with Q214-K224 residues of CKI δ . Interestingly, TTBK1 (rMT) significantly reduced temperature sensitivity in phosphorylation of two-serine substrate *CKI δ tide (Figures 7I and S10C), single-serine substrate *CKI δ tide(S10A) (Figure S10D), and a single-phosphorylated peptide CKI δ tide (Figure 7J). Therefore, incorporated residues in TTBK1 (rMT) would work as a regulatory module of temperature-dependent substrate- and/or product-binding mechanisms essential for temperature compensation in the CKI family.

STAR★METHODS

Detailed methods are provided in the online version of this paper and include the following:

- KEY RESOURCES TABLE
- CONTACT FOR REAGENT AND RESOURCE SHARING

- **EXPERIMENTAL MODEL AND SUBJECT DETAILS**

- Transfection and Luciferase Assay
- Mice Production

- **METHOD DETAILS**

- Protein Expression for Kinase Assay
- Mobility Shift Assay
- Substrate Screening
- Initial Velocity Analysis
- ATP-dependent Kinase Assay
- ATPase Activity Measurements
- Product Inhibition Assay for Kinase Activity
- ITC Assay
- Dephosphorylation Assay
- Mass Spectrometry for Dephosphorylation Assay
- Bayes Estimation of Rate Parameters
- Rate Equation for the ATPase Activity
- Rate Equation for the Phosphorylation Activity
- Chemical Screening
- Docking Simulation of ATA and Its Derivative
- Basic Residues around Phosphate Analogs
- Plasmid Construction
- Cultivation of Mouse ES Cells
- Targeting into Rosa26 Locus
- Locomotor Analysis of CK1 δ Mutant Mice
- Luminescence Monitoring of SCN Slice
- Multiple Sequence Alignment
- Protein Preparation for X-ray Crystallography
- Crystallization and Structure Determination
- Multiple Structural Alignment
- Molecular Dynamics Simulations
- Alanine Scanning of CK1 δ around K224
- Design of a Temperature-compensated Kinase

- **QUANTIFICATION AND STATISTICAL ANALYSIS**

- **DATA AND SOFTWARE AVAILABILITY**

SUPPLEMENTAL INFORMATION

Supplemental Information includes ten figures, one table, and three movies and can be found with this article online at <http://dx.doi.org/10.1016/j.molcel.2017.08.009>.

AUTHOR CONTRIBUTIONS

H.R.U. and Y.S. designed the study. Y.S. performed and analyzed most of the biochemical experiments. Y.M.K. constructed the computational model and performed Bayes estimation and MD simulation. Y.S. and H.F. performed chemical screening. T.H. performed chemical-enzyme docking simulation. Y.S., M.U.-T., and H.U. made the constructs. M.U.-T. performed dual-luciferase assay. M.U.-T. and H.U. generated CKI-KI mouse. R.G.Y. performed SCN slice experiment. Y.S. analyzed behavioral data. M.K. and T.U. performed X-ray crystal structure analysis. Y.S. and Y.M.K. designed synthetic temperature-compensated enzyme. H.R.U., K.T., Y.S., and Y.M.K. wrote the manuscript. All authors discussed the results and commented on the manuscript.

ACKNOWLEDGMENTS

We thank past and present lab members at RIKEN QBiC, and University of Tokyo, in particular M. Nakajima, M. Ishida, R. Narumi, C. Imai, J. Yoshida-Garcon, S. Morino, A. Kishimoto, J. Hara, S. Fujino, A. Nishiyama, K. Yamanaka, K. Sumiyama, and Y. Wada, for their kind help in preparing the materials and supporting experiments; LARGE, RIKEN CLST for housing the mice; K.L. Ode for

valuable comments; and H. Niwa (RIKEN CLST) and M. Yamamoto and G. Ueno (RIKEN SPring-8 Center) for assistance with X-ray data collection. We thank A. Millius and K. Wilkins for critical reading and valuable comments on the manuscript. We thank Y. Okada for valuable discussions. We thank M. Taiji, M. Takeichi, S. Hayashi, and F. Matsuzaki for encouraging the current study. We thank the RIKEN Integrated Cluster of Clusters (RICC). This work was supported by a grant from AMED-CREST (AMED/MEXT, H.R.U.), CREST (JST/MEXT, H.R.U.), Brain/MINDS (AMED/MEXT, H.R.U.), and Basic Science and Platform Technology Program for Innovative Biological Medicine (AMED/MEXT, H.R.U.); a Grant-in-Aid for Scientific Research (S) (JSPS KAKENHI Grant Number 25221004, H.R.U.); a Grant-in-Aid for Scientific Research on Innovative Areas (JSPS KAKENHI Grant Number 23115006, H.R.U.); a Grant-in-Aid for challenging Exploratory Research (JSPS KAKENHI Grant Number 16K15124, K.T.); the strategic programs for R&D (President's Discretionary Fund) of RIKEN (to H.R.U.); an intramural Grant-in-Aid from the RIKEN Quantitative Biology Center (to H.R.U.); Grants-in-Aid for Japan Society for the Promotion of Science (JSPS) Fellows 25-5989 (to Y.S.); and MEXT as "Priority Issue on Post-K computer" (Building Innovative Drug Discovery Infrastructure Through Functional Control of Biomolecular Systems) (hp160213) (to T.H.).

Received: May 12, 2017

Revised: July 4, 2017

Accepted: August 16, 2017

Published: September 7, 2017

REFERENCES

- Abe, T., Kiyonari, H., Shioi, G., Inoue, K., Nakao, K., Aizawa, S., and Fujimori, T. (2011). Establishment of conditional reporter mouse lines at ROSA26 locus for live cell imaging. *Genesis* **49**, 579–590.
- Adams, P.D., Afonine, P.V., Bunkóczy, G., Chen, V.B., Davis, I.W., Echols, N., Headd, J.J., Hung, L.W., Kapral, G.J., Grosse-Kunstleve, R.W., et al. (2010). PHENIX: a comprehensive Python-based system for macromolecular structure solution. *Acta Crystallogr. D Biol. Crystallogr.* **66**, 213–221.
- Bain, J., Plater, L., Elliott, M., Shpiro, N., Hastie, C.J., McLauchlan, H., Klevernic, I., Arthur, J.S., Alessi, D.R., and Cohen, P. (2007). The selectivity of protein kinase inhibitors: a further update. *Biochem. J.* **408**, 297–315.
- Barrett, R.K., and Takahashi, J.S. (1995). Temperature compensation and temperature entrainment of the chick pineal cell circadian clock. *J. Neurosci.* **15**, 5681–5692.
- Case, D.A., Darden, T.A., Cheatham, T.E., Simmerling, C.L., Wang, J., Duke, R.E., Luo, R., Crowley, M., Walker, R.C., Zhang, W., et al. (2008). AMBER 10 (San Francisco: University of California).
- Causton, H.C., Feeney, K.A., Ziegler, C.A., and O'Neill, J.S. (2015). Metabolic cycles in yeast share features conserved among circadian rhythms. *Curr. Biol.* **25**, 1056–1062.
- Cook, P., and Cleland, W.W. (2007). *Enzyme Kinetics and Mechanism* (Taylor & Francis Group).
- Doyle, E.L., Booher, N.J., Standage, D.S., Voytas, D.F., Brendel, V.P., Vandyk, J.K., and Bogdanove, A.J. (2012). TAL Effector-Nucleotide Targeter (TALE-NT) 2.0: tools for TAL effector design and target prediction. *Nucleic Acids Res.* **40**, W117–22.
- Dunlap, J.C., Loros, J.J., and DeCoursey, P.J. (2004). *Chronobiology: Biological Timekeeping* (Sinauer Associates).
- Emsley, P., Lohkamp, B., Scott, W.G., and Cowtan, K. (2010). Features and development of Coot. *Acta Crystallogr. D Biol. Crystallogr.* **66**, 486–501.
- Essmann, U., Perera, L., Berkowitz, M.L., Darden, T., Lee, H., and Pedersen, L.G. (1995). A smooth particle mesh Ewald method. *J. Chem. Phys.* **103**, 8577–8593.
- Flotow, H., and Roach, P.J. (1991). Role of acidic residues as substrate determinants for casein kinase I. *J. Biol. Chem.* **266**, 3724–3727.
- Friesner, R.A., Banks, J.L., Murphy, R.B., Halgren, T.A., Klicic, J.J., Mainz, D.T., Repasky, M.P., Knoll, E.H., Shelley, M., Perry, J.K., et al. (2004). Glide: a new approach for rapid, accurate docking and scoring. 1.

- Method and assessment of docking accuracy. *J. Med. Chem.* **47**, 1739–1749.
- Gallego, M., and Virshup, D.M. (2007). Post-translational modifications regulate the ticking of the circadian clock. *Nat. Rev. Mol. Cell Biol.* **8**, 139–148.
- Halgren, T. (2007). New method for fast and accurate binding-site identification and analysis. *Chem. Biol. Drug Des.* **69**, 146–148.
- Halgren, T.A. (2009). Identifying and characterizing binding sites and assessing druggability. *J. Chem. Inf. Model.* **49**, 377–389.
- Halgren, T.A., Murphy, R.B., Friesner, R.A., Beard, H.S., Frye, L.L., Pollard, W.T., and Banks, J.L. (2004). Glide: a new approach for rapid, accurate docking and scoring. 2. Enrichment factors in database screening. *J. Med. Chem.* **47**, 1750–1759.
- Hastings, J.W., and Sweeney, B.M. (1957). On the mechanism of temperature independence in a biological clock. *Proc. Natl. Acad. Sci. USA* **43**, 804–811.
- Hoguesch, J.B., and Ueda, H.R. (2011). Understanding systems-level properties: timely stories from the study of clocks. *Nat. Rev. Genet.* **12**, 407–416.
- Holm, L., and Rosenström, P. (2010). Dali server: conservation mapping in 3D. *Nucleic Acids Res.* **38**, W545–9.
- Hornak, V., Abel, R., Okur, A., Strockbine, B., Roitberg, A., and Simmerling, C. (2006). Comparison of multiple Amber force fields and development of improved protein backbone parameters. *Proteins* **65**, 712–725.
- Humphrey, W., Dalke, A., and Schulten, K. (1996). VMD: visual molecular dynamics. *J. Mol. Graph.* **14**, 33–38, 27–28.
- Isojima, Y., Nakajima, M., Ukai, H., Fujishima, H., Yamada, R.G., Masumoto, K.H., Kiuchi, R., Ishida, M., Ukai-Tadenuma, M., Minami, Y., et al. (2009). CK1epsilon/delta-dependent phosphorylation is a temperature-insensitive, period-determining process in the mammalian circadian clock. *Proc. Natl. Acad. Sci. USA* **106**, 15744–15749.
- Izumo, M., Johnson, C.H., and Yamazaki, S. (2003). Circadian gene expression in mammalian fibroblasts revealed by real-time luminescence reporting: temperature compensation and damping. *Proc. Natl. Acad. Sci. USA* **100**, 16089–16094.
- Kapust, R.B., Tózsér, J., Fox, J.D., Anderson, D.E., Cherry, S., Copeland, T.D., and Waugh, D.S. (2001). Tobacco etch virus protease: mechanism of autolysis and rational design of stable mutants with wild-type catalytic proficiency. *Protein Eng.* **14**, 993–1000.
- Kim, J.Y., Kwak, P.B., Gebert, M., Duong, H.A., and Weitz, C.J. (2015). Purification and analysis of PERIOD protein complexes of the mammalian circadian clock. *Methods Enzymol.* **551**, 197–210.
- Kiyonari, H., Kaneko, M., Abe, S., and Aizawa, S. (2010). Three inhibitors of FGF receptor, ERK, and GSK3 establishes germline-competent embryonic stem cells of C57BL/6N mouse strain with high efficiency and stability. *Genesis* **48**, 317–327.
- Kondo, T., Strayer, C.A., Kulkarni, R.D., Taylor, W., Ishiura, M., Golden, S.S., and Johnson, C.H. (1993). Circadian rhythms in prokaryotes: luciferase as a reporter of circadian gene expression in cyanobacteria. *Proc. Natl. Acad. Sci. USA* **90**, 5672–5676.
- Koyama, Y.M., Kobayashi, T.J., Tomoda, S., and Ueda, H.R. (2008). Perturbational formulation of principal component analysis in molecular dynamics simulation. *Phys. Rev. E Stat. Nonlin. Soft Matter Phys.* **78**, 046702.
- Koyama, Y.M., Kobayashi, T.J., and Ueda, H.R. (2011). Perturbation analyses of intermolecular interactions. *Phys. Rev. E Stat. Nonlin. Soft Matter Phys.* **84**, 026704.
- Lenhardt, R., and Sessler, D.I. (2006). Estimation of mean body temperature from mean skin and core temperature. *Anesthesiology* **105**, 1117–1121.
- Li, D.W., and Brüschweiler, R. (2010). NMR-based protein potentials. *Angew. Chem. Int. Ed. Engl.* **49**, 6778–6780.
- Lindorff-Larsen, K., Piana, S., Palmo, K., Maragakis, P., Klepeis, J.L., Dror, R.O., and Shaw, D.E. (2010). Improved side-chain torsion potentials for the Amber ff99SB protein force field. *Proteins* **78**, 1950–1958.
- Long, A., Zhao, H., and Huang, X. (2012). Structural basis for the interaction between casein kinase 1 delta and a potent and selective inhibitor. *J. Med. Chem.* **55**, 956–960.
- Longenecker, K.L., Roach, P.J., and Hurley, T.D. (1996). Three-dimensional structure of mammalian casein kinase I: molecular basis for phosphate recognition. *J. Mol. Biol.* **257**, 618–631.
- Lowrey, P.L., Shimomura, K., Antoch, M.P., Yamazaki, S., Zemenides, P.D., Ralph, M.R., Menaker, M., and Takahashi, J.S. (2000). Positional syntenic cloning and functional characterization of the mammalian circadian mutation tau. *Science* **288**, 483–492.
- Manning, G., Whyte, D.B., Martinez, R., Hunter, T., and Sudarsanam, S. (2002). The protein kinase complement of the human genome. *Science* **298**, 1912–1934.
- Meagher, K.L., Redman, L.T., and Carlson, H.A. (2003). Development of poly-phosphate parameters for use with the AMBER force field. *J. Comput. Chem.* **24**, 1016–1025.
- Mellor, J. (2016). The molecular basis of metabolic cycles and their relationship to circadian rhythms. *Nat. Struct. Mol. Biol.* **23**, 1035–1044.
- Meng, Q.J., Logunova, L., Maywood, E.S., Gallego, M., Lebiecki, J., Brown, T.M., Sládek, M., Semikhodskii, A.S., Glossop, N.R.J., Piggins, H.D., et al. (2008). Setting clock speed in mammals: the CK1 epsilon tau mutation in mice accelerates circadian pacemakers by selectively destabilizing PERIOD proteins. *Neuron* **58**, 78–88.
- Miller, J.C., Tan, S., Qiao, G., Barlow, K.A., Wang, J., Xia, D.F., Meng, X., Paschon, D.E., Leung, E., Hinkley, S.J., et al. (2011). A TALE nuclease architecture for efficient genome editing. *Nat. Biotechnol.* **29**, 143–148.
- Millius, A., and Ueda, H.R. (2017). Systems biology-derived discoveries of intrinsic clocks. *Front. Neurol.* **8**, 25.
- Murayama, Y., Mukaiyama, A., Imai, K., Onoue, Y., Tsunoda, A., Nohara, A., Ishida, T., Maéda, Y., Terauchi, K., Kondo, T., and Akiyama, S. (2011). Tracking and visualizing the circadian ticking of the cyanobacterial clock protein KaiC in solution. *EMBO J.* **30**, 68–78.
- Murshudov, G.N., Vagin, A.A., and Dodson, E.J. (1997). Refinement of macromolecular structures by the maximum-likelihood method. *Acta Crystallogr. D Biol. Crystallogr.* **53**, 240–255.
- Nakajima, M., Imai, K., Ito, H., Nishiwaki, T., Murayama, Y., Iwasaki, H., Oyama, T., and Kondo, T. (2005). Reconstitution of circadian oscillation of cyanobacterial KaiC phosphorylation in vitro. *Science* **308**, 414–415.
- Nakamura, W., Honma, S., Shirakawa, T., and Honma, K. (2002). Clock mutation lengthens the circadian period without damping rhythms in individual SCN neurons. *Nat. Neurosci.* **5**, 399–400.
- Narumi, R., Shimizu, Y., Ukai-Tadenuma, M., Ode, K.L., Kanda, G.N., Shinohara, Y., Sato, A., Matsumoto, K., and Ueda, H.R. (2016). Mass spectrometry-based absolute quantification reveals rhythmic variation of mouse circadian clock proteins. *Proc. Natl. Acad. Sci. USA* **113**, E3461–E3467.
- Ode, K.L., Ukai, H., Susaki, E.A., Narumi, R., Matsumoto, K., Hara, J., Koide, N., Abe, T., Kanemaki, M.T., Kiyonari, H., and Ueda, H.R. (2017). Knockout-rescue embryonic stem cell-derived mouse reveals circadian-period control by quality and quantity of CRY1. *Mol. Cell* **65**, 176–190.
- Otwinowski, Z., and Minor, W. (1997). [20] Processing of X-ray diffraction data collected in oscillation mode. *Methods Enzymol.* **276**, 307–326.
- Pittendrigh, C.S. (1954). On temperature independence in the clock system controlling emergence time in *Drosophila*. *Proc. Natl. Acad. Sci. USA* **40**, 1018–1029.
- Rappsilber, J., Mann, M., and Ishihama, Y. (2007). Protocol for micro-purification, enrichment, pre-fractionation and storage of peptides for proteomics using StageTips. *Nat. Protoc.* **2**, 1896–1906.
- Robert, X., and Gouet, P. (2014). Deciphering key features in protein structures with the new ENDscript server. *Nucleic Acids Res.* **42**, W320–4.
- Roe, D.R., and Cheatham, T.E., 3rd (2013). PTRAJ and CPPTRAJ: software for processing and analysis of molecular dynamics trajectory data. *J. Chem. Theory Comput.* **9**, 3084–3095.

- Sastry, G.M., Adzhigirey, M., Day, T., Annabhimoju, R., and Sherman, W. (2013). Protein and ligand preparation: parameters, protocols, and influence on virtual screening enrichments. *J. Comput. Aided Mol. Des.* *27*, 221–234.
- Sato, H., Amagai, K., Shimizukawa, R., and Tamai, Y. (2009). Stable generation of serum- and feeder-free embryonic stem cell-derived mice with full germline-competency by using a GSK3 specific inhibitor. *Genesis* *47*, 414–422.
- Schindelin, J., Arganda-Carreras, I., Frise, E., Kaynig, V., Longair, M., Pietzsch, T., Preibisch, S., Rueden, C., Saalfeld, S., Schmid, B., et al. (2012). Fiji: an open-source platform for biological-image analysis. *Nat. Methods* *9*, 676–682.
- Schlosser, A., Vanselow, J.T., and Kramer, A. (2005). Mapping of phosphorylation sites by a multi-protease approach with specific phosphopeptide enrichment and NanoLC-MS/MS analysis. *Anal. Chem.* *77*, 5243–5250.
- Segel, I.H. (1975). *Enzyme Kinetics: Behavior and Analysis of Rapid Equilibrium and Steady State Enzyme Systems* (New York: John Wiley & Sons).
- Sievers, F., Wilm, A., Dineen, D., Gibson, T.J., Karplus, K., Li, W., Lopez, R., McWilliam, H., Remmert, M., Söding, J., et al. (2011). Fast, scalable generation of high-quality protein multiple sequence alignments using Clustal Omega. *Mol. Syst. Biol.* *7*, 539.
- Soetaert, K., and Petzoldt, T. (2010). Inverse modelling, sensitivity and Monte Carlo analysis in R using package FME. *J. Stat. Softw.* *33*, 1–28.
- Soetaert, K., Petzoldt, T., and Setzer, R.W. (2010). Solving differential equations in R: package deSolve. *J. Stat. Softw.* *33*, 1–25.
- Susaki, E.A., Tainaka, K., Perrin, D., Kishino, F., Tawara, T., Watanabe, T.M., Yokoyama, C., Onoe, H., Eguchi, M., Yamaguchi, S., et al. (2014). Whole-brain imaging with single-cell resolution using chemical cocktails and computational analysis. *Cell* *157*, 726–739.
- Tomita, J., Nakajima, M., Kondo, T., and Iwasaki, H. (2005). No transcription-translation feedback in circadian rhythm of KaiC phosphorylation. *Science* *307*, 251–254.
- Tosini, G., and Menaker, M. (1998). The tau mutation affects temperature compensation of hamster retinal circadian oscillators. *Neuroreport* *9*, 1001–1005.
- Tsuchiya, Y., Akashi, M., and Nishida, E. (2003). Temperature compensation and temperature resetting of circadian rhythms in mammalian cultured fibroblasts. *Genes Cells* *8*, 713–720.
- Ukai, H., Kobayashi, T.J., Nagano, M., Masumoto, K.H., Sujino, M., Kondo, T., Yagita, K., Shigeyoshi, Y., and Ueda, H.R. (2007). Melanopsin-dependent photo-perturbation reveals desynchronization underlying the singularity of mammalian circadian clocks. *Nat. Cell Biol.* *9*, 1327–1334.
- Ukai-Tadenuma, M., Yamada, R.G., Xu, H., Ripperger, J.A., Liu, A.C., and Ueda, H.R. (2011). Delay in feedback repression by cryptochrome 1 is required for circadian clock function. *Cell* *144*, 268–281.
- Vagin, A., and Teplyakov, A. (2010). Molecular replacement with MOLREP. *Acta Crystallogr. D Biol. Crystallogr.* *66*, 22–25.
- Xu, R.M., Carmel, G., Sweet, R.M., Kuret, J., and Cheng, X. (1995). Crystal structure of casein kinase-1, a phosphate-directed protein kinase. *EMBO J.* *14*, 1015–1023.
- Xue, Y., Wan, P.T., Hillertz, P., Schweikart, F., Zhao, Y., Wissler, L., and Dekker, N. (2013). X-ray structural analysis of tau-tubulin kinase 1 and its interactions with small molecular inhibitors. *ChemMedChem* *8*, 1846–1854.
- Yoo, S.H., Yamazaki, S., Lowrey, P.L., Shimomura, K., Ko, C.H., Buhr, E.D., Siepka, S.M., Hong, H.K., Oh, W.J., Yoo, O.J., et al. (2004). PERIOD2:LUCIFERASE real-time reporting of circadian dynamics reveals persistent circadian oscillations in mouse peripheral tissues. *Proc. Natl. Acad. Sci. USA* *101*, 5339–5346.
- Zhou, M., Kim, J.K., Eng, G.W., Forger, D.B., and Virshup, D.M. (2015). A Period2 phosphoswitch regulates and temperature compensates circadian period. *Mol. Cell* *60*, 77–88.
- Zimmerman, W.F., Pittendrigh, C.S., and Pavlidis, T. (1968). Temperature compensation of the circadian oscillation in *Drosophila pseudoobscura* and its entrainment by temperature cycles. *J. Insect Physiol.* *14*, 669–684.

STAR★METHODS

KEY RESOURCES TABLE

REAGENT or RESOURCE	SOURCE	IDENTIFIER
Bacterial and Virus Strains		
<i>E. coli</i> Rosetta2 (DE3) (for X-ray crystallography)	Merck Millipore	Cat#71400-4
<i>E. coli</i> Rosetta2 (DE3) (for TTBK1 design)	Merck	Cat#71397
Chemicals, Peptides, and Recombinant Proteins		
Library of Pharmacologically Active Compounds (LOPAC 1280)	Sigma-Aldrich	Cat#LO3300-1KT
cOmplete, Mini, EDTA-free Protease Inhibitor Cocktail	Sigma-Aldrich	Cat#11836170001
PreScission Protease	GE Healthcare	Cat#27084301
Aurintricarboxylic acid	Sigma-Aldrich	Cat#A1895-5G
Farnesylthiosalicylic acid	Sigma-Aldrich	Cat#F8175-50MG
PD 169316	Sigma-Aldrich	Cat#P9248-5MG
SP600125	Sigma-Aldrich	Cat#S5567-10MG
Reactive Blue 2	Sigma-Aldrich	Cat#R115-10MG
SB 202190	Sigma-Aldrich	Cat#S7067-5MG
Morin hydrate	Sigma-Aldrich	Cat#M4008-2G
Methyl-3,4-dephostatin	Sigma-Aldrich	Cat#M9440-1MG
(<i>R</i>)-(+)-8-Hydroxy-DPAT hydrobromide	Sigma-Aldrich	Cat#H140-5MG
GW5074	Sigma-Aldrich	Cat#G6416-5MG
6-Hydroxy-DL-DOPA	Sigma-Aldrich	Cat#H2380-5MG
Mighty Cloning Reagent Set (Blunt End)	Takara Bio	Cat#6027
Lambda Protein Phosphatase	Bio-Rad	Cat#P0753L
HisGST-CKI δ (kinase domain)	This paper	N/A
HisGST-CKI homolog 1 (kinase domain)	This paper	N/A
His-TEV protease (S219V mutant)	Kapust et al., 2001	Addgene Plasmid #8827
λ phosphatase	Cosmo Bio	Cat#SC-200312A
Critical Commercial Assays		
FuGene6	Roche	Cat#11814443001
Dual-Luciferase Reporter Assay System	Promega	Cat#E1910
Deposited Data		
Raw images of SDS-PAGE analysis	This paper; Mendeley Data	http://dx.doi.org/10.17632/8v6y744r3t.1
CKI δ structure complexed with ADP	This paper	PDB: 5X17
CKI homolog 1 structure	This paper	PDB: 5X18
Experimental Models: Cell Lines		
Human: HEK293T	ATCC	CRL-3216
Experimental Models: Organisms/Strains		
Mouse: WT-KI: B6N-Gt(ROSA)26Sor (CAG-Csnk1d ^{WT/-})>	This paper	N/A
Mouse: K224D-KI: B6N-Gt(ROSA)26Sor (CAG-Csnk1d ^{K224D/-})>	This paper	N/A
Mouse: ROSA26 (+/+), PER2::LUC: B6.129S6(B6N)F1-mPER2::LUC ^{+/-} Gt(ROSA)26Sor (CAG-Csnk1d ^{-/-})>	This paper	N/A

(Continued on next page)

Continued

REAGENT or RESOURCE	SOURCE	IDENTIFIER
Mouse: ROSA26 (+/WT), PER2::LUC: B6.129S6(B6N)F1-mPER2::LUC ^{+/-} Gt(ROSA)26Sor < em(CAG-Csnk1d ^{WT/-})>	This paper	N/A
Mouse: ROSA26 (+/K224D), PER2::LUC: B6.129S6(B6N)F1-mPER2::LUC ^{+/-} Gt(ROSA)26Sor < em(CAG-Csnk1d ^{K224D/-})>	This paper	N/A
Mouse: ROSA26 (+/+), PER2::LUC(+/+): B6.129S6-mPER2::LUC	Yoo et al., 2004	RRID: IMSR_JAX:006852
Oligonucleotides		
Primers for CKI δ mutagenesis, see Table S1	This paper	N/A
Forward primer for the region upstream of the 5' homologous arm: 5'- TGCTGGCC TACTGCTGCCTCGATCTTAC-3'	Susaki et al., 2014	N/A
Reverse primer for the region downstream of the 5' homologous arm: 5'- AGGACAA CGCCACACACCAGGTTAGC -3'	Susaki et al., 2014	N/A
Forward primer annealing to the region upstream of the 3' homologous arm: 5'-CGTGGTGGAGCCG TTCTGTGAGACA-3'	Susaki et al., 2014	N/A
Reverse primer annealing to the region downstream of the 3' homologous arm: 5'-GGTAAATG CTTGACTCCTAGACTT-3'	Susaki et al., 2014	N/A
Reverse primer annealing to between 5' homologous arm and the CAG promoter: 5'-GGCTTTTAGTAAGCGAATTCGGTACC-3'	Susaki et al., 2014	N/A
Forward primer annealing to the poly-A region of the puromycin resistance gene: 5'-TCCATCA GAAGCTGGTCGATC-3'	Susaki et al., 2014	N/A
Recombinant DNA		
pGEX6P-1 vector (2-317 Δ CKI δ)	Isojima et al., 2009	N/A
pMU2-Luc	Isojima et al., 2009	N/A
pMU2-Per2::Luc	Isojima et al., 2009	N/A
phRL-CMV	Promega	Cat#E2261
pMU2-CKI δ vector	Narumi et al., 2016	N/A
pHisGST CKI δ	This paper	N/A
pHisGST CKI homolog 1	This paper	N/A
His-TEV protease (S219V mutant): pRK793	Kapust et al., 2001	Addgene Plasmid #8827
CKI homolog 1	Thermo Fisher Scientific	N/A
TTBK1	Thermo Fisher Scientific	N/A
Software and Algorithms		
Excel 2013	Microsoft	N/A
Origin 7.0	OriginLab	N/A
R	R Core Team	https://www.r-project.org
deSolve package	Soetaert et al., 2010	https://cran.r-project.org/web/packages/deSolve/index.html
FME package	Soetaert and Petzoldt, 2010	https://cran.r-project.org/web/packages/FME/index.html
Glide	Friesner et al., 2004; Halgren et al., 2004	https://www.schrodinger.com/
SiteMap	Halgren, 2007, 2009	https://www.schrodinger.com/
Maestro	Schrödinger, LLC	https://www.schrodinger.com/

(Continued on next page)

Continued

REAGENT or RESOURCE	SOURCE	IDENTIFIER
Protein Preparation Wizard	Sastry et al., 2013	https://www.schrodinger.com/
ClockLab	Actimetrics	http://actimetrics.com/products/clocklab/
MetaMorph	Molecular device	https://www.moleculardevices.com/
Fiji/ImageJ	Schindelin et al., 2012	https://fiji.sc/
Analysis of rhythmicity period length and oscillation phase of the SCN	Ukai-Tadenuma et al., 2011	N/A
Mathematica 9	Wolfram	https://www.wolfram.com/mathematica/
HKL2000	Otwinowski and Minor, 1997	http://www.hkl-xray.com
MOLREP	Vagin and Teplyakov, 2010	http://www.ccp4.ac.uk/html/molrep.html
Coot	Emsley et al., 2010	https://www2.mrc-lmb.cam.ac.uk/personal/pemsley/coot/
REFMAC	Murshudov et al., 1997	http://www.ccp4.ac.uk/html/refmac5.html
PHENIX	Adams et al., 2010	http://www.phenix-online.org/
PyMOL	Schrödinger, LLC	http://www.pymol.org/
Clustal Omega	Sievers et al., 2011	http://www.uniprot.org/align/
ESPrpt	Robert and Gouet, 2014	http://esprpt.ibcp.fr/ESPrpt/ESPrpt/
Dali server	Holm and Rosenström, 2010	http://ekhidna.biocenter.helsinki.fi/dali_server/
Amber 10	Case et al., 2008	http://ambermd.org/
PTRAJ	Roe and Cheatham, 2013	http://ambermd.org/
CPPTRAJ	Roe and Cheatham, 2013	http://ambermd.org/
VMD	Humphrey et al., 1996	http://www.ks.uiuc.edu/Research/vmd/

CONTACT FOR REAGENT AND RESOURCE SHARING

Further information and requests for resources and reagents should be directed to and will be fulfilled by the Lead Contact, Hiroki R. Ueda (uedah-ky@umin.ac.jp).

EXPERIMENTAL MODEL AND SUBJECT DETAILS**Transfection and Luciferase Assay**

HEK293T cells (American Type Culture Collection) were maintained in DMEM (Thermo Fisher Scientific) supplemented with 10% FBS (JRH Biosciences) and antibiotics (100 U/ml penicillin and 100 µg/ml streptomycin; Thermo Fisher Scientific) at 37°C with 5% CO₂. One day prior to transfection, cells were plated onto 35-mm dishes at a density of 4 × 10⁵ cells per well. The following day, HEK293T cells were co-transfected using FuGene6 (Roche) with 0.5 µg of a Luciferase reporter plasmid (pMU2-Per2::Luc for [Figures 5D, 5E, 7G, and S6D](#), or pMU2-Luc for [Figures S6B, S6C, S6E, and S10A](#); [Isojima et al., 2009](#)) in the presence of 0 or 1 µg each of wild-type or mutated pMU2-CKIδ ([Narumi et al., 2016](#); K224 mutants and R178 mutants for [Figures 5D and S6B](#), H185 mutants for [Figures S6D and S6E](#), D/E mutants for [Figures 5E and S6C](#), αF mutants for [Figures 7G and S10A](#), see “[Plasmid Construction](#)” section and [Table S1](#) for mutants construction; [Narumi et al., 2016](#)), according to the manufacturer’s instructions (n = 3), and cultured at 37°C. Empty vector was used to make up the total amount of DNA to 2 µg per well. Additionally, 50 ng of a phRL-CMV plasmid (Renilla luciferase (RLuc) reporter vector, Promega) was added into each transfection as an internal control for transfection efficiency. On the next day, cells in each well were harvested separately, and plated into two wells of 35-mm dishes. The following day, pre-warmed medium (27°C and 37°C) was added into each well, and then cells were cultured at 27°C and 37°C, respectively. After 24 hr, cells were harvested and assayed with Dual-Luciferase Reporter Assay System (Promega). Luciferase activity was normalized by RLuc activity. Data are representative of two independent experiments.

Mice Production

The ROSA26::P(CAG)-CKIδ knockin mouse strains were established in our laboratory (see “[Targeting into Rosa26 Locus](#)” section). mPer2^{Luc} mice were gifted from Joseph Takahashi ([Yoo et al., 2004](#)). CKIδ knockin × mPer2^{Luc} mice were produced by in vitro fertilization. All experimental procedures and housing conditions were approved by Institutional Animal Care and Use Committee of RIKEN Kobe Branch, and all of the animals were cared for and treated humanely in accordance with the Institutional Guidelines for Experiments Using Animals.

METHOD DETAILS

Protein Expression for Kinase Assay

Purification condition of CKI δ was described by reference to previous our paper (Isojima et al., 2009). After N-terminal GST tag was cleaved by PreScission Protease (GE Healthcare) overnight at 4°C, CKI δ was dephosphorylated by λ phosphatase 3–4 hr at 25°C. The dephosphorylated CKI δ was purified by cation exchange chromatography with 50 mM Tris-HCl buffer (pH 7.5) containing 600 mM NaCl and 1 mM DTT.

Mobility Shift Assay

Enzyme reaction was analyzed by mobility shift assay (LabChip EZ Reader; PerkinElmer). Substrate peptide and produced peptide were separated by applying a voltage in microchannel (Figure S1A). Reactant product was flowed with separation buffer (PerkinElmer). These peptides are labeled by the fluorescein amidite (FAM) fluorophore at N-terminal residue.

Substrate Screening

Substrate peptides based on the CKI δ peptide (KRRRALpSVASLPGL) were synthesized on a peptide synthesizer (Syrto Wave; Biotage) using Fmoc solid-phase chemistry. The synthesized peptide was purified using HPLC system and the product was confirmed by using MALDI-TOF Mass. Δ CKI δ protein (1 μ M) or Δ TTBK1 protein (Carna Biosciences; GST-fusion human TTBK1, catalytic domain (1–343 amino acids)) were added to the reaction buffer (25 mM Tris-HCl, pH 7.5, 7.5 mM MgCl₂, 1 mM ATP, 1 mM DTT, 0.1 mg/mL BSA and 20 μ M synthetic peptide) at 35°C and 25°C. Reaction was stopped by stop solution (20 mM Tris-HCl pH 7.5, 100 mM NaCl, 5 mM EDTA) at 30 min. These solutions were moved to 384-well plates and it was analyzed by mobility shift assay.

We prepared a series of single-serine substrates, *CKI δ (S10X) (KRRRALpSVAXLPGL), by mutating the second serine (at position 10) of *CKI δ to an amino acid X, and investigated their temperature dependency in Δ CKI δ -dependent phosphorylation. We also utilized a temperature-sensitive Δ TTBK1 (a catalytic domain of wild-type Tau-tubulin kinase 1, TTBK1) as a negative control. Activities at 25°C for the two-serine *CKI δ peptide were set as 1.0 in the relative activity (Figure 1B).

Initial Velocity Analysis

Initial velocities of product concentrations were computed by linear least square fittings conducted by Microsoft Excel 2013 or R 2.15.3 (<https://www.r-project.org/>). Substrate-saturation curve of initial velocities V were fitted by Michaelis-Menten equation

$$V = \frac{k_{\text{cat}}[E]_0[S]}{K_m + [S]},$$

where $[E]_0$, $[S]$, k_{cat} , and K_m represent enzyme concentration, substrate concentration, catalytic constant, and Michaelis constant, respectively. Nonlinear least square fittings were performed with R. Error of a ratio value y/x such as Q_{10} was computed by the error propagation formula

$$\varepsilon_{y/x} \approx \left| \frac{y}{x} \right| \sqrt{\left(\frac{\varepsilon_x}{x} \right)^2 + \left(\frac{\varepsilon_y}{y} \right)^2},$$

where x and y represent values such as means, ε_x and ε_y represent corresponding errors such as SEM.

In Figure 1D, ATP dependency of kinetic parameters are shown. Theoretical standard error (SE) of $k_{\text{catTS}}([T])/K_{\text{mTS}}([T])$ and $k_{\text{catTS}}([T])$ from $n = 1$ data shown in error bars in upper panels of Figure 1D were obtained from the result of nonlinear least square fittings. Theoretical SE of $K_{\text{mTS}}([T])$ was computed by the error propagation formula of the ratio of $y = k_{\text{catTS}}([T])$ to $x = k_{\text{catTS}}([T])/K_{\text{mTS}}([T])$ with theoretical covariance $\varepsilon_{x,y}$ obtained by fitting as

$$\varepsilon_{y/x} \approx \left| \frac{y}{x} \right| \sqrt{\left(\frac{\varepsilon_x}{x} \right)^2 + \left(\frac{\varepsilon_y}{y} \right)^2 - 2 \frac{\varepsilon_{x,y}}{xy}}.$$

Kinetic parameters $k_{\text{catTS}}([T])/K_{\text{mTS}}([T])$ and $k_{\text{catTS}}([T])$ were fitted according to equations in Figure 1C. Theoretical SE of $k_{\text{catTS}}/K_{\text{mTS}}$, K_T , k_{catTS} , and K_{TS} obtained from the result of nonlinear least square fittings are shown in error bars in bottom panels of Figure 1D. Theoretical SE of K_{mTS} was computed by the error propagation formula of the ratio of k_{catTS} to $k_{\text{catTS}}/K_{\text{mTS}}$ without theoretical covariance.

If not mentioned, we used product concentrations at 0, 5, 10, 15, 20, and 25 min to estimate initial velocities. For Figures 2A and S2A, 7B and S8C, S10C, and S10D (right), initial velocities were estimated with product concentrations at 0, 5, 10, and 15 min. For Figure 2A, due to the substrate inhibition observed at 320 μ M substrate (Figure S2A), we used initial velocities estimated at 20, 40, 80, and 160 μ M substrate for Michaelis-Menten analysis. Analysis including 320 μ M substrate was conducted in Figure 3 (Figures S3C and S3D).

ATP-dependent Kinase Assay

Δ CKI δ protein (1 μ M) was added to the reaction buffer (25 mM Tris-HCl, pH 7.5, 7.5 mM MgCl₂, 1 mM DTT, 0.1 mg/mL BSA, and 20, 40, 80, 160, 320 μ M *CKI_{tide}(S10A) (KRRRALSVAALPGL), respectively) at 35°C and 25°C. ATP concentration was changed the 20, 40, 80, 160, 320 μ M respectively. Reaction was stopped by stop solution (20 mM Tris-HCl pH7.5, 100 mM NaCl, 5 mM EDTA) at 0, 5, 10, 15, 20, 25 min. These solutions were moved to 384-well plates and were analyzed by mobility shift assay. Initial velocities were estimated with product concentrations at 0, 5, 10, and 15 min (Figure S1E). See also “Initial Velocity Analysis” section.

ATPase Activity Measurements

ATPase activity of Δ CKI δ was measured using an ACQUITY UPLC system (Waters Corporation, USA). The measurement condition was described by reference to ATPase activity of Kai protein (Murayama et al., 2011). Δ CKI δ protein (1 μ M) was added to the reaction buffer (25 mM Tris-HCl, pH 7.5, 7.5 mM MgCl₂, 1 mM DTT, 0.1 mg/mL BSA, and 10, 25, 50, 100 μ M ATP) at 35°C and 25°C. Reaction was auto-sampling by UPLC at 0, 5, 10, 15, 20, 25 min. ADP was separated from ATP on a BEH C18 column (2.1 \times 50 mm, 1.7 μ m) (Waters Corporation, USA) at a flow rate of 0.8 ml/min with mobile phase of 50 mM ammonium formate, 10 mM tetrabutylammonium hydrogen sulfate (pH 8.5) and 17% (v/v) acetonitrile. The ADP concentrations were calculated from their peak areas. See also “Initial Velocity Analysis” section.

Product Inhibition Assay for Kinase Activity

CKI_{tide}(2pS) (KRRRALpSVApSLPG) was synthesized by peptide synthesizer, see “Substrate Screening” section. Δ CKI δ protein (1 μ M) was added to the reaction buffer (25 mM Tris-HCl, pH 7.5, 7.5 mM MgCl₂, 640 μ M ATP, 1 mM DTT, 0.1 mg/mL BSA and 20 μ M CKI_{tide} (KRRRALpSVASLPGL)) at 35°C and 25°C. Synthesized CKI_{tide}(2pS) peptide and ADP (80, 160, 320 μ M) was added reaction mixture. Reaction was stopped by stop solution (20 mM Tris-HCl pH7.5, 100 mM NaCl, 5 mM EDTA) at 0, 5, 10, 15, 20, 25 min. These solutions were moved to 384-well plates and analyzed by mobility shift assay. See also “Initial Velocity Analysis” section.

ITC Assay

For ITC assay, MicroCal iTC200 was used. With Origin 7.0 software provided by MicroCal, data were fitted with a one-site binding model and the baselines were corrected automatically with minor manual adjustment. Δ CKI δ (WT, K224D, and K224E) purified as described above, were both dialyzed against a buffer consisting of 25 mM Bis-Tris pH 7.5, 50 mM NaCl and 10 mM MgCl. Protein concentrations were determined by UV spectra. CKI_{tide}(2pS) (500 μ M at 25°C and 750 μ M at 35°C) was loaded into the syringe and 50 μ M Δ CKI δ into the sampling cell in presence of 1 mM ADP. Titrations were performed at 25°C and 35°C using an initial injection of 0.5 μ l, followed by 2 μ L injections. CKI_{tide}(2pS) was titrated with amount of Δ CKI δ protein until saturation was reached.

Dephosphorylation Assay

Δ CKI δ protein (0.2 μ M at 25°C and 0.05 μ M at 35°C) was added to the reaction buffer (25 mM Tris-HCl, pH 7.5, 7.5 mM MgCl₂, 640 μ M ADP, 1 mM DTT, 0.1 mg/mL BSA and CKI_{tide}(2pS) (KRRRALpSVApSLPGL)) at 35°C and 25°C. The reaction was sampled at a series of time points at 0, 5, 10, 15, 20, and 25 min. These solutions were added to the stop solution at each time point. The solutions were moved to 384-well plates and were analyzed by mobility shift assay. See also “Initial Velocity Analysis” section.

Mass Spectrometry for Dephosphorylation Assay

We confirmed contamination in purified protein and the dephosphorylation activity of Δ CKI δ using LC-MS analysis. The dephosphorylation assay was performed conditions described in “Dephosphorylation Assay” section and time series sampling at 0 min and 30 min. The trypsin digested sample was prepared to a phase transfer surfactant protocol (Ode et al., 2017). The samples in a buffer (12 mM sodium deoxycholate, 12 mM sodium N-lauroylsarcosinate, 50 mM NH₄HCO₃) were digested with 1 μ g trypsin using microwave (Rapid Enzyme Digestion System, AMR, Japan) for 20 min. After the digestion, an equal volume of ethyl acetate was added to the sample, which was acidified with 0.5% TFA and well mixed to transfer the detergents into organic phase. The sample was centrifuged at 10,000 \times g for 10 min at room temperature, and an aqueous phase containing peptides was collected and dried with SpeedVac (Thermo Fisher Scientific). The dried peptides were solubilized in 100 μ L of 2% acetonitrile and 0.1% TFA and then cleaned up by self-prepared C18 tips (Rappsilber et al., 2007). The LC-MS analyses were performed by data-dependent MS/MS with IT-FT mass spectrometer (Orbitrap velos mass spectrometer, Thermo Fisher Scientific) equipped with an HPLC system containing a nano HPLC equipment (Advance UHPLC, Bruker Daltonics) and an HTC-PAL autosampler (CTC Analysis) with a trap column (0.3 \times 5 mm, L-column, ODS, Chemicals Evaluation and Research Institute, Japan). An analytical sample solubilized in 2% acetonitrile and 0.1% TFA was loaded to the LC-MS system to be separated by a gradient using mobile phases A (0.5% acetic acid) and B (0.5% acetic acid and 80% acetonitrile) at a flow rate 300 nL/min. The eluted peptides were electrosprayed (2.4 kV) and introduced into the MS equipment (positive ion mode, data-dependent MS/MS). The obtained raw data was subjected to database search with MASCOT (Matrix Science) algorithm running on Proteome Discoverer (Thermo Fisher Scientific).

Bayes Estimation of Rate Parameters

Figure 3A is a comprehensive model to explain experimental data observed in the current work. Since the model includes many rate parameters (16 parameters), it is possible to fit experimental data by several combination of parameters (Figures S3A–S3D).

Therefore, we cannot determine a parameter set uniquely (point estimation). Instead of determining a parameter set, we generate several rate parameter set to fit experimental data (Bayes estimation). For Bayes estimation of rate parameters, the statistical computing platform R 3.1.1 (<https://www.r-project.org/>) was used. Since the model equations cannot be solved analytically, we solved equations numerically. To determine the initial parameter set to fit experimental data, we applied global fittings. Then, we sampled rate parameters by Markov chain Monte Carlo (MCMC) simulations with the initial best fit parameters. Finally, we performed perturbation analyses of sampled rate parameters to identifying key parameters for temperature compensated reactions. These procedures are described in detail as follows:

Ordinary Differential Equations (ODE) of the Model

ODEs of the model shown in Figure 3A are described as follows:

$$\frac{d[T]}{dt} = k_{dT}[ET] - k_{aT}[E][T], \quad (\text{Equation 1})$$

$$\frac{d[D]}{dt} = k_{dD}[ED] - k_{aD}[E][D], \quad (\text{Equation 2})$$

$$\frac{d[S0]}{dt} = k_{dTSo}[ETS0] - k_{aTSo}[ET][S0], \quad (\text{Equation 3})$$

$$\frac{d[S1]}{dt} = k_{dDS1}[EDS1] - k_{aDS1}[ED][S1] + k_{dTTS1}[ETS1] - k_{aTTS1}[ET][S1], \quad (\text{Equation 4})$$

$$\frac{d[S2]}{dt} = k_{dDS2}[EDS2] - k_{aDS2}[ED][S2], \quad (\text{Equation 5})$$

$$\frac{d[E]}{dt} = k_{dT}[ET] - k_{aT}[E][T] + k_{dD}[ED] - k_{aD}[E][D], \quad (\text{Equation 6})$$

$$\frac{d[ET]}{dt} = k_{aT}[E][T] - k_{dT}[ET] - k_D[ET] + k_{dTSo}[ETS0] - k_{aTSo}[ET][S0] + k_{dTTS1}[ETS1] - k_{aTTS1}[ET][S1], \quad (\text{Equation 7})$$

$$\frac{d[ED]}{dt} = k_D[ET] + k_{aD}[E][D] - k_{dD}[ED] + k_{dDS1}[EDS1] - k_{aDS1}[ED][S1] + k_{dDS2}[EDS2] - k_{aDS2}[ED][S2], \quad (\text{Equation 8})$$

$$\frac{d[ETS0]}{dt} = k_{aTSo}[ET][S0] - k_{dTSo}[ETS0] - k_{DS1}[ETS0], \quad (\text{Equation 9})$$

$$\frac{d[EDS1]}{dt} = k_{DS1}[ETS0] + k_{aDS1}[ED][S1] - k_{dDS1}[EDS1], \quad (\text{Equation 10})$$

$$\frac{d[ETS1]}{dt} = k_{aTTS1}[ET][S1] - k_{dTTS1}[ETS1] + k_{TTS1}[EDS2] - k_{DS2}[ETS1], \quad (\text{Equation 11})$$

$$\frac{d[EDS2]}{dt} = k_{DS2}[ETS1] - k_{TTS1}[EDS2] + k_{aDS2}[ED][S2] - k_{dDS2}[EDS2]. \quad (\text{Equation 12})$$

ODEs were numerically solved with deSolve package (Soetaert et al., 2010).

Experimental Data to Construct a Computational Model

We used the following experimental data to construct a computational model:

- (1) ATPase assay: T to D (Figure S1D; $n = 3$)
 - $[E]_0 = 1 \mu\text{M}$, $[T]_0 = 10, 25, 50, 100 \mu\text{M}$
- (2) Phosphorylation assay: S0 to S2 (Figures 1A and S1C; $n = 3$)
 - $[E]_0 = 1 \mu\text{M}$, $[T]_0 = 640 \mu\text{M}$, $[S0]_0 = 20, 40, 80, 160, 320 \mu\text{M}$
 - Data for $[S0]_0 = 640 \mu\text{M}$ were excluded in the current analysis
- (3) Phosphorylation assay: S1 to S2 (Figures 2A and S2A; $n = 3$)
 - $[E]_0 = 0.005 \mu\text{M}$, $[T]_0 = 640 \mu\text{M}$, $[S1]_0 = 20, 40, 80, 160, 320 \mu\text{M}$
- (4) Dephosphorylation assay: S2 to S1 (Figure 2G; $n = 3$)
 - $[E]_0 = 0.2 \mu\text{M}$, $[D]_0 = 640 \mu\text{M}$, $[S2]_0 = 20, 40, 80, 160, 320 \mu\text{M}$ for 25°C
 - $[E]_0 = 0.05 \mu\text{M}$, $[D]_0 = 640 \mu\text{M}$, $[S2]_0 = 20, 40, 80, 160 \mu\text{M}$ for 35°C
- (5) Product inhibition assay: S1 to S2 (Figures 2B, S2B, and S2C; $n = 5$)
 - (a) with ADP
 - $[E]_0 = 0.005 \mu\text{M}$, $[T]_0 = 640 \mu\text{M}$, $[S1]_0 = 20 \mu\text{M}$, $[D]_0 = 80, 160, 320 \mu\text{M}$
 - $n = 3$ data were used for the current analysis
 - (b) with ADP + S2
 - $[E]_0 = 0.005 \mu\text{M}$, $[T]_0 = 640 \mu\text{M}$, $[S1]_0 = 20 \mu\text{M}$, $[D]_0 = [S2]_0 = 80, 160, 320 \mu\text{M}$
 - $n = 3$ data were used for the current analysis

Global Fitting to Experimental Data

To find a rate parameter set to represent experimental data, product concentrations of ATPase, phosphorylation, dephosphorylation, and product inhibition assays were fitted simultaneously with identical parameter set (global fitting). To circumvent to search in unphysical values, association rate parameters were searched between $1 \text{ M}^{-1}\text{s}^{-1}$ and $10^{10} \text{ M}^{-1}\text{s}^{-1}$. Reaction or dissociation rate constants were searched between 10^{-5} s^{-1} and 10^6 s^{-1} . Numerical optimizations with box constraints were performed by “optim” function with “L-BFGS-B” option in R. To search wide range of parameters, rate parameters

$$\mathbf{k} \equiv (k_{\text{AT}}, k_{\text{dT}}, k_{\text{D}}, k_{\text{AD}}, k_{\text{dD}}, k_{\text{ATSO}}, k_{\text{dTSO}}, k_{\text{DS1}}, k_{\text{ADS1}}, k_{\text{dDS1}}, k_{\text{ATS1}}, k_{\text{dTS1}}, k_{\text{DS2}}, k_{\text{TS1}}, k_{\text{ADS2}}, k_{\text{dDS2}}) \quad (\text{Equation 13})$$

were converted to

$$\mathbf{x} \equiv \log_{10} \mathbf{k}. \quad (\text{Equation 14})$$

The score function for the global fitting is a squared sum of relative error of experimental product concentrations with respect to simulated ones:

$$\text{Score}(\mathbf{x}) = \sum_{i=1}^{n_a} \sum_{j=1}^{n_{\text{int}}} \sum_{l=1}^n \sum_{m=1}^{n_t} \left(\frac{[P]_{\text{exp}}(t_m; j, l) - [P]_{\text{sim}}(t_m; j, \mathbf{k} = 10^{\mathbf{x}})}{[P]_{\text{sim}}(t_m; j, \mathbf{k} = 10^{\mathbf{x}})} \right)^2. \quad (\text{Equation 15})$$

$[P]_{\text{exp}}(t_m; j, l)$ represents an experimental product concentration of i -th assay at time t_m and l -th measurement. The index j expresses initial concentrations of substrate or product in the i -th assay. For the production inhibition assay, the product concentration was computed by subtracting initial product concentration from the total product concentration. $[P]_{\text{sim}}(t_m; j, \mathbf{k})$ represents a simulated product concentration of i -th assay at time t_m with rate parameters \mathbf{k} and initial concentrations indexed by j . Initial parameters \mathbf{x} were generated from uniform distribution with box constraints. The best fit parameter set \mathbf{x}_0 was determined by global fittings generated from 1000 random parameter set.

Markov Chain Monte Carlo (MCMC) Simulation to Sample Rate Parameters

For Bayes estimation, parameters \mathbf{x} were sampled from the posterior distribution $p(\mathbf{x}|\text{data})$. Based on Bayes' theorem, the posterior distribution can be represented as $p(\mathbf{x}|\text{data}) \propto p(\text{data}|\mathbf{x})p(\mathbf{x})$, where $p(\text{data}|\mathbf{x})$ and $p(\mathbf{x})$ represent the likelihood function and the prior distribution, respectively. We used a normal distribution for the likelihood function $p(\text{data}|\mathbf{x}) \propto \exp(-\text{Score}(\mathbf{x})/2\sigma^2)$. The model variance σ^2 was determined from the score function $\text{Score}(\mathbf{x}_0)$ of the best fit parameter \mathbf{x}_0 by dividing the total number of all experimental data points. We used non-informative prior ($p(\mathbf{x}) = \text{const}$) with box constraints identical to the global fitting.

With the likelihood function and the prior, parameters that follow the posterior distribution can be generated numerically by the MCMC simulation. We used FME package (Soetaert and Petzoldt, 2010) for MCMC simulations. For the MCMC simulation, trial parameters were generated from a multivariate normal distribution. To determine the SD of the normal distribution, we conducted 10,000 step MCMC simulations by changing the SD value. Then, we determined the SD from the simulation whose acceptance ratio was around 40%. With this criterion, SDs were determined to 0.008 at 25°C and 0.007 at 35°C . The best fit parameter set \mathbf{x}_0 was used as an initial parameter set. MCMC simulations were performed for 10^8 steps (Figures S3A and S3B). As a result, we obtained well-fitted plots in all experimental data (Figures S3C and S3D), which provided detailed information on each reaction process in multi-site

phosphorylation (Figures S3E and S3F). For analysis, 10,000 rate parameter sets were sampled from 10^8 steps MCMC simulation with 10,000 step interval.

Perturbation Analyses of Rate Parameters Sampled by the MCMC Simulation

To understand the contribution of each rate parameter to ATPase, phosphorylation, and dephosphorylation activities, we performed perturbation analyses by observing the response by changing rate parameters at 35°C. First, we quantify the impact of each rate parameter to overall time course of product concentrations ([S2]) for S0 to S2 reaction (Figure 3B). As an example, we consider the perturbation analysis of the association rate parameter k_{aTS0} as follows: (i) Pick up a rate parameter set from the MCMC simulation. (ii) k_{aTS0} is multiplied by 2 or 0.5. Other 15 rate parameters are not changed. (iii) ODE for S0 to S2 reaction is solved under these 16 rate parameters. (iv) Compute the root mean square relative error (RMSRE) between experimental and simulated product time course [S2](t). By repeating (i)–(iv) for sampled parameter set by the MCMC simulation, we obtain (10,000 in the current analysis) values of RMSRE. From these values, we can compute the mean and the SD of RMSRE. The bar graph in Figure 3B was computed in this way. The large deviation from experimental data suggests that the perturbed rate parameter is important process for S0 to S2 reaction. The contribution of the parameter to the reaction can be investigated in detail by observing perturbed time courses of product concentrations. The ratio (Q_{10}) of perturbed mean product concentrations at 35°C to unperturbed one at 25°C is shown in Figure 3B.

We also conducted the perturbation analysis of rate parameters by observing the response of kinetic parameters such as k_{cat}/K_m , k_{cat} , and K_m , which characterize the reaction quantitatively. In the following sections, we derive kinetic parameters by rate parameters. Procedures (i) and (ii) are identical to the previous ones. (iii) Compute kinetic parameters by using 16 parameters. By repeating (i)–(iii), we can compute the mean and the SD of the perturbed kinetic parameter. In Figure 3C, unperturbed k_{cat}/K_m , k_{cat} , and K_m at 25°C and 35°C, and perturbed one at 35°C are shown.

Rate Equation for the ATPase Activity

As shown in Figure S1D, $\Delta CKI\delta$ has ATPase activity. To understand the contribution of ATPase activity to the phosphorylation process, we derive the rate equation. Since $\Delta CKI\delta$ also has dephosphorylation activity (Figures 2D–2G), the ADP binding process was explicitly introduced. ODEs of the ATPase with product (ADP) binding are given as

$$\frac{d[T]}{dt} = k_{dT}[ET] - k_{aT}[E][T], \quad (\text{Equation 16})$$

$$\frac{d[D]}{dt} = k_{dD}[ED] - k_{aD}[E][D], \quad (\text{Equation 17})$$

$$\frac{d[E]}{dt} = k_{dT}[ET] - k_{aT}[E][T] + k_{dD}[ED] - k_{aD}[E][D], \quad (\text{Equation 18})$$

$$\frac{d[ET]}{dt} = k_{aT}[E][T] - k_{dT}[ET] - k_D[ET], \quad (\text{Equation 19})$$

$$\frac{d[ED]}{dt} = k_D[ET] + k_{aD}[E][D] - k_{dD}[ED]. \quad (\text{Equation 20})$$

Under quasi steady state approximation (QSSA), $d[E]/dt = d[ET]/dt = d[ED]/dt = 0$, Equation 17 is expressed as

$$\frac{d[D]}{dt} = \frac{k_{catT}[E]_0[T]}{K_{mT} \left(1 + \frac{[D]}{K_{dD}} \right) + [T]}, \quad (\text{Equation 21})$$

where we defined

$$k_{catT} \equiv \frac{k_{dD}k_D}{k_{dD} + k_D} = \frac{\alpha_D}{1 + \alpha_D} k_{dD}, \quad (\text{Equation 22})$$

$$\alpha_D \equiv \frac{k_D}{k_{dD}}, \quad (\text{Equation 23})$$

$$K_{mT} \equiv \frac{(k_{dT} + k_D)k_{dD}}{k_{aT}(k_{dD} + k_D)}, \quad (\text{Equation 24})$$

$$K_{dD} \equiv \frac{k_{dD}}{k_{aD}}. \quad (\text{Equation 25})$$

Thus, the rate Equation 21 follows Michaelis-Menten kinetics with ADP independent k_{cat} denoted by k_{catT} and ADP dependent K_m denoted by $K_{mT}(1 + [D]/K_{dD})$. The inhibition that does not change k_{cat} but k_{cat}/K_m is called competitive inhibition. Therefore, the product (ADP) behaves as a competitive inhibitor and the competitive inhibition constant is identical to the dissociation constant of the ADP (K_{dD}) in the current model.

Rate Equation for the Phosphorylation Activity

Derivation of the Rate Equation

To understand phosphorylation process S0 to S1 and S1 to S2 quantitatively, we derive rate equations and represent kinetic parameters by rate parameters. To proceed from S1 to S2, the binding process between ET and S1 is required. Therefore, we included the process in the model S0 → S1 (Figure S3G). In a similar way, the binding process between ED and S1 was included in the model S1 → S2 (Figure S3H). Instead of deriving each rate equation for S0 → S1 and S1 → S2, we use the model S → P that includes both models as shown in Figure S3I. To derive the rate equation, we applied the King-Altman method (Cook and Cleland, 2007). The King-Altman method is a schematic method to derive the rate equation by systematically deriving concentrations of all enzyme complexes under QSSA. The ODE of the product concentration is given as

$$\frac{d[P]}{dt} = k_{dDP}[EDP] - k_{aDP}[ED][P] + k_{dTP}[ETP] - k_{aTP}[ET][P]. \quad (\text{Equation 26})$$

After expressing all enzyme complex concentrations by [T], [D], [S], [P], and $[E]_0$ with the King-Altman method, Equation 26 can be expressed as

$$\frac{d[P]}{dt} = -\frac{d[S]}{dt} = \frac{n([T], [D], [S], [P])}{d([T], [D], [S], [P])} [E]_0, \quad (\text{Equation 27})$$

$$n([T], [D], [S], [P]) \equiv n_{TS}[T][S] - n_{TP}[T][P] - n_{DP}[D][P], \quad (\text{Equation 28})$$

$$\begin{aligned} d([T], [D], [S], [P]) &\equiv d_1 + d_T[T] + d_D[D] + d_S[S] + d_P[P] \\ &+ d_{TS}[T][S] + d_{TP}[T][P] + d_{DS}[D][S] + d_{DP}[D][P] \\ &+ d_{TSS}[T][S][S] + d_{TSP}[T][S][P] + d_{TTP}[T][P][P] \\ &+ d_{DSS}[D][S][S] + d_{DSP}[D][S][P] + d_{DPP}[D][P][P]. \end{aligned} \quad (\text{Equation 29})$$

We note that the equality $d[P]/dt = -d[S]/dt$ holds in Equation 27 under QSSA. Coefficients in the numerator and the denominator are given as

$$n_{TS} \equiv k_{aT}k_{dD}k_{aTS}k_{dTP}k_{DP}k_{dDP}k_{dDS}, \quad (\text{Equation 30})$$

$$n_{TP} \equiv k_{aT}k_Dk_{dTS}k_{dTP}k_{TS}k_{aDP}k_{dDS}, \quad (\text{Equation 31})$$

$$n_{DP} \equiv (k_{dT} + k_D)k_{aD}k_{dTS}k_{dTP}k_{TS}k_{aDP}k_{dDS}, \quad (\text{Equation 32})$$

$$d_1 \equiv (k_{dT} + k_D)k_{dD}k_{dTP}(k_{dTS}k_{TS} + k_{DP}k_{dDP} + k_{dTS}k_{dDP})k_{dDS}, \quad (\text{Equation 33})$$

$$d_T \equiv k_{aT}(k_D + k_{dD})k_{dTP}(k_{dTS}k_{TS} + k_{DP}k_{dDP} + k_{dTS}k_{dDP})k_{dDS}, \quad (\text{Equation 34})$$

$$d_D \equiv (k_{dT} + k_D)k_{aD}k_{dTP}(k_{dTS}k_{TS} + k_{DP}k_{dDP} + k_{dTS}k_{dDP})k_{dDS}, \quad (\text{Equation 35})$$

$$d_S \equiv k_{dD}k_{aTS}k_{dTTP}k_{DP}k_{dDP}k_{dDS}, \quad (\text{Equation 36})$$

$$d_P \equiv k_{dT}k_{dTS}k_{dTTP}k_{TS}k_{aDP}k_{dDS}, \quad (\text{Equation 37})$$

$$d_{TS} \equiv k_{aT}k_{dTTP}(k_{aTS}(k_{DP}k_{dDP} + k_{dD}(k_{TS} + k_{dDP} + k_{DP}))k_{dDS} + k_D(k_{dTS}k_{TS} + k_{DP}k_{dDP} + k_{dTS}k_{dDP})k_{aDS}), \quad (\text{Equation 38})$$

$$d_{TP} \equiv k_{aT}(k_{dTTP}k_{aDP}(k_{dTS}k_{TS} + k_D(k_{TS} + k_{DP} + k_{dTS})) + k_{dD}k_{aTP}(k_{dTS}k_{TS} + k_{DP}k_{dDP} + k_{dTS}k_{dDP}))k_{dDS}, \quad (\text{Equation 39})$$

$$d_{DS} \equiv k_{aD}k_{dTTP}(k_{aTS}k_{DP}k_{dDP}k_{dDS} + (k_{dT} + k_D)(k_{dTS}k_{TS} + k_{DP}k_{dDP} + k_{dTS}k_{dDP})k_{aDS}), \quad (\text{Equation 40})$$

$$d_{DP} \equiv k_{aD}k_{dTTP}((k_{dT} + k_D + k_{dTS})k_{TS} + (k_{dT} + k_D)(k_{dTS} + k_{DP}))k_{aDP}k_{dDS}, \quad (\text{Equation 41})$$

$$d_{TSS} \equiv k_{aT}k_{aTS}k_{dTTP}k_{DP}k_{dDP}k_{aDS}, \quad (\text{Equation 42})$$

$$d_{TSP} \equiv k_{aT}k_{aTS}k_{dTTP}(k_{DP} + k_{TS})k_{aDP}k_{dDS}, \quad (\text{Equation 43})$$

$$d_{TPP} \equiv k_{aT}k_{dTS}k_{aTP}k_{TS}k_{aDP}k_{dDS}, \quad (\text{Equation 44})$$

$$d_{DSS} \equiv k_{aD}k_{aTS}k_{dTTP}k_{DP}k_{dDP}k_{aDS}, \quad (\text{Equation 45})$$

$$d_{DSP} \equiv k_{aD}k_{aTS}k_{dTTP}(k_{DP} + k_{TS})k_{aDP}k_{dDS}, \quad (\text{Equation 46})$$

$$d_{DPP} \equiv k_{aD}k_{dTS}k_{aTP}k_{TS}k_{aDP}k_{dDS}. \quad (\text{Equation 47})$$

In the model $S0 \rightarrow S1$ (Figure S3G), the dephosphorylation rate is zero. By putting $k_{TS} = 0$ into Equations 44 and 47, we have that $d_{TPP} = d_{DPP} = 0$. In the model $S1 \rightarrow S2$ (Figure S3H), the binding process between ET and S2 is not included. By putting $k_{aTP} = 0$ into Equations 44 and 47, we have that $d_{TPP} = d_{DPP} = 0$. Thus, in the both models $S0 \rightarrow S1$ and $S1 \rightarrow S2$, equalities

$$d_{TPP} = d_{DPP} = 0 \quad (\text{Equation 48})$$

hold. In the following derivations, we assume Equation 48 hold.

Rate Equation for the Phosphorylation without Initial ADP and Product

Without initial ADP and product ($[D] = [P] = 0$), Equation 27 is expressed as

$$\frac{d[P]}{dt} = \frac{k_{catTS}([T])}{K_{mTS}([T])} \frac{[E]_0[S]}{1 + \frac{[S]}{K_{mTS}([T])} \left(1 + \frac{[S]}{K_{TS}([T])}\right)}, \quad (\text{Equation 49})$$

where we defined

$$\frac{k_{catTS}([T])}{K_{mTS}([T])} \equiv \frac{n_{TS}[T]}{d_1 + d_T[T]} = \frac{k_{catTS}}{K_{mTS}} \frac{[T]}{K_T + [T]}, \quad (\text{Equation 50})$$

$$\frac{k_{catTS}}{K_{mTS}} \equiv \frac{n_{TS}}{d_T}, \quad (\text{Equation 51})$$

$$K_T \equiv \frac{d_I}{d_T}, \quad (\text{Equation 52})$$

$$k_{\text{catTS}}([T]) \equiv \frac{n_{\text{TS}}[T]}{d_S + d_{\text{TS}}[T]} = k_{\text{catTS}} \frac{[T]}{K_{\text{TS}} + [T]}, \quad (\text{Equation 53})$$

$$k_{\text{catTS}} \equiv \frac{n_{\text{TS}}}{d_{\text{TS}}}, \quad (\text{Equation 54})$$

$$K_{\text{TS}} \equiv \frac{d_S}{d_{\text{TS}}}, \quad (\text{Equation 55})$$

$$K_{\text{mTS}}([T]) = K_{\text{mTS}} \frac{K_T + [T]}{K_{\text{TS}} + [T]}, \quad (\text{Equation 56})$$

$$K_{\text{mTS}} = \frac{d_T}{d_{\text{TS}}}, \quad (\text{Equation 57})$$

$$K_{\text{ITS}}([T]) \equiv \frac{d_S + d_{\text{TS}}[T]}{d_{\text{TSS}}[T]} = K_{\text{ITS}} \frac{K_{\text{TS}} + [T]}{[T]}, \quad (\text{Equation 58})$$

$$K_{\text{ITS}} \equiv \frac{d_{\text{TS}}}{d_{\text{TSS}}}. \quad (\text{Equation 59})$$

The term $[S]/K_{\text{ITS}}([T])$ in Equation 49 represents the inhibition effect for higher substrate concentration and is known for the substrate inhibition (Cook and Cleland, 2007). We denote ATP saturated kinetic parameters (such as k_{catTS}) by omitting the ATP concentration from the ATP dependent kinetic parameters (such as $k_{\text{catTS}}([T])$). By putting Equations 33 and 34 into Equation 52, we have that

$$K_T = \frac{(k_{dT} + k_D)k_{dD}}{k_{aT}(k_D + k_{dD})} = K_{\text{mT}}. \quad (\text{Equation 60})$$

Thus, K_T is identical to K_m of the ATPase activity (K_{mT} ; Equation 24) in the current model.

If we do not incorporate the binding between enzyme-ADP complex and substrate ($k_{\text{aDS}} = 0$) as models for $S_0 \rightarrow S_1$ (Figures 1C and S3G), Equations 42 and 45 lead to $d_{\text{TSS}} = d_{\text{DSS}} = 0$. In this case, Equation 49 is described by the Michaelis-Menten model

$$\frac{d[P]}{dt} = \frac{k_{\text{catTS}}([T])[E]_0[S]}{K_{\text{mTS}}([T]) + [S]}. \quad (\text{Equation 61})$$

Thus, the substrate inhibition term is present due to the binding between enzyme-ADP complex and substrate (Cook and Cleland, 2007) in the current model.

We consider ATP saturated kinetic parameters for $S_0 \rightarrow S_1$. By putting Equations 30, 34, and $k_{\text{TS}} = 0$ into Equation 51, we have that

$$\frac{k_{\text{catTS}}}{K_{\text{mTS}}} = \frac{k_{dD}}{k_D + k_{dD}} \frac{k_{\text{aTS}}k_{\text{DP}}}{k_{\text{DP}} + k_{\text{dTS}}} = \frac{1}{1 + \alpha_D} \frac{k_{\text{aTS}}k_{\text{DP}}}{k_{\text{DP}} + k_{\text{dTS}}}. \quad (\text{Equation 62})$$

By putting Equations 30, 38, and $k_{\text{TS}} = k_{\text{aDS}} = 0$ into Equation 54, we have that

$$k_{\text{catTS}} = \frac{k_{dD}k_{\text{DP}}k_{\text{dDP}}}{k_{\text{DP}}k_{\text{dDP}} + k_{dD}k_{\text{dDP}} + k_{dD}k_{\text{DP}}} = \frac{1}{\frac{1}{k_{dD}} + \frac{1}{k_{\text{DP}}} + \frac{1}{k_{\text{dDP}}}}, \quad (\text{Equation 63})$$

$$K_{mTS} = (1 + \alpha_D) \frac{k_{DP} + k_{dTS}}{\frac{k_{aTS}k_{DP}}{k_{dD} + k_{DP} + k_{dDP}}}. \quad (\text{Equation 64})$$

We note that Equations 62, 63, and 64 hold for both models in Figures 1C and S3G. If the rate limiting step of ATPase is the forward reaction ($\alpha_D < 1$; Equation 23), α_D do not contribute to k_{catTS}/K_{mTS} in Equation 62. On the other hand, the rate limiting step of ATPase is the ADP dissociation ($\alpha_D \gg 1$), the temperature dependence of α_D largely contribute to k_{catTS}/K_{mTS} . Therefore, we consider the estimation of α_D . From Equations 53, 54, 30, and 38, we can show inequalities

$$k_{catTS}([T]) \leq k_{catTS} \leq k_{dD}. \quad (\text{Equation 65})$$

By using Equations 22 and 65, the inequality

$$\alpha_D \leq \frac{k_{catT}}{k_{catTS}([T]) - k_{catT}} \quad (\text{Equation 66})$$

holds. Thus, the upper bound of α_D can be evaluated with k_{cat} values of ATPase and phosphorylation activities. We note that the inequality Equation 66 holds for S0 to S1 and S1 to S2 models. Therefore, the upper bound of α_D can be tightly estimated by using the maximum value of k_{cat} for S0 to S1 or S1 to S2 reactions.

By using results for S1 to S2 ($k_{cat} = 681 \text{ min}^{-1}$; Figure 2A) and ATPase ($k_{cat} = 2.32 \text{ min}^{-1}$; Figure S1D) at 35°C, Equation 66 leads to $\alpha_D < 0.0035$. Thus, the rate limiting step of the ATPase is not the ADP dissociation but the forward reaction. The result was also confirmed by the perturbation analysis of k_{cat} for the ATPase (Figure S4A). Under the condition $\alpha_D < 1$, Equation 62 can be further simplified for the magnitude relation between k_{dTS} and k_{DP} as

$$\frac{k_{catTS}}{K_{mTS}} \approx \begin{cases} k_{aTS}, & \text{for } \alpha_D \ll 1 \text{ and } k_{dTS} \ll k_{DP} \\ \frac{k_{DP}}{K_{dTS}}, & \text{for } \alpha_D \ll 1 \text{ and } k_{dTS} \gg k_{DP} \end{cases}, \quad (\text{Equation 67})$$

$$K_{dTS} \equiv \frac{k_{dTS}}{k_{aTS}}. \quad (\text{Equation 68})$$

For $k_{dTS} \ll k_{DP}$, the temperature independency of k_{catTS}/K_{mTS} is accounted for by the temperature independency of the association rate between enzyme-ATP complex and substrate (k_{aTS}). For $k_{dTS} \gg k_{DP}$, the temperature independency of k_{catTS}/K_{mTS} is explained by cancelling the change of the reaction rate (k_{DP}) with the change of the affinity between enzyme-ATP complex and substrate (K_{dTS}).

Rate Equation for the Dephosphorylation due to the ATPase Activity without Initial ADP and Substrate

The term $-n_{TP}[T][P]$ in Equation 28 represents the dephosphorylation activity by adding ATP and product (for simplicity, we use the term product for [P] that is a product of the phosphorylation and the substrate of the dephosphorylation). Without ATPase activity ($k_D = 0$), the equality $n_{TP} = 0$ holds in Equation 31. Therefore, the dephosphorylation activity is caused by using ADP produced from ATP by the ATPase activity. Without initial ADP and substrate ($[D] = [S] = 0$), Equation 27 is expressed as the Michaelis-Menten model

$$\frac{d[S]}{dt} = \frac{k_{catTP}([T])[E]_0[P]}{K_{mTP}([T]) + [P]}, \quad (\text{Equation 69})$$

where we defined

$$\frac{k_{catTP}([T])}{K_{mTP}([T])} \equiv \frac{n_{TP}[T]}{d_1 + d_T[T]} = \frac{k_{catTP}}{K_{mTP}} \frac{[T]}{K_T + [T]}, \quad (\text{Equation 70})$$

$$\frac{k_{catTP}}{K_{mTP}} \equiv \frac{n_{TP}}{d_T}, \quad (\text{Equation 71})$$

$$k_{catTP}([T]) \equiv \frac{n_{TP}[T]}{d_p + d_{TP}[T]}. \quad (\text{Equation 72})$$

Rate Equation for the Dephosphorylation without Initial ATP and Substrate

Without initial ATP and substrate ($[T] = [S] = 0$), Equation 27 is expressed as the Michaelis-Menten model

$$\frac{d[S]}{dt} = \frac{k_{\text{catDP}}([D])[E]_0[P]}{K_{\text{mDP}}([D]) + [P]}, \quad (\text{Equation 73})$$

where we defined

$$\frac{k_{\text{catDP}}([D])}{K_{\text{mDP}}([D])} \equiv \frac{n_{\text{DP}}[D]}{d_1 + d_D[D]} = \frac{k_{\text{catDP}}}{K_{\text{mDP}}} \frac{[D]}{K_D + [D]}, \quad (\text{Equation 74})$$

$$\frac{k_{\text{catDP}}}{K_{\text{mDP}}} \equiv \frac{n_{\text{DP}}}{d_D}, \quad (\text{Equation 75})$$

$$K_D \equiv \frac{d_1}{d_D}, \quad (\text{Equation 76})$$

$$k_{\text{catDP}}([D]) \equiv \frac{n_{\text{DP}}[D]}{d_P + d_{\text{DP}}[D]} = k_{\text{catDP}} \frac{[D]}{\frac{d_P}{d_{\text{DP}}} + [D]}, \quad (\text{Equation 77})$$

$$k_{\text{catDP}} \equiv \frac{n_{\text{DP}}}{d_{\text{DP}}}, \quad (\text{Equation 78})$$

$$K_{\text{mDP}} = \frac{d_D}{d_{\text{DP}}}. \quad (\text{Equation 79})$$

By putting Equation 33 and Equation 35 into Equation 76, we have that

$$K_D = \frac{k_{\text{dD}}}{k_{\text{aD}}} = K_{\text{dD}}. \quad (\text{Equation 80})$$

Thus, K_D is identical to the dissociation constant between enzyme and ADP (K_{dD}).

Rate Equation for the Phosphorylation with Initial ADP and Product

For S0 to S2 reaction, S2 were produced almost linearly with respect to the progression of time (Figures S3C and S3D). In these conditions, produced ADP and peptide do not largely affect the reaction rate. For S1 to S2 reaction, on the other hand, nonlinearities were observed (Figures S3C and S3D). Although nonlinearities for lower substrate concentrations are considered as a result of depletion of the substrate (e.g., over 50% conversion at 25 min for $[S]_0 = 20 \mu\text{M}$), nonlinearities were observed even for higher substrate concentrations (e.g., less than 20% conversion at 25 min for $[S]_0 = 320 \mu\text{M}$). This indicates produced ADP and peptide affect the reaction rate. To consider effects of products, we discuss the rate equation with initial ADP and product.

First, we consider the numerator term $n([T],[D],[S],[P])$ in Equation 27. Its sign determines the direction of the reaction. To quantify contributions of two negative terms in Equation 28, we represent $n([T],[D],[S],[P])$ as

$$n([T],[D],[S],[P]) = n_{\text{TS}}[T][S] \left(1 - \alpha_{\text{TP}} \frac{[P]}{[S]} - \alpha_{\text{DP}} \frac{[D][P]}{[T][S]} \right), \quad (\text{Equation 81})$$

$$\alpha_{\text{TP}} \equiv \frac{n_{\text{TP}}}{n_{\text{TS}}} = \frac{d_{\text{T}}}{n_{\text{TS}}} = \frac{k_{\text{catTP}}}{k_{\text{catTS}}}, \quad (\text{Equation 82})$$

$$\alpha_{\text{DP}} \equiv \frac{n_{\text{DP}}}{n_{\text{TS}}} = \frac{\frac{d_{\text{D}}}{d_{\text{T}}} \frac{d_1}{d_{\text{T}}}}{\frac{n_{\text{TS}}}{d_{\text{T}}} \frac{d_1}{d_{\text{T}}}} = \frac{k_{\text{catDP}}}{k_{\text{catTS}}} \frac{1}{K_D}. \quad (\text{Equation 83})$$

To relate α_{TP} and α_{DP} in Equations 82 and 83 to kinetic parameters, we used Equations 51, 52, 71, 75, and 76. The equilibrium condition $d[P]/dt = 0$ is achieved for $n([T],[D],[S],[P]) = 0$. We denote equilibrium concentrations of $[T]$, $[D]$, $[S]$, and $[P]$ as $[T]_{eq}$, $[D]_{eq}$, $[S]_{eq}$, and $[P]_{eq}$, respectively. By solving $n([T]_{eq}, [D]_{eq}, [S]_{eq}, [P]_{eq}) = 0$ for Equation 81, we have that

$$\alpha_{TP} \frac{[P]_{eq}}{[S]_{eq}} + \alpha_{DP} \frac{[D]_{eq}[P]_{eq}}{[T]_{eq}[S]_{eq}} = \frac{k_{catTP}[P]_{eq}}{K_{mTP}} + \frac{k_{catDP}[P]_{eq}}{K_{mDP}} \frac{[D]_{eq}}{K_D} = 1. \quad (\text{Equation 84})$$

The relation between equilibrium concentrations and kinetic parameters for a reversible reaction is known as the Haldane relationship (Cook and Cleland, 2007). Therefore, Equation 84 corresponds to the Haldane relationship in our model.

If initial concentrations $[T]$, $[D]$, $[S]$, and $[P]$ satisfy following conditions

$$\alpha_{TP} \frac{[P]}{[S]} \ll 1, \quad (\text{Equation 85})$$

$$\alpha_{DP} \frac{[D][P]}{[T][S]} \ll 1, \quad (\text{Equation 86})$$

Equation 81 can be approximated as

$$n([T], [D], [S], [P]) \approx n_{TS}[T][S]. \quad (\text{Equation 87})$$

If these conditions are satisfied, Equation 27 can be represented by the substrate inhibition model

$$\frac{d[P]}{dt} = \frac{\frac{k_{catTS}([T], [D], [P])}{K_{mTS}([T], [D], [P])} [E]_0 [S]}{1 + \frac{[S]}{K_{mTS}([T], [D], [P])} \left(1 + \frac{[S]}{K_{ITS}([T], [D], [P])}\right)}, \quad (\text{Equation 88})$$

where we defined the apparent k_{cat}/K_m that depends on ATP, ADP, and product as

$$\frac{k_{catTS}([T], [D], [P])}{K_{mTS}([T], [D], [P])} \equiv \frac{k_{catTS}([T])}{K_{mTS}([T])} \frac{1}{1 + \frac{[D]}{K_{cD}([T])} + \frac{[P]}{K_{cP}([T])} + \frac{[D][P]}{K_{cD}([T])K_{cDP}}}, \quad (\text{Equation 89})$$

$$K_{cD}([T]) \equiv \frac{d_1 + d_T[T]}{d_D} = K_D \left(1 + \frac{[T]}{K_T}\right), \quad (\text{Equation 90})$$

$$K_{cP}([T]) \equiv \frac{d_1 + d_T[T]}{d_P + d_{TP}[T]}, \quad (\text{Equation 91})$$

$$K_{cDP} \equiv \frac{d_D}{d_{DP}}. \quad (\text{Equation 92})$$

$K_{cD}([T])$, $K_{cP}([T])$, and K_{cDP} represent competitive inhibition constants by adding ADP, product, and both, respectively. By comparing Equations 79 and 92, we can show the identity

$$K_{cDP} = K_{mDP}. \quad (\text{Equation 93})$$

Thus, the competitive inhibition constant by addition of ADP and product (K_{cDP}) is identical to the ADP saturated K_m for the dephosphorylation (K_{mDP}) in the current model. We also introduced the apparent k_{cat} as

$$k_{catTS}([T], [D], [P]) \equiv k_{catTS}([T]) \frac{1}{1 + \frac{[D]}{K_{uD}([T])} + \frac{[P]}{K_{uP}([T])} + \frac{[D][P]}{K_{uD}([T])K_{uDP}}}, \quad (\text{Equation 94})$$

$$K_{uD}([T]) \equiv \frac{d_S + d_{TS}[T]}{d_{DS}}, \quad (\text{Equation 95})$$

$$K_{uP}([T]) \equiv \frac{d_S + d_{TS}[T]}{d_{TSP}[T]}, \quad (\text{Equation 96})$$

$$K_{uDp} \equiv \frac{d_{DS}}{d_{DSP}}. \quad (\text{Equation 97})$$

$K_{uD}([T])$, $K_{uP}([T])$, and K_{uDp} represent uncompetitive inhibition constants for adding ADP, product, and both, respectively. The apparent substrate inhibition constant is defined as

$$K_{ITS}([T], [D], [P]) \equiv \frac{d_S + d_{TS}[T] + d_{DS}[D] + d_{TSP}[T][P] + d_{DSP}[D][P]}{d_{TSS}[T] + d_{DSS}[D]}. \quad (\text{Equation 98})$$

In some cases, K_{cDP} or K_{uDp} can be represented by the dissociation constant between enzyme-ADP complex and product

$$K_{cDP} \equiv \frac{k_{dDP}}{k_{aDP}}. \quad (\text{Equation 99})$$

Without the dephosphorylation activity, by putting [Equation 35](#), [Equation 41](#), and $k_{TS} = 0$ into [Equation 92](#), K_{cDP} can be expressed as

$$K_{cDP} = K_{dDP}. \quad (\text{Equation 100})$$

Without the dephosphorylation activity and the binding between enzyme-ADP complex and substrate, by putting [Equation 40](#), [Equation 46](#), and $k_{TS} = k_{aDS} = 0$ into [Equation 97](#), K_{uDp} can be expressed as

$$K_{uDp} = K_{dDP}. \quad (\text{Equation 101})$$

For $S_0 \rightarrow S_1$ models in [Figures 1C](#) and [S3G](#), the dephosphorylation activity and the binding between enzyme-ADP and substrate are missing. Therefore, identities [Equations 100](#) and [101](#) hold for $S_0 \rightarrow S_1$ models.

We noted the following table provided Bayes estimators of α_{TP} and α_{DP} ([Equations 82](#) and [83](#)) for S_1 to S_2 reaction. Data are mean \pm SD (sampled from 10^8 step MCMC simulation with 10,000 step interval).

	25°C	35°C
α_{TP}	$< 1.88 \times 10^{-6}$	$< 9.38 \times 10^{-6}$
α_{DP}	$(6.87 \pm 0.82) \times 10^{-4}$	$(1.24 \pm 0.22) \times 10^{-3}$

We also noted the following table provided Bayes estimators of magnitudes of dephosphorylation activity ([Equations 85](#) and [86](#)) for S_1 to S_2 reaction. ATP, substrate, ADP, and product concentrations correspond to the product inhibition assay in [Figures 2B](#) and [S2B](#). Data are mean \pm SD (sampled from 10^8 step MCMC simulation with 10,000 step interval).

	$[T] = 640 \mu\text{M}$, $[S] = 20 \mu\text{M}$, $[D] = [P] = 320 \mu\text{M}$	
	25°C	35°C
$\alpha_{TP}[P]/[S]$	$< 3.00 \times 10^{-5}$	$< 1.51 \times 10^{-4}$
$\alpha_{DP}[D][P]/([T][S])$	$(5.49 \pm 0.65) \times 10^{-3}$	$(9.93 \pm 1.73) \times 10^{-3}$

Since values are smaller compared to 1, dephosphorylation activities in product inhibition assays are ignorable.

Chemical Screening

Chemical screening was performed by using Library of Pharmacologically Active Compounds (LOPAC¹²⁸⁰, Sigma-Aldrich) consists of 1259 chemicals. Each chemical was transferred twice into eight 384-well plates filled with phosphorylated peptide (2pS) (20 μM) and ADP solution (1 mM). Next, $\Delta\text{CKI}\delta$ solution (1 μM) was dispensed to each 384-well plate, $n = 2$. Then each plate was incubated at 35°C for 3 hr. After that, stop solution were dispensed to each 384-well plate to stop enzyme reaction. All dispensing steps described above were performed by using Biomek FX (Beckman Coulter). To quantify dephosphorylated form of peptide, mobility shift assay was done. After normalization of all assay data, fold change against negative control (DMSO) was calculated. Finally,

we selected chemicals that fold change was less than mean - 3 SD. We performed second chemical screening against it discovered chemicals.

To evaluate chemicals, we performed second screening both kinase assay and dephosphorylation assay. For kinase assay, each chemical (10 μ M) was added to the reaction buffer (1 μ M Δ CKI δ , 25 mM Tris-HCl, pH 7.5, 7.5 mM MgCl₂, 1 mM DTT, 0.1 mg/mL BSA, 1 mM ATP and 20 μ M *CKItide (KRRRALSVASLPGL), respectively) at 35°C. Kinase reaction was stopped by using a stop solution (20 mM Tris-HCl pH7.5, 100 mM NaCl, 5 mM EDTA) at 30 min. These solutions were analyzed by mobility shift assay in 384-well plates (see also “ATP-dependent Kinase Assay” section). For dephosphorylation assay, each chemical (10 μ M) was added to the reaction buffer (1 μ M Δ CKI δ , 25 mM Tris-HCl, pH 7.5, 7.5 mM MgCl₂, 1 mM DTT, 0.1 mg/mL BSA, 1 mM ADP and 20 μ M CKItide(2pS) (KRRRALpSVApSLPG), respectively) at 35°C. Dephosphorylation reaction was stopped by using a stop solution (20 mM Tris-HCl pH7.5, 100 mM NaCl, 5 mM EDTA) at 30 min. These solutions were analyzed by mobility shift assay in 384-well plates (see also “Dephosphorylation Assay” section). Since N-arachidonylglycine and MRS 2211 sodium salt hydrate were not available at the second screening stage, they were not included in Figure 4D.

Docking Simulation of ATA and Its Derivative

Our approach to docking ATA molecule to the potential binding sites of Δ CKI δ utilized four main steps: (1) structure preparation of Δ CKI δ for docking, (2) binding site prediction, (3) docking of ATA molecule, and (4) clustering and re-scoring according to the calculated binding free energy. An initial structure of mouse CKI δ was modeled from the chain A of rat CKI δ (PDB: 1CKJ) (Longenecker et al., 1996). Amino acid sequences of mouse CKI δ and rat CKI δ is identical. To incorporate the ATP, the N-lobe (1-86 residues) was superposed to ATP and Mg²⁺ complex of fission yeast CK1 (PDB: 1CSN) (Xu et al., 1995). The mouse CKI δ structure with ATP and Mg²⁺ was refined for docking simulations using the Protein Preparation Wizard (Sastry et al., 2013) Script within Maestro. For small molecule, ionization and energy minimization were performed by the OPLS3 force field in the LigPrep Script in the Maestro (Schrödinger, LLC, New York, NY, USA). These minimized structures were employed as input structures for docking simulations. Next, putative druggable sites on Δ CKI δ -ATP complex were detected and represented by small dummy atoms using the grid-based energy calculation (Halgren, 2007, 2009) incorporated in the SiteMap program with shallow binding site mode (Schrödinger, LLC, New York, NY, USA). As a result, we obtained five binding regions (Figure 4H). In this work, we searched for ATA binding sites other than a known ATP binding site. Docking simulations were performed using the Glide (Friesner et al., 2004; Halgren et al., 2004) SP docking program (Schrödinger, LLC, New York, NY, USA). Up to 100 docking poses of ATA molecule were generated in a grid box defined by each potential binding site position from previous step. We obtained 500 poses of ATA molecule in total. After the docking simulations were completed, nine representative poses of cluster center from 500 poses on all potential binding sites were selected by clustering analysis with average linkage method using Conformer Cluster Script in the Maestro. RMSD cutoff of clustering analysis was 10 Å. Finally, ligand binding free energy of the representative poses was calculated using the MM-GBSA (Schrödinger, LLC, New York, NY, USA) (Figure 4I). The docking procedure of NS-05199909 was identical to ATA. For NS-05199909, ten representative poses were selected (Figure S5E).

Basic Residues around Phosphate Analogs

To identify basic amino acid residues that could interact with a phosphate group, we used two structures that bind phosphate analogs. One is the rat CKI δ with tungstate ions (WO₄²⁻), which contains 2 chains A and B (PDB: 1CKJ) (Longenecker et al., 1996). The other is the human CKI δ with sulfate ions (SO₄²⁻), which contains 4 chains A, B, C, and D (PDB: 3UYS) (Long et al., 2012). There are 4 binding sites among 6 chains (two chains from 1CKJ and four chains from 3UYS). We labeled them as site 1, 2, 3, and 4 (Figure 5A). In the following table, we show which chain binds the phosphate analog in the specified site.

	1CKJ (Rat CKI δ with WO ₄ ²⁻)	3UYS (Human CKI δ with SO ₄ ²⁻)
Site 1	Chain A and B	Chain A, B, C, and D
Site 2	Chain B	Chain A and B
Site 3	Chain A and B	Chain B
Site 4	Nothing	Chain A, C, and D

We note that all chain bind a phosphate analog in site 1. On the other hand, the phosphate analog in site 4 is only contained in chains of 3UYS.

Since phosphate analogs are negatively charged, we searched basic amino acid residues (histidine, arginine, and lysine) whose minimum distance to a phosphate analog in the specified site is less than 10 Å. Identified residues are shown in Figures 5A and 5B. Mean and SD of minimum distances between identified basic residues and the phosphate analog in the specified site is shown in Figure 5B. The sample number in the computation of mean and SD corresponds to the number of chains which bind the phosphate analog in the specified PDB ID (e.g., n = 2 for site 1 of 1CKJ and n = 1 for site 2 of 1CKJ).

Plasmid Construction

Per2 and CKI δ plasmid used in this study were subcloned in the pMU2 vector (Ukai et al., 2007) as described in a previous study (Narumi et al., 2016) and expressed under the CMV promoter as a Flag-tag fusion to their N terminus. CKI δ mutagenesis with inverse PCR followed by self-ligation of blunt-end product was performed using Mighty Cloning Reagent Set (Takara Bio, Japan). Primer sequences used CKI δ mutagenesis were summarized in Table S1.

Cultivation of Mouse ES Cells

ES cells were cultured without feeder cells as described in a previous report (Ode et al., 2017). Before beginning cultivation, surface of BD PURECoat amine dishes were exposed to medium which are containing LIF plus 6-bromoindirubin-3'-oxime (BIO) (Sato et al., 2009) for more than 5 hr at 37°C with 5% CO₂. ES cells were cultured without feeder cells in iSTEM medium (Clontech Laboratories A Takara Bio Company) at 37°C with 5% CO₂.

Targeting into Rosa26 Locus

The ROSA26::P(CAG)-CKI δ knockin mouse strains were established in our laboratory. All of the required elements, including P(CAG)-CKI δ -polyA from pMU2-CKI δ (wild-type and K224D mutant, see “Plasmid Construction” section) and the Puromycin resistance gene cassette (P(PGK)-Puro^R-polyA), were inserted into pENTR-1A (Invitrogen). The resulting sequence (pENTR-P(CAG)-CKI δ -polyA-P(PGK)-Puro^R-polyA) was then inserted into the ROSA26 targeting vector (Abe et al., 2011), which contains the Reading Frame Cassette B from the Gateway Conversion System (Invitrogen), using the Gateway system. In the resulting targeting vector, the insertion cassette was in the same orientation as the ROSA26 gene.

C-terminal-truncated (+63) TALENs (Miller et al., 2011) that bind target sequence (5'-CTGCAACTCCAGTCTTTCTAGAA GATGGGCGGGAGTCTTCTGGGCAGGCTTA-3', TALEN binding sequences are indicated with italics) were designed using TALE-NT (Doyle et al., 2012).

Purified 0.9 μ g of the targeting vector and 1.2 μ g each of the TALEN-L and TALEN-R expression vector were co-transfected into 4 \times 10⁵ cells of C57BL/6 mouse ES cells, HK3i, (Kiyonari et al., 2010) by using Xfect Transfection Reagent (Clontech Laboratories A Takara Bio Company). The homologous recombined, puromycin resistant ES cell clones were isolated for further culture and expansion.

The screened for successful homologous recombination and the confirmation of genome integrity were performed as previously described (Susaki et al., 2014) by PCR using the following primers (Hokkaido System Science): 1) forward primer annealing to the region upstream of the 5' homologous arm: 5'-TGCTGGCCTACTGCTGCCTCGATCTTAC-3', 2) reverse primer annealing to the region downstream of the 5' homologous arm: 5'-AGGACAACGCCACACACCAGGTTAGC-3', 3) forward primer annealing to the region upstream of the 3' homologous arm: 5'-CGTGGTGGAGCCGTTCTGTGAGACA-3', 4) reverse primer annealing to the region downstream of the 3' homologous arm: 5'-GGTAAAATGCTTGACTCCTAGACTT-3', 5) reverse primer annealing to between 5' homologous arm and the CAG promoter: 5'-GGCTTTTAGTAAGCGAATTCGGTACC-3', and 6) forward primer annealing to the poly-A region of the puromycin resistance gene: 5'-TCCATCAGAAGCTGGTGCATC-3'. The copy number of the inserted cassette was confirmed with quantitative PCR assay (Susaki et al., 2014).

The selected ES cell clones were injected into 8-cell-stage ICR embryos to generate ~100% ES cell-derived chimeras (Kiyonari et al., 2010).

Locomotor Analysis of CKI δ Mutant Mice

Either 6, 10, or 20 weeks old male WT-KI mice were maintained under LD cycles (light 12 hr, dark 12 hr) for 16 days. Then the mice were released into DD (constant dark) environment, and maintained for 21 days. The mice were resynchronized with LD cycle environment (light 12 hr, dark 12 hr) for 16 days, before they were released into LL (constant light) environment (18 days). K224D-KI mice of same ages were also exposed to the similar sequence of light conditions, that is LD for 21 days, DD for 18 days, LD for 14 days, and then LL for 16 days. The circadian period of each light condition was estimated by using whole data obtained in the corresponding condition. The LL data of non-significant circadian rhythmicity (chi-square test) were excluded. The behavior was monitored by an infrared monitoring system (NS-AS01, Neuroscience), and data were analyzed with ClockLab software (Actimetrics).

Luminescence Monitoring of SCN Slice

The mice were maintained in 24 hr light dark cycle (12 hr dark, 12 hr light) before sampling. The 7-day old pups of mice carrying luciferase reporter gene with mutated or wild-type *Csnk1d* gene inserted into ROSA26 locus were anesthetized on crushed ice and decapitated. Mice with intact ROSA26 locus were also used as a control. Brain was rapidly removed and trimmed down to a small block containing the medial basal hypothalamus. The coronal brain slices of 300 μ m thickness were obtained from the block by using a McIlwain tissue chopper. The slices were then transferred into cooled Hanks buffer, and the one slice including suprachiasmatic nucleus (SCN) was selected under a stereoscopic microscope. The extra region outside SCN were trimmed out. The SCN slice was then placed on Millicell-CM (PICMORG50, Millipore) in a 35 mm Petri dish which was sealed with silicone grease. The SCN slice was cultured with 1.2 mL of DMEM/F12 (12400-024, Thermo Fisher Scientific) supplemented with serum-free growth supplements (Nakamura et al., 2002). The measurement of bioluminescence from each SCN slice was performed with a photomultiplier tube (PMT) detector assemblies (LM-2400, Hamamatsu Photonics) for 7 days either at 37°C or 30°C, followed by a medium exchange and

another 7 days measurement at the complementary temperature (i.e., if a SCN slice was first measured at 37°C, the same slice was measured at 30°C in the following measurement). Graphs of oscillations were plotted by Mathematica 9 (Wolfram). The detector assemblies were maintained in an incubator without CO₂ gas, and interfaced with computers for continuous data-acquisition. Photons were counted for 1 min with 15 min intervals.

The rhythmicity period length and oscillation phase of the SCN were determined as described previously (Ukai-Tadenuma et al., 2011), with a slight change. Briefly, bioluminescence time course data beginning 24 hr after measurement-start were used for analysis in order to distinguish endogenous circadian oscillation from acute effects of culture preparation. Bioluminescence data were detrended using the trend curve calculated by smoothing spline method. Then, autocorrelation of the detrended bioluminescence time courses data was calculated within the range of 14–34 hr to determine the circadian period of oscillation. The average time course and its standard deviation were calculated by aligning time courses from SCN slices in a same genotypic group according to their oscillation phases.

Q₁₀ was calculated with the formula

$$Q_{10} = \left(\frac{R_2}{R_1} \right)^{\frac{10}{T_2 - T_1}},$$

where T_1 and T_2 are the measurement temperatures, R_1 and R_2 are wave-numbers of the observed luminescence at the corresponding temperature (Barrett and Takahashi, 1995).

For the timelapse imaging, samples were prepared as described above. Sealed 35-mm culture dishes were placed on the stage of a macrozoom microscope (MVX10; Olympus) in a dark hood. The culture dishes were kept at approximately 30 or 37°C in a heated chamber (Tokai Hit) on the microscope stage. Bioluminescence was imaged using a 1.6 × Plan Apochromat objective (NA 0.24; Olympus) with 2.5 × zoom and transmitted to an electron-multiplying charge-coupled device (EM-CCD) camera cooled to –80°C (ImagEM C9100-13, Hamamatsu Photonics). The dimension of an image is 512 × 512 pixels, and each pixel is 16 bits. Exposure time was 540 s with EM gain of 300 ×. Images were transferred at 690 kHz to minimize readout noise, and recorded using MetaMorph software (Molecular device). Subsequent image processing including noise-reduction, intensity extraction and construction of the multi-slice movie was performed by Fiji/ImageJ software (Schindelin et al., 2012).

Multiple Sequence Alignment

The multiple sequence alignment was performed by Clustal Omega (Sievers et al., 2011) in UniProt (<http://www.uniprot.org/align/>) and was rendered by ESPript (Robert and Gouet, 2014) (<http://esprict.ibcp.fr/ESPript/ESPript/>) (Figure 7A).

Protein Preparation for X-ray Crystallography

The cDNAs encoding mouse CKIδ (residues 1–294) and CKI homolog 1 derived from yeast (residues 62–355) were amplified by PCR and subcloned into a pET28a(+) derivative vector, which has a glutathione *S*-transferase-encoding sequence inserted after an N-terminal polyhistidine tag. The constructs contained a tobacco etch virus (TEV) protease recognition site at the junction between GST and the protein sequences. The recombinant proteins were expressed in *E. coli* Rosetta2 (DE3) (Merck Millipore) cells in LB broth at 37°C until the OD₆₀₀ reached 0.6, at which point the temperature was shifted to 15°C. Protein expressions were induced by addition of isopropyl-β-D-thiogalactopyranoside to a final concentration of 200 μM. The cultures were grown for an additional 20 hr and harvested by centrifugation. Cell pellets were resuspended in 50 mM Tris-HCl buffer (pH 8.0) containing 500 mM NaCl and 20 mM imidazole. Cells were lysed by sonication and clarified by centrifugation. The cell lysates were loaded onto a HisTrap HP column (GE Healthcare), and CKIδ and CKI homolog 1 was respectively eluted with 50 mM Tris-HCl buffer (pH 8.0) containing 500 mM NaCl and 500 mM imidazole. Then, the CKIδ and CKI homolog 1 proteins were dephosphorylated and the N-terminal histidine-GST tags were cleaved by incubating with λ phosphatase (Cosmo Bio) and TEV protease (Kapust et al., 2001) overnight at 4°C. The dephosphorylated proteins were further purified by cation exchange chromatography, followed by size-exclusion column chromatography using a HiLoad Superdex 200 16/60 (GE Healthcare). The CKIδ protein stored in 50 mM Tris-HCl buffer (pH 7.5) containing 200 mM NaCl, 5 mM β-octyl glucoside, 1 mM EDTA and 1 mM DTT, and the CKI homolog 1 protein stored in 10 mM MOPS buffer (pH 7.0) containing 100 mM NaCl, 100 μM EGTA and 2 mM DTT was subjected to crystallization.

Crystallization and Structure Determination

Crystallization was performed by the sitting-drop vapor-diffusion method under 20°C by mixing equal volumes (200 nl) of Δ294CKIδ (13.5 mg/ml) and a reservoir solution of 100 mM sodium citrate buffer (pH 5.0) containing 25 mM (NH₄)₂SO₄ and 7% (w/v) PEG 8000. The crystals were soaked with 2 mM of ADP for 24 hr in mother liquor. Reservoir solution for CKI homolog 1 (10 mg/ml) was 200 mM sodium malonate buffer (pH 7.0) containing 20% (w/v) polyethylene glycol 3350. The crystals were briefly soaked in a cryoprotectant drop composed of the reservoir solution supplemented with 20% glycerol and then flash-cooled in liquid nitrogen for X-ray diffraction data collection. The datasets were collected at the beamline BL26B2, SPring-8 (Harima, Japan), and were indexed, integrated, and merged using the HKL2000 program suite (Otwinowski and Minor, 1997). The crystal structures were determined by molecular replacement using MOLREP (Vagin and Teplyakov, 2010) with the apo form structure of CKIδ (PDB: 3UYS) as the search model.

Model building was accomplished with *Coot* (Emsley et al., 2010), and structural refinement was performed with *REFMAC* (Murshudov et al., 1997) and *PHENIX* (Adams et al., 2010). The structural models in the figures were depicted using *PyMOL* version 1.8 software (Schrödinger, LLC).

Multiple Structural Alignment

Multiple structural alignment was performed by Dali server (Holm and Rosenström, 2010) with the “Expand gaps” option. Following structures were used: Rat CKI δ (PDB: 1CKJ and 1CKI); Human CKI δ (PDB: 3UYS); Human CKI ϵ (PDB: 4HOK); Fission yeast CK1 (PDB: 1CSN); Human CKI γ 3 (PDB: 4G17); Human TTBK1 (PDB: 4BTJ); Human VPK2 (PDB: 2V62); Human AurA (PDB: 4DEE); Human CDK2 (PDB: 1HCK). If a PDB file includes multiple chains, the chain that had the highest Dali score (Z-score) from 1CKJ:B structure was used. Secondary structures (α helix, 3_{10} helix, turn, bend, β strand, β bridge, and no secondary structure assigned) were labeled based on the “DSSP Legend” of the corresponding PDB ID in the PDB website (<http://www.rcsb.org/>). Labels of secondary structure elements such as β 7 and α D were based on previous studies (Longenecker et al., 1996; Xu et al., 1995). In Figure 7D, WO4, SO4, MG, PO4, and EDO represent tungstate ion WO $_4^{2-}$, sulfate ion SO $_4^{2-}$, magnesium ion Mg $^{2+}$, phosphate ion PO $_4^{3-}$, and 1,2-ethanediol, respectively. The binding sites in “CKI δ WO4/SO4 site” are shown (see also Figure 5A) if the minimum distance between the amino acid and a phosphate analogs (WO $_4^{2-}$ /SO $_4^{2-}$) is less than 10 Å among chain A and B of 1CKJ (Longenecker et al., 1996) and chain A-D of 3UYS (Long et al., 2012). Underlined site indicates the contact residue (minimum distance is less than 3.5 Å).

Molecular Dynamics Simulations

For MD simulations, the chain B of rat CKI δ (PDB: 1CKJ) (Longenecker et al., 1996) was used as an initial structure. The modeling procedure of the initial structure of mouse CKI δ (apo form; Figure S9A) and ATP bound structure (Figure 7E) is described in “Docking Simulation of ATA and Its Derivative.” The ADP binding structure (Figure 7E) was modeled by removing the γ -phosphate from the ATP bound structure. Protonation states of histidine were determined from neighboring atoms as follows: 46 HID, 50 HIP, 120 HIP, 126 HIP, 162 HIP, 164 HIP, 185 HIP, and 278 HIE, where HID, HIE, and HIP indicate δ nitrogen is protonated, ϵ nitrogen is protonated, and both nitrogens are protonated, respectively. The first methionine (Met1) was excluded and Glu2-Leu293 residues were used for MD simulations.

MD simulations were conducted by MD package Amber 10 (Case et al., 2008). The ff99SB force field parameter (Hornak et al., 2006) with additional modifications (Li and Brüschweiler, 2010; Lindorff-Larsen et al., 2010) was used for proteins. Force field of ATP and ADP (Meagher et al., 2003) were obtained from AMBER parameter database (<http://research.bmh.manchester.ac.uk/bryce/amber>). Truncated octahedron periodic boundary condition was applied. TIP3P water molecules were added with 15 Å buffer from the protein surface. To neutralize the system, Cl $^-$ atoms were included. Electrostatic interactions were evaluated by smooth particle mesh Ewald (Essmann et al., 1995) with 10 Å direct space cutoff. After performing energy minimizations with 1000 steps, 100 ps MD simulations were conducted at 1 atm and 25°C or 35°C. Production MD simulations were performed for 1.5 μ s with the constant volume condition at 25°C or 35°C. Langevin dynamics with collision frequency 1.0 ps $^{-1}$ and 2 fs time step was used for MD simulations. Movies S2 and S3 were created by using VMD (Humphrey et al., 1996).

Root mean square fluctuation (RMSF) for each C α atom (Figures 7E and S9A) and minimum distances between residues (Figures S9D–S9G) were computed with PTRAJ and CPPTRAJ programs (Roe and Cheatham, 2013), respectively. Potential energy principal component analyses (PEPCA; Figures S9D–S9I) (Koyama et al., 2008, 2011) were performed with a C++ program written by us. Residue based potential energies were computed without cutoff distance. PCA was implemented by diagonalization of the centered Gram matrix (Koyama et al., 2008) with 1500 structures.

Alanine Scanning of CKI δ around K224

In structural analyses (Figures 7F and S8F) and MD simulations (Figures 7E and S9A), CKI specific domain K217–Q223 (Figure 7D) showed large fluctuations. Furthermore, fluctuations of α F helix (K221–S234, Figure 7D) showed temperature sensitivity in MD simulations (Figures 7E and S9A). To understand the contribution of each residue to the temperature compensation, we performed alanine scanning of these residues:

K217A, (A218), (A219), T220A, K221A, R222A, Q223A, K224A, Y225A, E226A, R227A, I228A, S229A, E230A, K231A, K232A, M233A, S234A.

We also performed the alanine scanning of interaction residues of K217–S234. Since the 1st principal component (PC1) of PEPCA corresponds to the conformational change of α F helix for Δ CKI δ -ADP at 35°C (Figures S9D and S9E) and Δ CKI δ -ATP at 25°C (Figures S9F and S9G), we selected residues including K217–S234 from the top 20 components of the 1st eigenvector (bar graphs in Figures S9D–S9G). As a result, we performed following alanine mutations:

K45A, D128A, K130A, D149A, L173A, T176A, (A177), R178A, (A180), H185A, D194A, E197A, Y201A, W213A, Q214A, T235A, R256A.

For MD simulations of Δ CKI δ -ADP at 25°C and Δ CKI δ -ATP at 35°C, large conformational changes of α F helix were not observed (Figure 7E). To check whether interaction residues with K217–S234 specific to these conditions could change the temperature dependency, we also performed PEPCA in these conditions (Figures S9H and S9I). By comparing the top 20 components of the 1st

eigenvector (Figures S9D–S9I), there is only one specific interaction, that is the vdW interaction between L216 and R227 found in Δ CKI δ -ADP at 25°C (Figure S9H). We also created the alanine mutation of the residue:

L216A.

We confirmed that the mutation did not induce the large change of Q_{10} (Figure 7G).

Dual-luciferase assay of these CKI δ mutants are shown in Figure 7G. See also “Transfection and Luciferase Assay” and “Plasmid Construction” sections.

Design of a Temperature-compensated Kinase

TTBK1 was deficient in K217 to Q223 regions of CKI δ (Figure 7D; PDB: 4BTJ; Xue et al., 2013). We also note that contact residues of phosphate analogs in site 1 of CKI δ are R178, Q214, G215, and K224 (“CKI δ WO4 / SO4 site” in Figure 7D). Since R178 of CKI δ and the corresponding residue of TTBK1 (R204) is conserved (Figure 7D), introduction of residues corresponding to Q214, G215, and K224 into TTBK1 is expected to recognize a phosphate group. With these considerations, we rationally designed TTBK1 mutant (rMT; reconstituted mutant type) by replacing 5 amino acid residues (R240–D244) of TTBK1 with 11 amino acid residues (Q214–K224) (Figure 7H).

The double strand DNA of TTBK1(WT) and TTBK1(rMT) were synthesized by DNA synthesis (Thermo Fisher Scientific). Human TTBK1(WT) (residues 1–343) and TTBK1(rMT) were amplified by PCR and subcloned into a pGEX-6P vector. The recombinant protein was expressed in *E. coli* Rosetta2 (DE3) cells in LB broth at 30°C until the OD_{600} reached 0.4, at which point the temperature was shifted to 37°C. Protein expression was induced by addition of isopropyl- β -D-thiogalactopyranoside (IPTG) to a final concentration of 100 μ M. The cultures were grown for an additional 20 hr and harvested by centrifugation. Cell pellets were resuspended in 50 mM Tris-HCl buffer (pH 7.5) containing 300 mM NaCl, 1 mM EDTA, 1 mM DTT, 10% glycerine and cComplete mini (Roche). Cells were lysed by sonication and clarified by centrifugation on ice. TTBK1(WT) and TTBK1(rMT) were purified from the cell lysate by GST-tag. Purified proteins were incubated with λ phosphatase 5 hr at 25°C. The dephosphorylated proteins were further purified by HiTrap HP column (GE Healthcare). Elution buffer used was 50 mM Tris-HCl buffer (pH 8.0) containing 600 mM NaCl and 1 mM DTT. Quality of protein was confirmed by SDS-PAGE and UV spectra.

QUANTIFICATION AND STATISTICAL ANALYSIS

Sample numbers of mean and SEM/SD are described in figure legends. Two-tailed Welch’s t tests were performed by Microsoft Excel 2013.

DATA AND SOFTWARE AVAILABILITY

The accession numbers for CKI δ structure complexed with ADP and CKI homolog 1 structure are PDB: 5X17 and 5X18, respectively. Raw images of SDS-PAGE analysis have been deposited to Mendeley Data and are available at <http://dx.doi.org/10.17632/8v6y744r3t.1>.

Molecular Cell, Volume 67

Supplemental Information

Temperature-Sensitive Substrate and Product

Binding Underlie Temperature-Compensated

Phosphorylation in the Clock

Yuta Shinohara, Yohei M. Koyama, Maki Ukai-Tadenuma, Takatsugu Hirokawa, Masaki Kikuchi, Rikuhiro G. Yamada, Hideki Ukai, Hiroshi Fujishima, Takashi Umehara, Kazuki Tainaka, and Hiroki R. Ueda

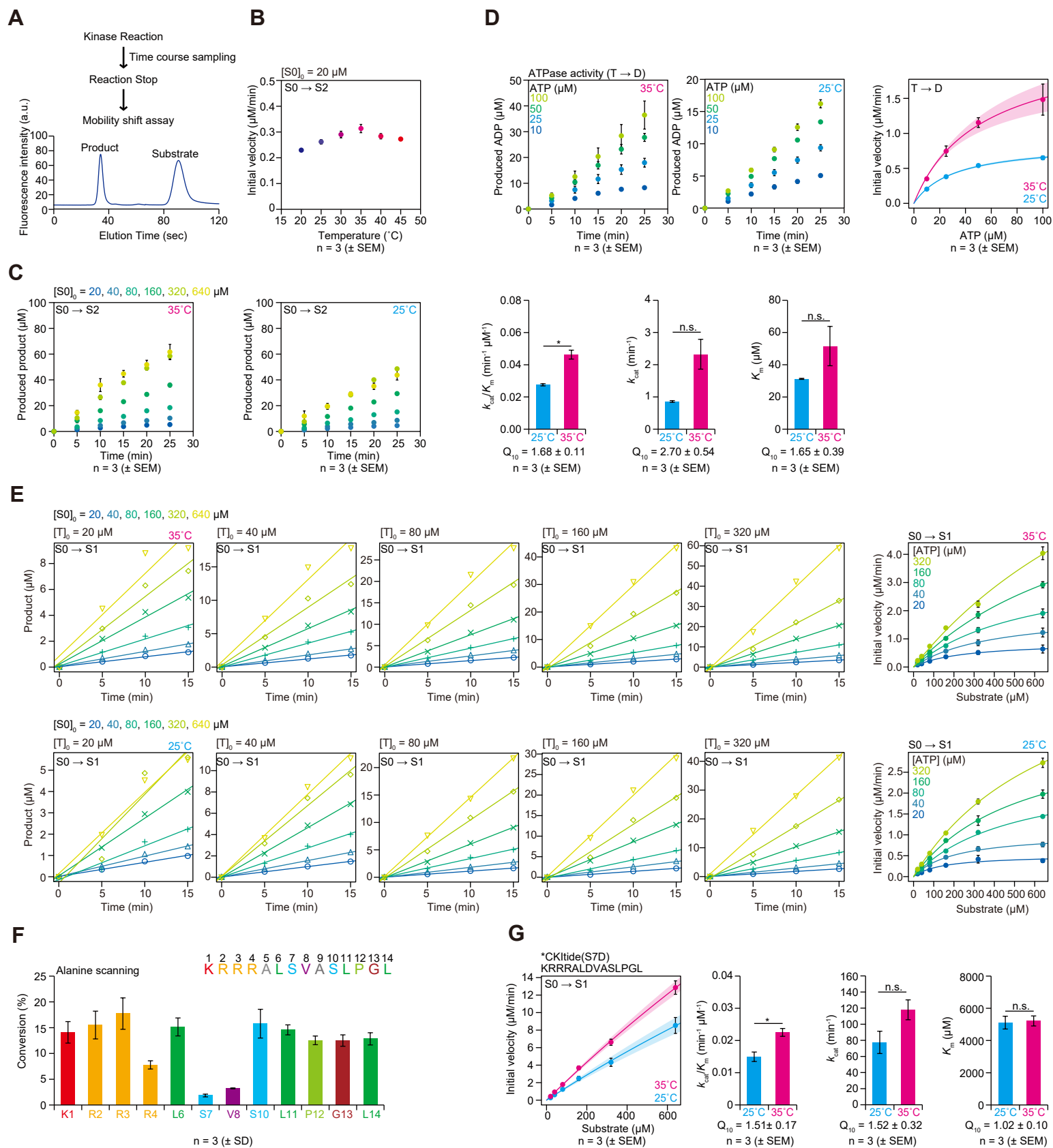


Figure S1: Shinohara et al.

Figure S1. Temperature-sensitive binding of a substrate to an enzyme underlies the temperature compensation of CKI δ -dependent single-serine phosphorylation, related to Figure 1.

(A) Workflow of the phosphorylation assay by using the mobility shift assay system.

(B) Initial velocity of a two-serine substrate *CKItide (KRRRALSVASLPGL) (20 μ M) to a double-phosphorylated product CKItide(2pS) (KRRRALpSVApSLPGL) at 20°C to 45°C. Data are mean \pm SEM (n = 3).

(C) Time course of products of Δ CKI δ -dependent phosphorylation on a two-serine substrate *CKItide (20 to 640 μ M) at 35°C (left) and 25°C (right). Their substrate saturation curves are shown in **Figure 1A**. Data are mean \pm SEM (n = 3).

(D) Time course of produced ADP (upper left and middle), their substrate saturation curves (upper right), and kinetic parameters (lower) of Δ CKI δ -dependent ATPase activity (10 to 100 μ M ATP) without a peptide substrate at 25°C and 35°C.

(E) Time course of products (left 5 columns; 20 to 320 μ M ATP) and their substrate saturation curves (right column) of Δ CKI δ -dependent phosphorylation on a single-serine substrate *CKItide(S10A) (KRRRALSVAAALPGL) (20 to 640 μ M) at 35°C (upper) and 25°C (lower). For substrate saturation curves, data are initial velocity \pm SE estimated from the linear fitting for the initial velocity (n = 1).

(F) Phosphorylation activity of a series of alanine mutants of *CKItide by Δ CKI δ . Data are mean \pm SEM (n = 3).

(G) Substrate saturation curves (left) and kinetic parameters (right) of Δ CKI δ -dependent phosphorylation on a single-serine substrate *CKItide(S7D) (KRRRALDVASLPGL) at 25°C and 35°C.

For (D) and (G), data are mean \pm SEM (n = 3); * $p < 0.05$ and n.s. (not significant); two-tailed Welch's t-test. Solid line and shade represent mean \pm SEM of curves of Michaelis-Menten model with estimated parameters.

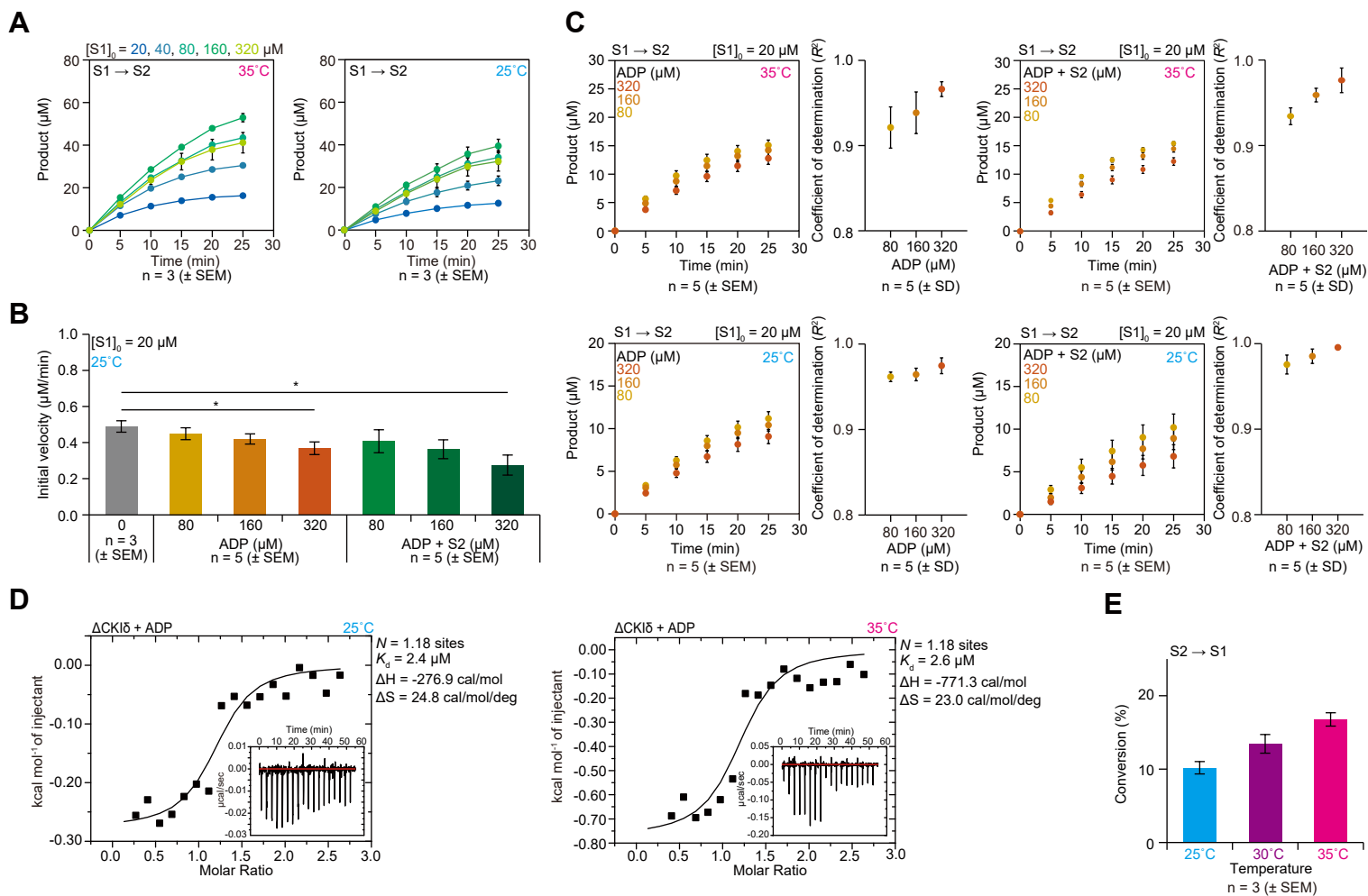


Figure S2. Temperature-sensitive and ADP-dependent binding of a product to an enzyme underlies the temperature compensation of CKI δ -dependent multi-site phosphorylation, related to Figure 2.

(A) Time course of products of phosphorylation on a single-phosphoserine substrate CKItide (20 to 320 μ M) at 35°C (left) and 25°C (right). Their substrate saturation curves and kinetic parameters are shown in **Figure 2A**. Data are mean \pm SEM (n = 3).

(B) Initial velocities of CKItide-phosphorylation at 25°C with initial ADP or mixture of ADP and CKItide(2pS). Data are mean \pm SEM (n = 3 for [ADP] = [S2] = 0 μ M and n = 5 for otherwise); **p* < 0.05; two-tailed Welch's t-test.

(C) Time course of products of phosphorylation on a single-phosphoserine substrate CKItide (20 μ M) at 35°C (upper) and 25°C (lower) with initial ADP (left) or mixture of ADP and CKItide(2pS) (right). The coefficient of determination (R^2) for the linear fitting to estimate the initial velocity became closer to 1.0 (i.e. the dynamics of the reaction became more linear) in the presence of higher dose of ADP or mixture of ADP and CKItide at the beginning of the reaction. Data are mean \pm SEM (n = 5) for the time course of product and mean \pm SD (n = 5) for the coefficient of determination. Initial velocities are shown in **Figures 2B and S2B**.

(D) ITC assay for the binding of ADP to Δ CKI δ at 25°C (left) and 35°C (right).

(E) Temperature dependency of dephosphorylation activity by Δ CKI δ on CKItide(2pS). Data are mean \pm SEM (n = 3).

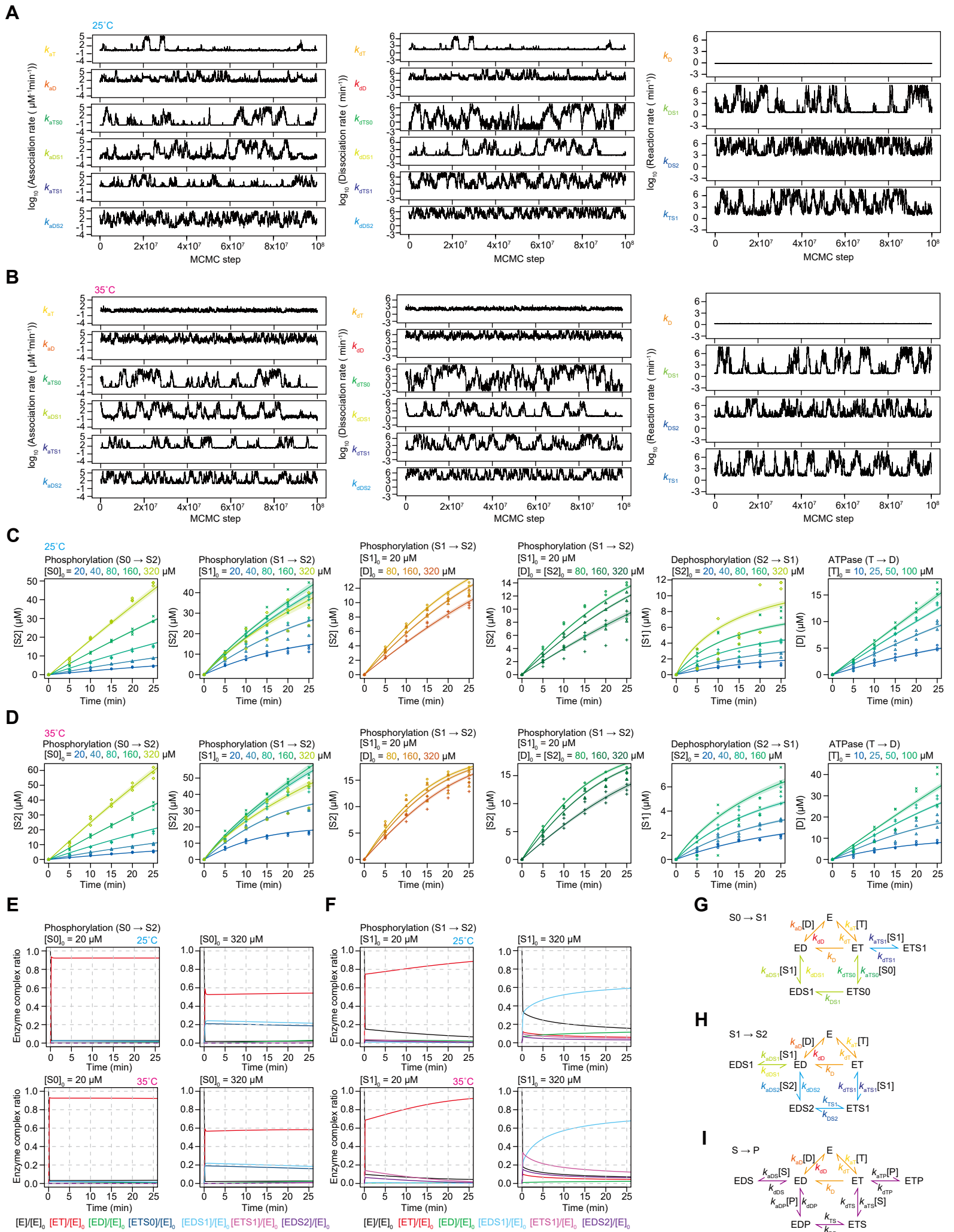


Figure S3: Shinohara et al.

Figure S3. Bayes estimation of rate parameters in a computational model of temperature-compensated CKI δ -dependent multi-site phosphorylation, related to Figure 3.

(A and B) Sampling of 16 rate parameters by Markov chain Monte Carlo (MCMC) simulations at 25°C (A) and 35°C (B). MCMC simulations were performed for 10^8 steps. The distribution of 10,000 rate parameter sets were sampled from 10^8 step MCMC simulation with 10,000 step interval. Some rate parameters such as k_{aT} and k_{dT} fluctuate similarly. However, these data are not identical. We confirmed that dissociation constants (such as k_{dT}/k_{aT}) fluctuated.

(C-D) Experimental (points) and simulated (curves) time course at 25°C (C) and 35°C (D). In each experiment, three independent datasets were used for the MCMC simulation. Bold curves represent mean time courses obtained by MCMC simulations. Shaded curves represent the region for mean \pm SD of simulated time courses (sampled from 10^8 step MCMC simulation with 10,000 step interval).

(E-F) Mean time courses of ratios of enzyme complexes for S0 to S2 (E) and S1 to S2 (F) reactions.

(G-I) Computational models of reactions from S0 to S1 (G), from S1 to S2 (H), and the unified reaction (I).

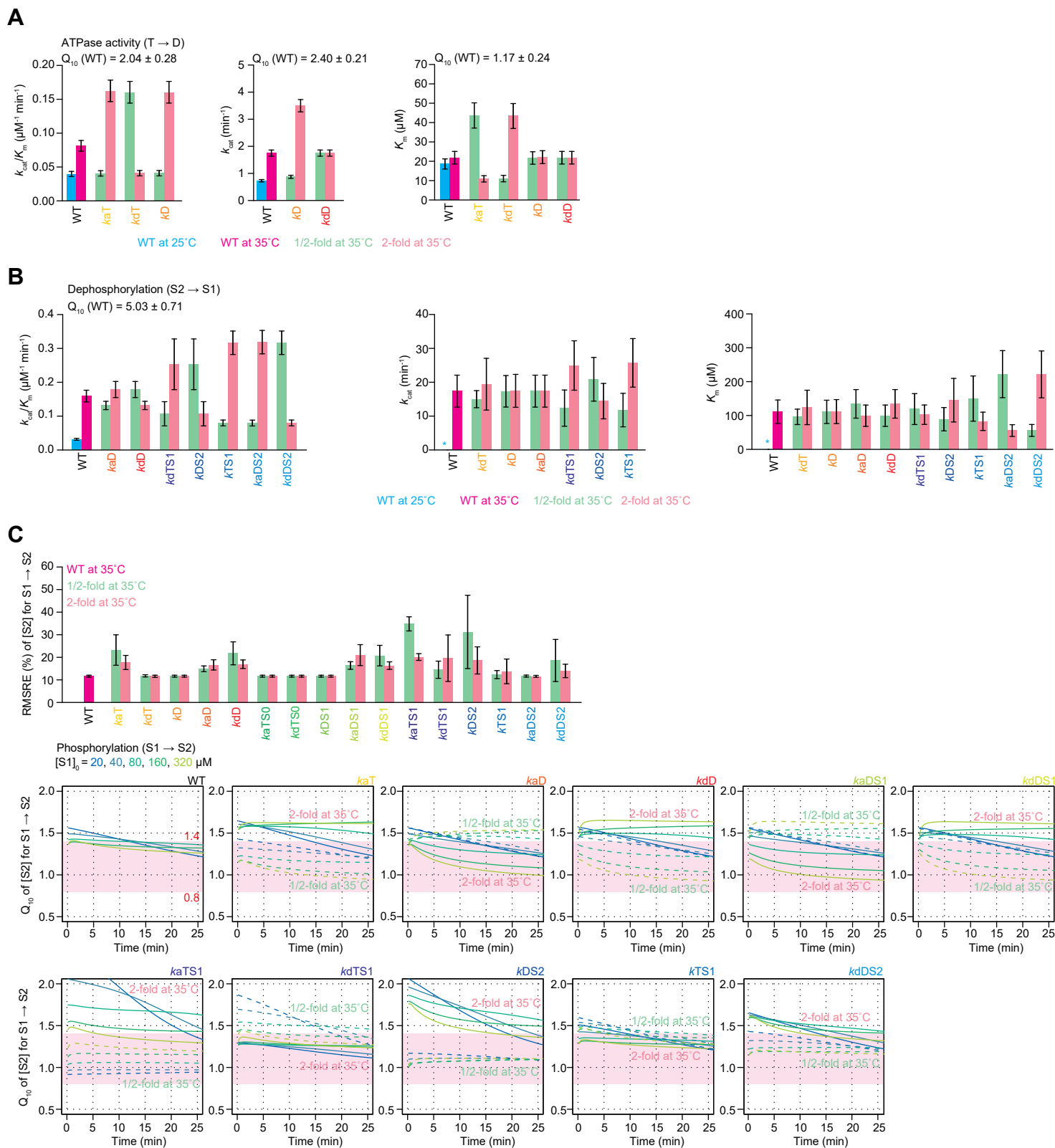


Figure S4: Shinohara *et al.*

Figure S4. A computational model recapitulated the importance of substrate and product binding in temperature-compensated CKI δ -dependent multi-site phosphorylation, related to Figure 3.

(A and B) Perturbation analysis of kinetic parameters for ATPase activity (A) and dephosphorylation from S2 to S1 (B) by changing each rate parameter value 2-fold or 1/2-fold at 35°C. A label * indicates that the mean value could not be determined precisely (the SD value was greater than the mean).

(C) Perturbation analysis of the product concentration ([S2]) from S1 to S2 phosphorylation by changing each rate parameter value 2-fold or 1/2-fold at 35°C. The upper panel shows RMSRE from experimental product concentration by the perturbation. Lower panels show the ratio (Q_{10}) of perturbed mean time course of [S2] at 35°C to unperturbed one at 25°C. The shaded region (pink) indicates that the reaction is temperature-compensated ($0.8 \leq Q_{10} \leq 1.4$) in this region.

For (A), (B), and the upper panel in (C), data are mean \pm SD (sampled from 10^8 step MCMC simulation with 10,000 step interval).

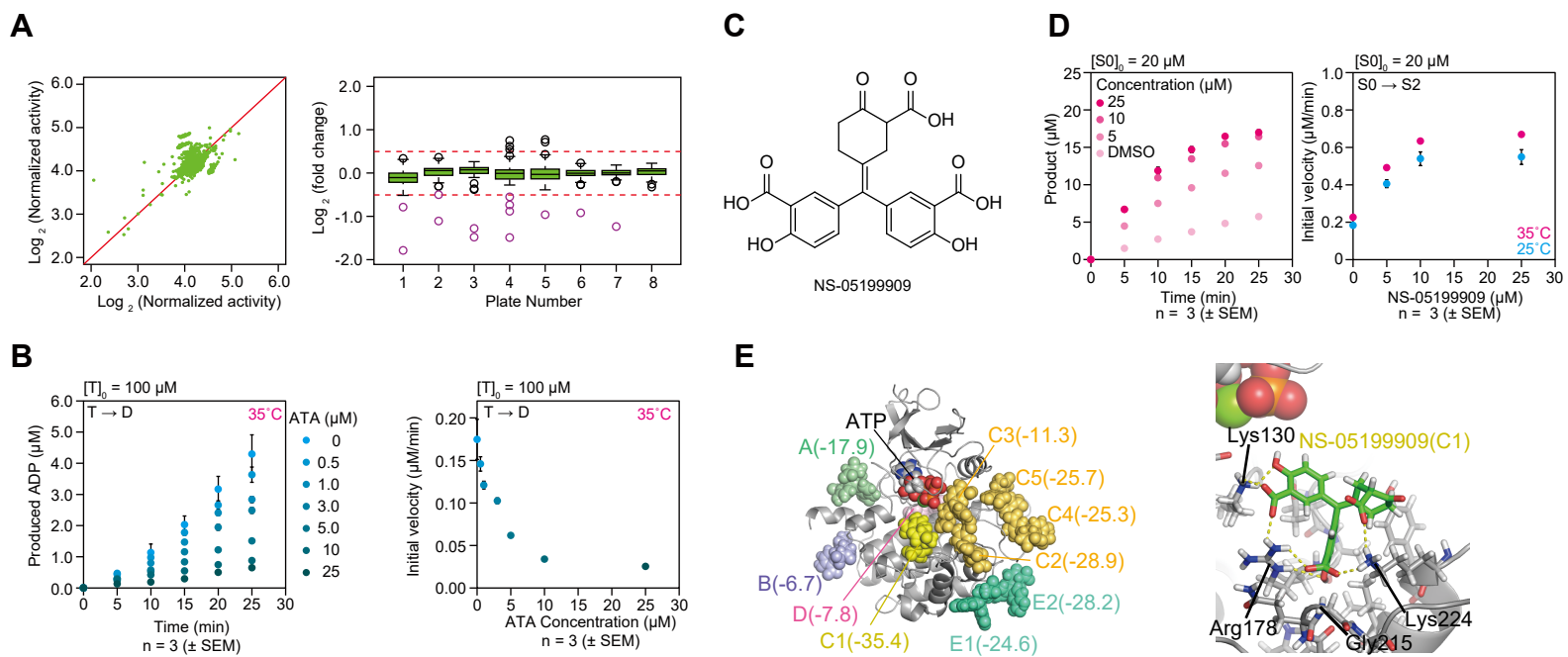


Figure S5: Shinohara *et al.*

Figure S5. Identification of ATA that inhibits ADP-dependent product binding of CKI δ by comprehensive chemical screening and putative ATA-binding site of CKI δ by in silico docking simulation, related to Figure 4.

(A) Chemical inhibitor screening against Δ CKI δ -dependent dephosphorylation activity by using LOPAC¹²⁸⁰ chemical library. Scatter plot (left panel) was constructed by calculating the normalized value among different 384-well plates. Box plot (right panel) was constructed by calculating the ratio between dephosphorylation activities with or without chemicals, which was represented as a fold change in a logarithmic scale with base 2. Chemicals that exceed the 3 SD (dashed red line) indicated as purple circles.

(B) Δ CKI δ -dependent ATPase activity (100 μ M ATP at 35°C) without a peptide substrate was inhibited by ATA in a dose-dependent manner. Data are mean \pm SEM (n = 3).

(C) Chemical structure of NS-05199909, which is similar to ATA structure (**Figure 4C**).

(D) NS-05199909-concentration dependency of Δ CKI δ -dependent phosphorylation on *CKI δ tide was enhanced by NS-05199909 in a dose-dependent manner. Data are mean \pm SEM (n = 3).

(E) Putative NS-05199909 binding sites identified by in silico docking simulation. The binding free energy (kcal/mol) was indicated in parentheses (left panel). The detailed structure of putative NS-05199909-binding site C1 with the lowest binding free energy was indicated in the right panel.

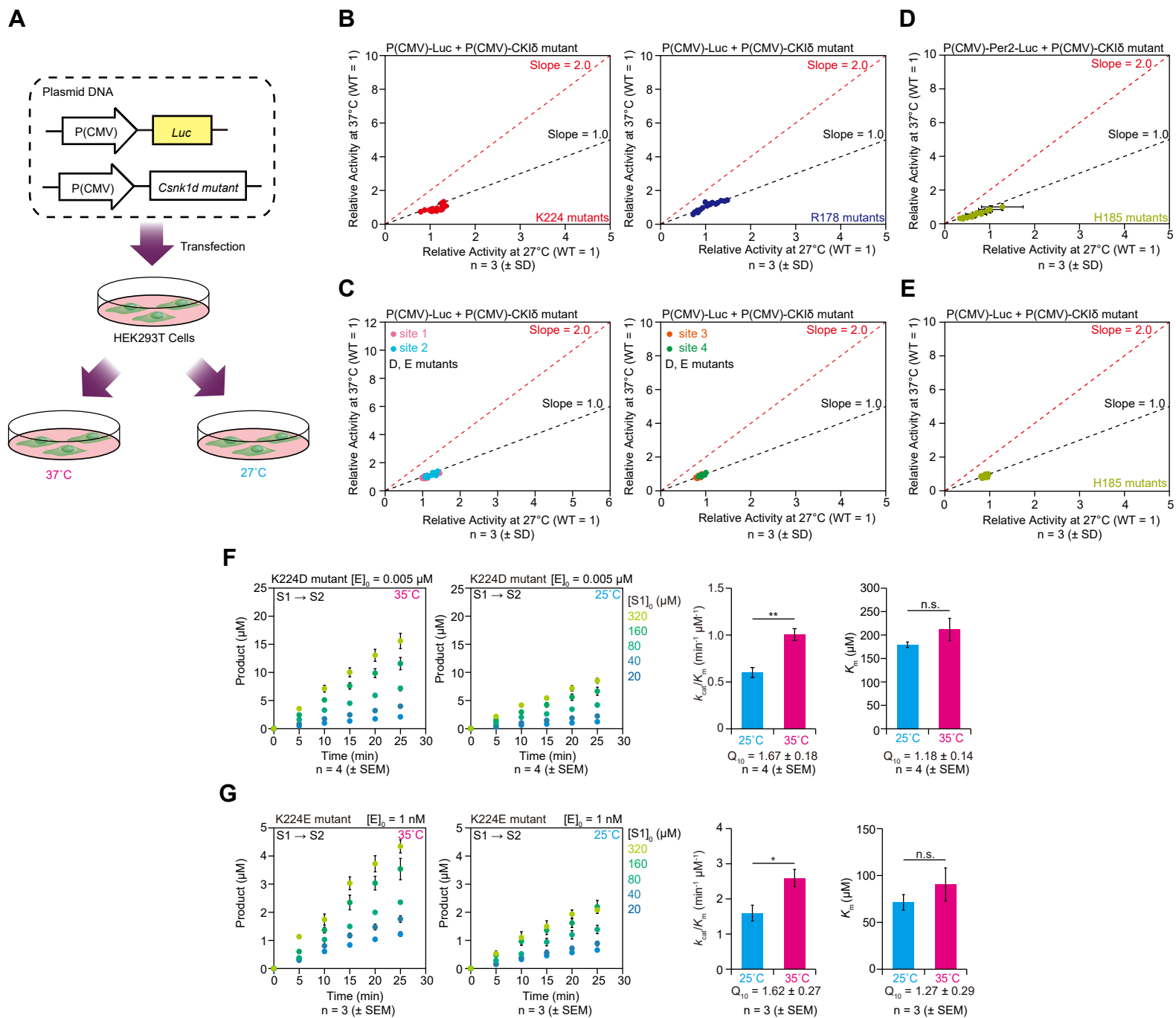


Figure S6: Shinohara et al.

Figure S6. Comprehensive genetic screening identified K224D and K224E mutants of CKI δ that impaired ADP-dependent product binding and temperature compensation of multi-site phosphorylation, related to Figure 5.

(A) Workflow of the dual-luciferase assay to examine a series of CKI δ mutants for their effect on temperature dependency of the stability of the LUC protein in HEK293T cells. See “**Transfection and Luciferase Assay**” section.

(B) K224 (left) and R178 (right) mutation did not promote the degradation of LUC protein in a temperature-dependent manner. The relative CKI δ -dependent LUC destabilization activity at 27°C or 37°C was calculated as the reciprocal of the normalized LUC value of a sample, and calibrated so that that of a wild-type sample was set as 1.0.

(C) The aspartate D or glutamate E mutation of all other candidate residues in four sites did not promote the degradation of LUC protein in a temperature-dependent manner.

(D and E) H185 mutation did not promote the degradation of PER2::LUC (D) or LUC (E) proteins in a temperature-dependent manner. The relative CKI δ -dependent PER2::LUC or LUC destabilization activity at 27°C or 37°C was calculated as the reciprocal of the normalized LUC value of a sample, and calibrated so that that of a wild-type sample was set as 1.0.

For (B)-(E), data are mean \pm SD (n = 3).

(F and G) Temperature and substrate-concentration dependency of the phosphorylation activity on a single-phosphorylated CKI tide (KRRRALpSVASLPGL) by K224D (F) and K224E (G) Δ CKI δ mutants. Kinetic parameters such as catalytic efficiency (k_{cat}/K_m) and the Michaelis constant of the substrate (K_m) were estimated for 35°C and 25°C, respectively. For (F) and (G), data are mean \pm SEM ((F) n = 4 and (G) n = 3); * p < 0.05, ** p < 0.01, and n.s. (not significant); two-tailed Welch's t-test.

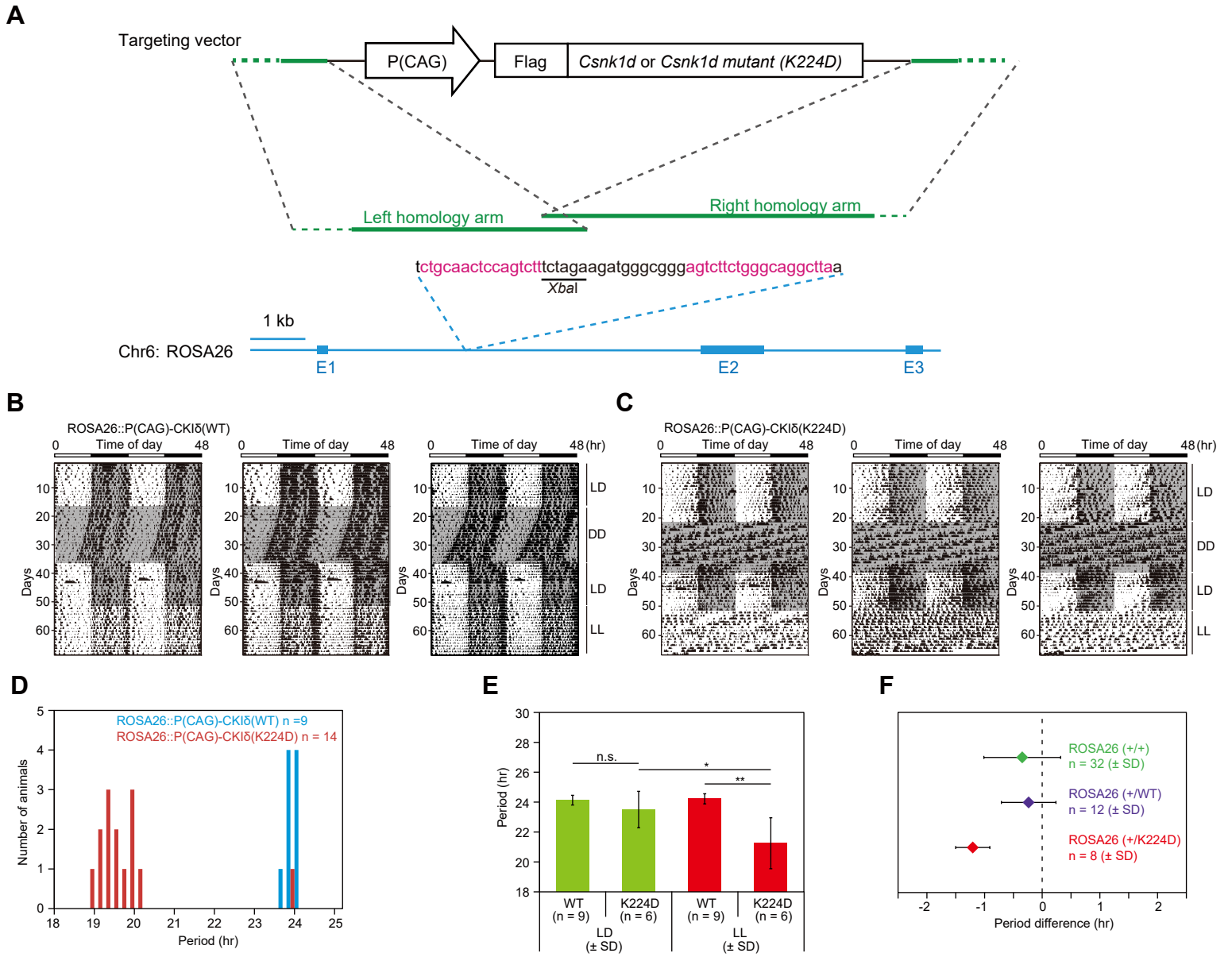


Figure S7: Shinohara *et al.*

Figure S7. K224D mutation of CKI δ remarkably shortens behavioral circadian rhythm and significantly changed the temperature-dependency of circadian rhythm of SCN in mammalian circadian clocks, related to Figure 6.

(A) Schematic of structure of the targeting vector and TALEN-targeting site on the ROSA26 locus. The FLAG-tagged CKI δ genes (wild type and K224D mutant) under the control of CAG promoter were knocked into the ROSA26 locus of ES cells by using TALEN-based gene targeting. Genomic DNA is shown as blue lines. Three of the exons (E1, E2, and E3) are indicated as blue boxes. The short nucleotide sequence of the target site containing the TALEN recognition sites (labelled in magenta) and an *Xba*I-recognition site sequence (tctaga) is shown. Corresponding regions for the 3'-terminal of left homology arm of the targeting vector and the 5'-terminal of right homology arm, which are overlapped by 6 base pairs (tctaga: *Xba*I-recognition site sequence), are shown as green lines.

(B and C) Locomotor activity of other individuals of wild-type CKI δ knock-in mice (WT-KI mice, B) and K224D mutant knock-in mice (K224D-KI mice, C) in the light-dark (LD) cycle, constant light (LL), or constant darkness (DD) conditions.

(D) The distribution of circadian period of WT-KI (n = 9) and K224D-KI (n = 14) mice under DD condition.

(E) Behavioral period of WT-KI and K224D-KI mice in the second LD and LL conditions. K224D-KI mice showed markedly shorter circadian period (21.3 ± 1.7 hr) than WT-KI mice (24.2 ± 0.3 hr) in LL condition while no significant circadian period difference was observed in LD condition. Data are mean \pm SD (n = 9 for WT-KI mice and n = 6 for K224D-KI mice); * $p < 0.05$, ** $p < 0.01$, and n.s. (not significant); two-tailed Welch's t-test.

(F) The period difference in circadian rhythms between 30°C and 37°C in the suprachiasmatic nucleus (SCN) from WT-KI or K224D-KI mice. To record endogenous circadian rhythms of SCN slices, WT-KI or K224D-KI mice were mated with PER2::Luciferase (PER2::LUC) protein-fused reporter mice (*Per2^{Luc}*). Time course of luciferase activity in each long-term cultured organotypic SCN slice was monitored by photomultiplier tubes (PMTs) over 6 days under 30°C and 37°C. Data are mean \pm SD (n = 32 for control mice without knock-in, n = 12 for WT-KI mice, and n = 8 for K224D-KI mice).

A

Accession	Entry	Length	Identical positions	Similar positions
Q9DC28	KC1D_MOUSE	415	-	-
P23291	KC11_YEAST	538	176	131
P23292	KC12_YEAST	546	169	125
P39962	KC13_YEAST	524	177	123
P29295	HRR25_YEAST	494	215	115

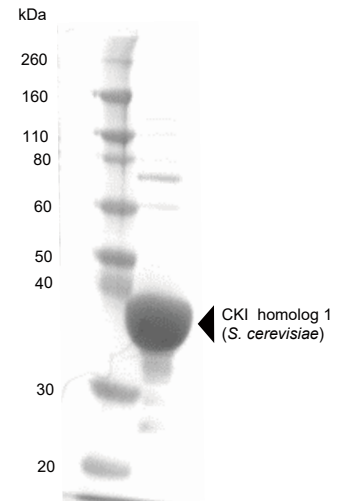
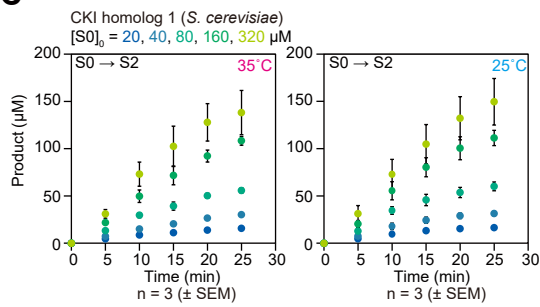
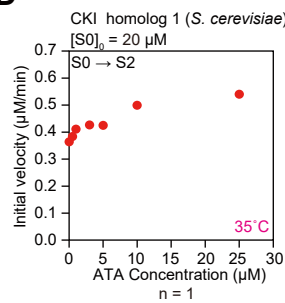
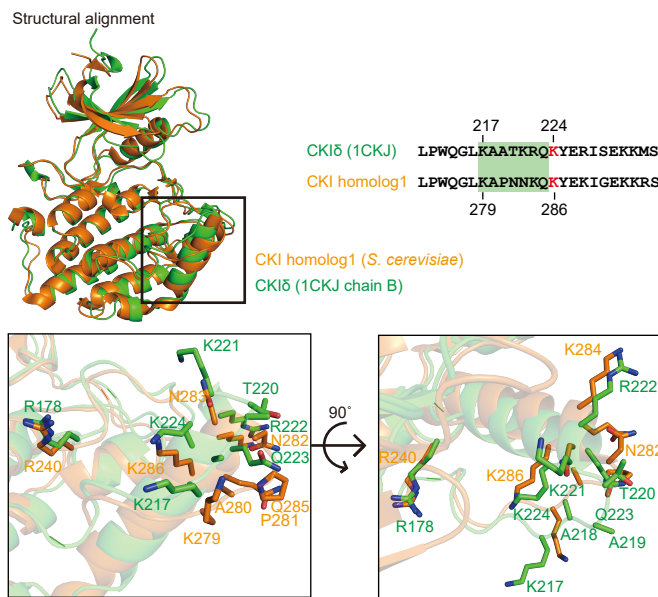
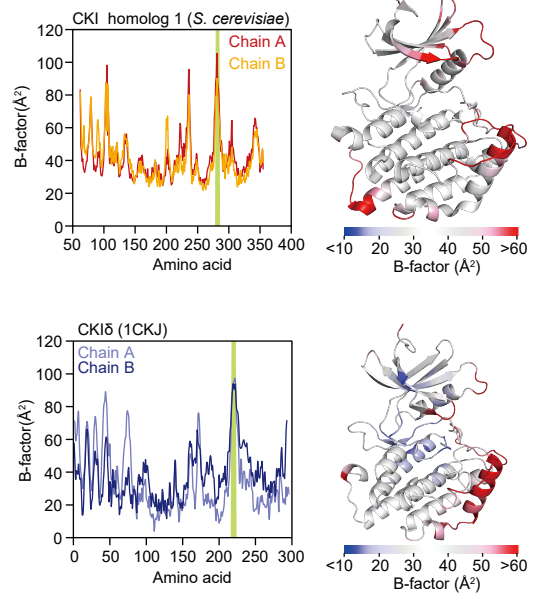
B**C****D****E****F**

Figure S8: Shinohara *et al.*

Figure S8. Temperature compensation of multi-site phosphorylation is evolutionary conserved in CKI family, related to Figure 7.

(A) Pairwise sequence alignment between CKI δ from a mouse (*Mus musculus*, MOUSE) and CKI homologs from a budding yeast (*Saccharomyces cerevisiae*, YEAST). Pairwise sequence alignments were performed by Clustal Omega program in UniProt (<http://www.uniprot.org/align/>).

(B) SDS-PAGE analysis of the purified budding yeast CKI homolog 1. The gel was stained with Coomassie Brilliant Blue (CBB).

(C) Temperature and substrate-concentration dependency of CKI homolog 1-dependent phosphorylation on a two-serine substrate, *CKItide (KRRRALSVASLPGL). Data are mean \pm SEM (n = 3). See also **Figure 7B**.

(D) ATA-concentration dependency of Δ CKI δ -dependent phosphorylation on *CKItide at 35°C (n = 1).

(E) Structural comparison between CKI δ (*Rattus norvegicus*, 1CKJ) and CKI homolog 1 (*S. cerevisiae*). Green and orange colors indicated CKI δ (*Rattus norvegicus*, 1CKJ) and CKI homolog 1 (*S. cerevisiae*), respectively.

(F) CKI-specific regions (green) located in K217-Q223 of CKI δ (*Rattus norvegicus*, 1CKJ; lower left panel) and K279-Q285 of CKI homolog 1 (*S. cerevisiae*; upper left panel) were highly fluctuated in X-ray crystal structures of apo- Δ CKI δ (lower right panel) or apo-CKI homolog 1 (upper right panel). Structural fluctuation among the three-dimensional structural polymorphism was represented as its B-factor for each C $_{\alpha}$ atom. See also **Figure 7F**.

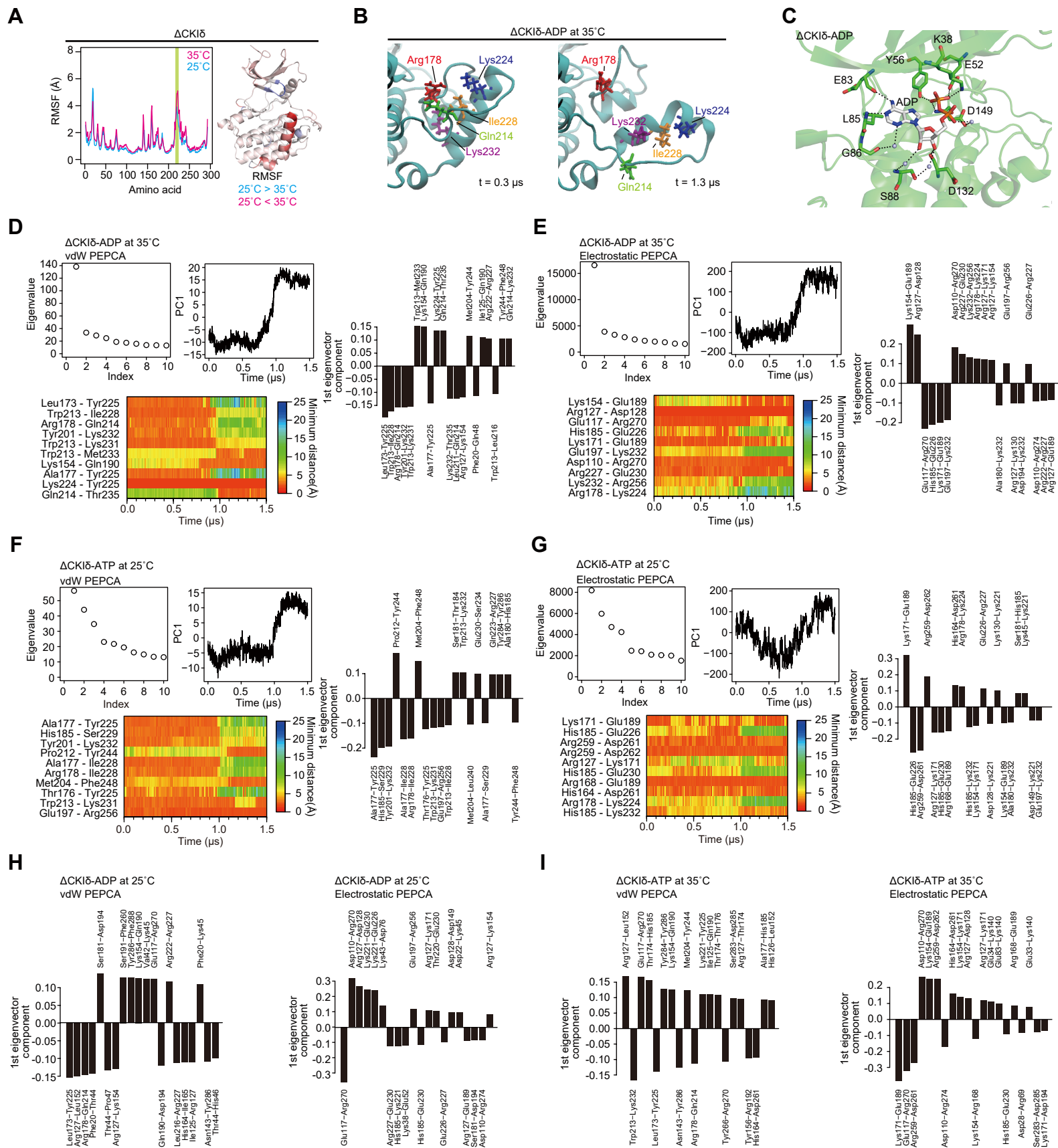


Figure S9: Shinohara *et al.*

Figure S9. A CKI-specific domain around K224 can be a structural basis of temperature compensation of CKI δ -dependent multi-site phosphorylation, related to Figure 7.

(A) 1.5 μ s molecular dynamics (MD) simulation of an apo- Δ CKI δ protein at higher (35°C) and lower (25°C) temperatures. MD simulation revealed that CKI-specific region located from K217 to Q223 (green) around α F helix was highly fluctuated in apo- Δ CKI δ protein. Structural fluctuation during MD simulation was represented as its Root Mean Square Fluctuation (RMSF) for each C α atom. See also **Figure 7E**.

(B) The conformational change of α F helix observed in 1.5 μ s MD simulation of Δ CKI δ -ADP complex at 35°C. See also **Movie S2**.

(C) ADP-binding site identified by X-ray crystal structure analysis of Δ CKI δ -ADP complex.

(D-G) Analysis of conformational changes of Δ CKI δ -ADP complex at 35°C (**D** and **E**) and Δ CKI δ -ATP complex at 25°C (**F** and **G**) by PEPCA. PCA of potential energies of van der Waals (vdW) (**D** and **F**) or electrostatic (**E** and **G**) interactions between residues were performed. Eigenvalues represent the magnitude of the conformational change due to interactions identified by the corresponding eigenvector. PC1 represents the 1st principal component that discriminates conformational states due to interactions by the 1st eigenvector. The bar graph shows the top 20 components (interactions) of the 1st eigenvector. The heat map represents the minimum distance between two residues identified by the top 10 components of the 1st eigenvector. Interactions to stabilize conformational states with negative values of PC1 can be identified by interactions with negative components of the 1st eigenvector. For example, PC1 in (**D**) shows the state transition around 0.9 μ s. The state corresponding to negative values is stabilized by negative components of the 1st eigenvector such as vdW interaction between Leu173 and Tyr 225. We can confirm that contacted two residues are detached from 0.9 μ s as shown in the heat map.

(H-I) Top 20 components of the 1st eigenvector of PEPCA for Δ CKI δ -ADP at 25°C (**H**) and Δ CKI δ -ATP at 35°C (**I**). In these MD simulations, the large conformational changes of α F helix were not observed (**Figure 7E**).

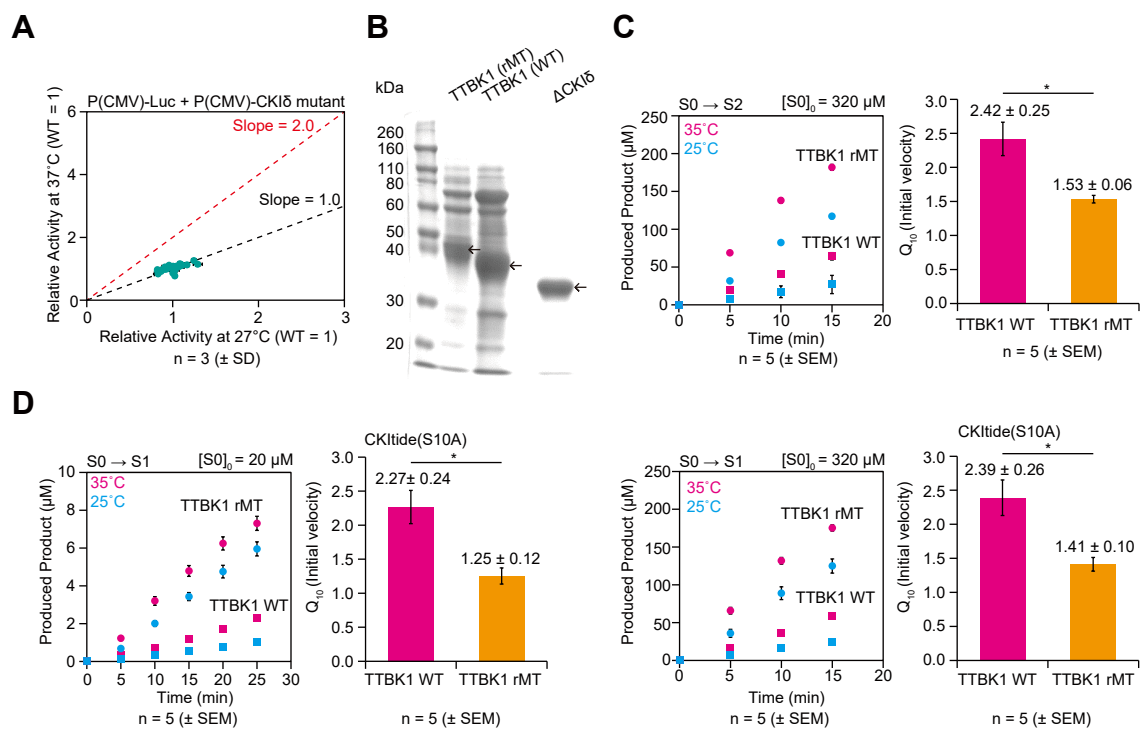


Figure S10: Shinohara *et al.*

Figure S10. A CKI δ -specific domain around K224 can confer temperature compensation on TTBK1, which shows temperature sensitivity in the first- and second-serine phosphorylation, related to Figure 7.

(A) Dual-luciferase assay to examine a series of CKI δ mutants for their effect on temperature dependency of CKI δ -dependent phosphorylation measured by the stability of the LUC protein in HEK293T cells. The alanine mutations on α F helix or on its spatially adjacent regions did not promote the degradation of LUC protein in a temperature-dependent manner. The relative CKI δ -dependent LUC destabilization activity at 27°C or 37°C was calculated as the reciprocal of the normalized LUC value of a sample, and calibrated so that that of a wild-type sample was set as 1.0. Data are mean \pm SD (n = 3).

(B) SDS-PAGE analysis of the purified wild-type TTBK1 (WT) and rationally designed TTBK1 mutant (rMT). The gel was stained with Coomassie Brilliant Blue (CBB).

(C) Temperature dependency of phosphorylation on a two-serine substrate *CKI δ tide (KRRRALSVASLPGL) by wild-type TTBK1 (WT) and rationally designed TTBK1 mutant (rMT) at higher substrate concentration (320 μ M). Temperature-sensitive TTBK1 (WT) ($Q_{10} = 2.42 \pm 0.25$) was converted to significantly less temperature-sensitive TTBK1 (rMT) ($Q_{10} = 1.53 \pm 0.06$). See also **Figure 7I**.

(D) Temperature dependency of phosphorylation on a single-serine substrate *CKI δ tide(S10A) (KRRRALSVAALPGL) by wild-type TTBK1 (WT) and rationally designed TTBK1 mutant (rMT) at lower (left panels; 20 μ M) and higher (right panels; 320 μ M) substrate concentrations. Temperature-sensitive TTBK1 (WT) ($Q_{10} = 2.27 \pm 0.24$ for 20 μ M and $Q_{10} = 2.39 \pm 0.26$ for 320 μ M substrate concentrations) was converted to significantly less temperature-sensitive TTBK1 (rMT) ($Q_{10} = 1.25 \pm 0.12$ for 20 μ M and $Q_{10} = 1.41 \pm 0.10$ for 320 μ M substrate concentrations).

For (C) and (D), data are mean \pm SEM (n = 5); * $p < 0.05$; two-tailed Welch's t-test.